AARON JOSEPH AVERBUCH

A PHOTO-ELECTRIC METHOD FOR DETECTING ACOUSTICALLY INDUCED BIREFRINGENCE IN LIQUIDS

UNIVERSITY OF ILLINOIS AT URBANA-CHAMPAIGN

THE GRADUATE COLLEGE

October, 1971

I HEREBY RECOMMEND THAT THE THESIS PREPARED UNDER MY SUPERVISION BY AARON JOSEPH AVERBUCH

ENTITLED A PHOTO-ELECTRIC METHOD FOR DETECTING ACOUSTICALLY INDUCED BIREFRINGENCE IN LIQUIDS

BE ACCEPTED IN PARTIAL FULFILLMENT OF THE REQUIREMENTS FOR THE DEGREE OF DOCTOR OF PHILOSOPHY

Floyd Dunn
In Charge of Thesis

E. Jakobsen
Head of Department

Recommendation concurred in†

O. L. Gaddy
J. R. Pierce
[illegible]
H. W. Culver

Committee on Final Examination†

† Required for doctor's degree but not for master's.

D517

A PHOTO-ELECTRIC METHOD FOR DETECTING ACOUSTICALLY INDUCED BIREFRINGENCE IN LIQUIDS

BY

AARON JOSEPH AVERBUCH
B.S.E.E., Illinois Institute of Technology, 1962
M.S., University of Illinois, 1965

THESIS

Submitted in partial fulfillment of the requirements
for the degree of Doctor of Philosophy in Electrical Engineering
in the Graduate College of the
University of Illinois at Urbana-Champaign, 1971

Urbana, Illinois

ACKNOWLEDGEMENT

The author wishes to express his grateful appreciation to his advisor Professor Floyd Dunn for suggesting the problem and for his continued interest and guidance throughout this investigation. Appreciation is also extended to Professor W. R. Klein for his many helpful discussions. The author especially wishes to thank his wife for her patience and understanding throughout this difficult period.

TABLE OF CONTENTS

I. INTRODUCTION

The purpose of this study is the investigation, by optical means, of the acoustical forces orienting anisotropic molecules of a liquid. The study is related to the interaction of sound waves with biological structures. A method of photoelectrically detecting the acoustically induced birefringence in liquids is developed to obtain the highest sensitivity possible, since the effect is measurable in only a few liquids. This method takes into account the phenomenon of light diffraction by acoustic waves in fluids. By using the acoustic pressure wave as a reference, the phase by which the acoustically induced birefringence lags the velocity gradient can be determined. If sufficient numbers of fluids could be measured, some indication of the direct mechanical forces exerted on the molecules comprising a liquid, due to the passage of acoustical waves, might be found and determinations of whether these forces are sufficient to cause molecular degradation could be made.

Biological structures *in vivo* can be modified by interaction with intense, non-cavitating, high frequency acoustic waves. Early investigations of these interactions showed that lesions can be produced in the white matter of the cat central nervous system when irradiated with acoustic waves (Barnard *et al.*, 1956). The lesions produced were not

observable until about 10 min after the end of irradiation but for longer survival times, the tissue in the lesion area showed progressive deterioration. Welkowitz and Fry (1956) irradiated amphibian skeletal muscle with acoustic intensities of the order of 100 watts/cm^2 at 980 KHz causing irreversible blockage of the action potential which propogates along the muscle fiber. A histological study showed no fiber tearing or vacuole formation, and yet, the blockage occurred within 10 seconds. Fry and Dunn (1956) were able to paralyze the hind legs of day old mice by irradiating the lumbar enlargement of the spinal cord using 982 KHz acoustic waves of 100 watts/cm^2 acoustic waves and 1 sec duration. Histological examination (light microscopy) showed no apparent damage until about 10-15 min after exposure.

Welkowitz and Fry (1956) and Fry and Dunn (1956) both showed, by means of thermocouples imbedded in the specimen, that the temperature increase due to absorption of the acoustic waves was too small to account for the irreversible effect by thermal mechanisms. Dunn (1958) has argued that hydrostatic pressure would not cause the effect and that acoustic cavitation (the production of small bubbles which form and then collapse causing shock waves) was not present. Fry and Dunn (1956) showed also that the irradiation time required to obtain paralysis of the hind legs in 50 per cent of the mice irradiated was inversely proportional to the square root of the acoustic intensity, i.e., field variables

such as pressure amplitude, particle velocity amplitude, velocity gradient amplitude, etc. The general conclusion was reached that the interaction between sound waves and biological media must occur at the microscopic level. However, the details of the physical interaction are, as yet, poorly understood. Another study employed to elucidate the interaction mechanisms involved irradiation of solutions of bio-molecules with very high acoustic intensities followed by examination of the molecular weight or, in the case of enzymes, examination for altered biological activity. Macleod (1966) found that acoustic irradiation of various enzyme solutions with acoustic intensities sufficient to cause functional damage in tissues had no effect on either the structure or function of the enzymes when examined after the irradiation procedure. It was also shown that the enzymes were not inhibited while catalyzing a reaction during the acoustic irradiation, leading to the conclusion that at the high acoustic intensities used (10^4 w/cm^2), no chemically important changes in the secondary or tertiary structure occurred in the enzyme molecules.

Although large molecular weight enzymes were not degraded by high intensity acoustic waves, deoxyribonucleic acid (DNA) prepared from B. subtilus was degraded by Hawley et al. (1963) by irradiation with 1 MHz acoustic waves of about 30 w/cm^2. The degradation was found to occur principally as backbone scission, i.e., breakage transverse

to the molecular axis. Similar concluclusions were reached by Levinthal and Davison (1961) who degraded DNA from T-2 bacteriophage by passing solutions through capillary tubes 250 microns in diameter. In addition, they were able to calculate the approximate forces which act on the DNA molecule in such a velocity gradient. The stretching force τ at the center of a long thin rod representing the molecule with radius r and length L is

$$\tau = \frac{1}{2} \int_0^{\frac{L}{2}} f G L \sin\theta \, dL$$

where G is the velocity gradient assumed uniform over the distance L, θ is the angle the rod makes with direction of fluid flow and f is a friction term given by

$$f = 3\pi\eta / \ln(L/r)$$

where η is the solvent viscosity. The calculation also assumes that the center of the rod travels at the same velocity as the fluid. If the rod is rigid, straight, and oriented at 45° to the direction of fluid flow, then

$$\tau_{max} = \frac{3\pi}{16} (\eta G L / \ln(L/r)$$

For the T-2 bacteriophage DNA molecule (length about 52 microns and radius about 10 Å measured by Cairns (1961) using an autoradiograph technique), the force at the center of the molecule for a flow rate of 0.046 ml/sec was calculated to be 1.1×10^3 dynes and compares well with the

estimated value of the force required to break a carbon-carbon band, viz., 0.8×10^3 dynes. The acoustic intensity necessary to produce an equivalent shear gradient over the T-2 DNA is calculated as follows. The velocity gradient developed in the capillary to rupture the DNA was 1.5×10^4 sec^{-1}. The velocity gradient for an acoustic wave is given by

$$G = \left.\frac{du}{dx}\right|_{max} = u_{max} \cdot k$$

or in terms of acoustic intensity,

$$G = k\sqrt{2 I_{avg} / \rho_o c}$$

where u is the particle velocity, k is the acoustic wave-number ($k = 2\pi/\lambda$), x is the direction of sound propogation, ρ_o is the undisturbed density of the fluid, c is the velocity of sound in the fluid, and I_{avg} is the average intensity of the acoustic wave. Taking ρ_o for water as 1 g/cc^3, c as 1.46×10^5 cm/sec and k as 42 cm^{-1}, and f as 1 MHz, the required intensity is 8.7×10^2 $watts/cm^2$.

Frenkel (1944) used a different approach to the problem in which he treated the bonds of a flexible polymer as a linear elastic link whose value could be determined from the bulk properties of the polymer. Following Frenkel, let

$$e = 1/El$$

where e is the elasticity coefficient of the link between two beads of a polymer consisting of N spherical beads of separation l and radius a and E is the elasticity of a body

constituted by the monomeric groups. A critical value of the velocity gradient G occurs when the change in link length becomes infinite where

$$\Delta l = \frac{3\pi\eta r G l e}{1 - 3\pi\eta r G l e}$$

and therefore

$$G = \frac{1}{3\pi\eta r l e}$$

for the dimer. For a random coil model polymer stretched out into a long thin rod, the force of extension at the center of the molecule is given by

$$f = 3\pi\eta r G l N^2$$

If η is 0.01 poise, r is 10^{-7} cm, l is 3×10^{-7} cm, G is 1.5×10^{4} sec^{-1}, and f is 10^{-3} dyne, then N is found to be about 4500 giving a molecular length of Nxl or about 14 microns, which is one fourth of the T-2 phage DNA molecular length. For a given molecule and flow gradient, Frenkel's method results in a calculated force 16 times larger than that calculated by Leventhal and Davison (1961), since the force developed is proportional to the square of the molecular length. Thus, to degrade the T-2 phage DNA, an acoustic intensity of only 3.4 watts/cm^2 would be required. Further, the acoustic intensity required to degrade a molecule varies as the inverse fourth power of the length, so that the acoustic intensities required to degrade molecules smaller than those of DNA increases very rapidly to levels beyond

those possible to generate.

In order to determine the forces acting on the molecules in a fluid, it was necessary, in the above discussion, for a change in molecular structure to occur. However, an alternative method for determining the forces on the molecules in a fluid uses the fact that, if the molecules are anisotropic both in shape and in optical properties, the presence of an acoustic wave causes the normally random distribution of molecular orientations to be perturbed resulting in anisotropy of the index of refraction. This is called acoustically induced birefringence and is discussed extensively in the following chapters. The study of acoustically induced birefringence allows determination of the statistical average of the forces on the molecule, together with the degree of orientation and the rotational diffusion constant. The theories describing this effect are only approximate and it is not possible to calculate a priori the birefringence expected in any given fluid. The most sophisticated attempts thus far involves measuring the effect and comparing the observed optical properties with those obtained in flow birefringence studies.

The present investigation was undertaken to examine the previous work in detail with the hope of improving the methods of measurement in order to obtain more precise birefringence data. The second chapter of this thesis describes some of the current theories which predict the

resultant index of refraction change when acoustic waves are present in the fluid. These theories all begin with the assumption that shear forces resulting from the presence of a velocity gradient perturb the molecules in a fluid so that their orientations are no longer completely random, although the forces are not calculated explicitly. Chapter III contains descriptions of several schemes for measuring acoustically induced birefringence, wherein the methods of Lucas (1939) and Klein (1969) are discussed in detail. This chapter also introduces a new method which allows the use of a photomultiplier to measure the degree of anisotropy while minimizing the effects of source intensity variations and of changes in the transmission characteristics in the optical path. Chapter IV describes some of the limitations of the new detection method and describes a correction which must be made when working at the limit of resolution of the apparatus to account partially for the deficiencies of the optical system. Chapter V describes the instrumentation used in this investigation and Chapter VI deals with the experimental methods and procedures of this study. The experimental data obtained using the new measurement technique are presented in Chapter VII. The fluids studied exhibited rotary relaxation frequencies which extended from frequencies below those used for measurement to frequencies well above the frequency range of the equipment used allowing the system to identify properly the phase angle between the acoustically

induced birefringence and the pressure wave. Concluding remarks showing that new theories are required to describe the effect of temperature on the mechanical and optical properties of some fluids are presented in Chapter VIII. Three appendices follow which describe a computer program to evaluate the diffraction of light by acoustical waves, contains tables of the amplitude of the electric vector in a number of diffraction orders as well as for different frequencies of operation, and, last describes the theory of the rotary mica compensator used to provide a variable phase shift in the optical path.

II. THEORIES OF ACOUSTICALLY INDUCED BIREFRINGENCE

This chapter deals with several theories proposed to explain the magnitude of the observed acoustically induced birefringence for the three cases of pure liquids, solutions of flexible molecules and solutions of rigid molecules. Theories for pure liquids have been proposed by Lucas (1939), Frenkel (1946) and Peterlin (1950). Peterlin (1967a) has also proposed a theory for flexible molecules and his (1950) paper could also be interpreted as a theory for rigid molecules in solution.

Lucas bases his theory of acoustically induced birefringence on results from the theory of flow birefringence proposed by Raman and Krishnan (1928) in which the hydrodynamic theory of Stokes (1845) is employed to account for the forces tending to orient anisotropic molecules in a flow gradient, the theory of Boltzmann employed to account for the disorienting forces, and the optical treatment of Langevin (1910) and Born (1918) to relate the polarizability of the oriented molecule to the birefringence of the medium. In the case of flow birefringence, Stokes showed that each element of liquid in a velocity gradient is subject to tensile and compressive forces acting along two mutually perpendicular directions inclined at an angle of 45^{o} to the direction of flow with magnitude

$$F = \eta \frac{dv}{dx} \qquad (2\text{-}1)$$

where F is the normal force acting on the element, η is the dynamic coefficient of viscosity, dv/dx is the velocity gradient evaluated at the element, and v is the velocity of the molecules in the x direction, which varies as a function of the x coordinate only. Using the Navier-Stokes equations, Lucas concludes that the acoustically induced forces on the molecules in a liquid act in the direction of wave propagation (x-direction) with magnitude given by

$$\delta F = 2\eta \frac{du}{dx} \tag{2-2}$$

where u is the velocity of the molecule in the x direction which varies as a function of the x coordinate only. Also, Lucas assumes that the sound is present in the form of a plane wave. Using relationships among the acoustic variables, Lucas arrives at the relationship

$$\delta F_{max} = 2\eta \frac{\omega}{c} \sqrt{\frac{2I}{\rho_0 c}} \tag{2-3}$$

where δF_{max} is the peak value of the sinusoidally varying force (actually force per unit area), ω is the angular frequency of the sound wave, c is the velocity of sound propagation in the medium, I is the intensity of the acoustic wave, and ρ_c is the undisturbed density of the medium. To relate the orienting forces with the observed birefringence, Lucas employs the relation

$$n_y - n_x = n M \delta F_{max} = n M \left(2\eta \frac{\omega}{c} \sqrt{\frac{2I}{\rho_0 c}}\right) \tag{2-4}$$

where n_y is the index of refraction for the extraordinary wave, n_x is the index of refraction for the ordinary wave, and n is the index of refraction of the undisturbed medium. M, the proportionality constant between the orienting force and the observed birefringence, is the Maxwell constant which contains the relationship between the orienting force and the optical anisotropy of the molecule. Hilyard and Jerrard (1962) combine the formuli of Lucas (1939) and Raman and Krishnan (1928) to give finally

$$(n_y - n_x)_{max} = \frac{2\omega (n^2-1)(n^2+2)}{10\, n\, k\, T\, N_o} \left(\frac{2I}{\rho_o c^3}\right)^{1/2} f(\gamma) \qquad (2\text{-}5)$$

where N_o is the number of molecules per unit volume, k is Boltzmann's constant, $f(\gamma)$ is a function of molecular size and polarizability, and

$$M = \frac{(n^2-1)(n^2+2)}{10 n^2 N_o k T} f(\gamma) \qquad (2\text{-}6)$$

Raman and Krishnan give $f(\gamma)$ as

$$f(\gamma) = \frac{(a_1-a_2)(b_{11}-b_{22}) + (a_2-a_3)(b_{22}-b_{33}) + (a_3-a_1)(b_{33}-b_{31})}{(a_1+a_2+a_3)(b_{11}+b_{22}+b_{33})} \qquad (2\text{-}7)$$

where a is the axis of the ellipsoid representing the molecule and b is the optical anisotropy along the axis a.

Lucas did not include a time dependence for $n_y - n_x$, though he does assume a spatial dependence

$$\delta = \delta_{max} \sin kx$$

where δ is the phase shift between the x and y vectors. Hilyard and Jerrard (1962) add a factor $\sin(wt-kx-\phi)$ to Eq. 2-4

where ϕ is the angle by which the oscillations of the molecules lag behind those of the sound waves.

The theory of Lucas has been modified by Frenkel (1946) who considers the same mechanism of molecular orientation, but introduces the fact that when the acoustic wave disappears, a finite time is required (the relaxation time) for the birefringence to disappear. Unfortunately, Frenkel does not derive an expression for $(n_y - n_x)$ but only derives the form the correction for a single relaxattion time should take, viz.,

$$| S_{11} | = \frac{2}{3} \cdot \frac{\Lambda \tau G_{11}}{(1+\omega^2\tau^2)^{1/2}} \qquad (2\text{-}8)$$

where S_{11} is an anisotropy tensor of the molecule, Λ is a constant, τ is the relaxation time, and G_{11} is a velocity tensor, which, if the time dependence is inserted into Eq. 2-4 gives

$$(n_y - n_x) = n M K \frac{\omega\tau}{(1+\omega^2\tau^2)^{1/2}} \left(\frac{2I}{\rho_0 c^3}\right)^{1/2} \qquad (2\text{-}9)$$

where K is a constant.

Peterlin (1950) has also proposed a theory of acoustically induced birefringence based upon the work of Jeffery (1922) who considers the molecules of the solution to be rigid, anisotropic ellipsoids of revolution having major and minor axes of lengths $2a_1$ and $2a_2$, respectively.

Peterline assumes that the optical axes of the molecule coincide with the geometrical axes. The mechanism of orientation is considered to be the same as that proposed by Lucas, i.e, the orientation is the result of a kinematic equilibrium between the flow gradient set up by the acoustic wave and thermal agitation. However, Jeffery's analysis takes into account the regular precession of the molecule about its geometrical axes with the result

$$\dot{\theta} = -\frac{Gb}{2}\sin 2\theta \qquad (2\text{-}10)$$

where θ is the angle between the major axis of the ellipse and the direction of propagation of the sound wave, G is the velocity gradient, and b is given by

$$b = \frac{a_1^2 - a_2^2}{a_1^2 + a_2^2}$$

The distribution of the molecule at any time t is given by Peterlin as

$$F = \frac{N_o}{4\pi}\left[1 + \frac{3U_o b\,\omega\gamma}{c(1+\omega^2\gamma^2)^{1/2}}\left(\cos^2\theta - \tfrac{1}{3}\right)\sin(\omega t - kx - \phi)\right] \qquad (2\text{-}11)$$

where N_o is the number of molecules per unit volume, and U_o is the amplitude of displacement of the sound wave. A polar plot of F for $(\omega t - kx - \phi)$ equal to 90° and 270° is shown in Fig. 2-1. The magnitude of the induced birefringence is now found by differentiation of the equation giving the molar polarization [P] of the liquid, i.e.,

$$[P] = \frac{n^2-1}{n^2+2}\frac{M}{\rho_o} = \frac{4\pi}{3}N_A\bar{\alpha} \qquad (2\text{-}12)$$

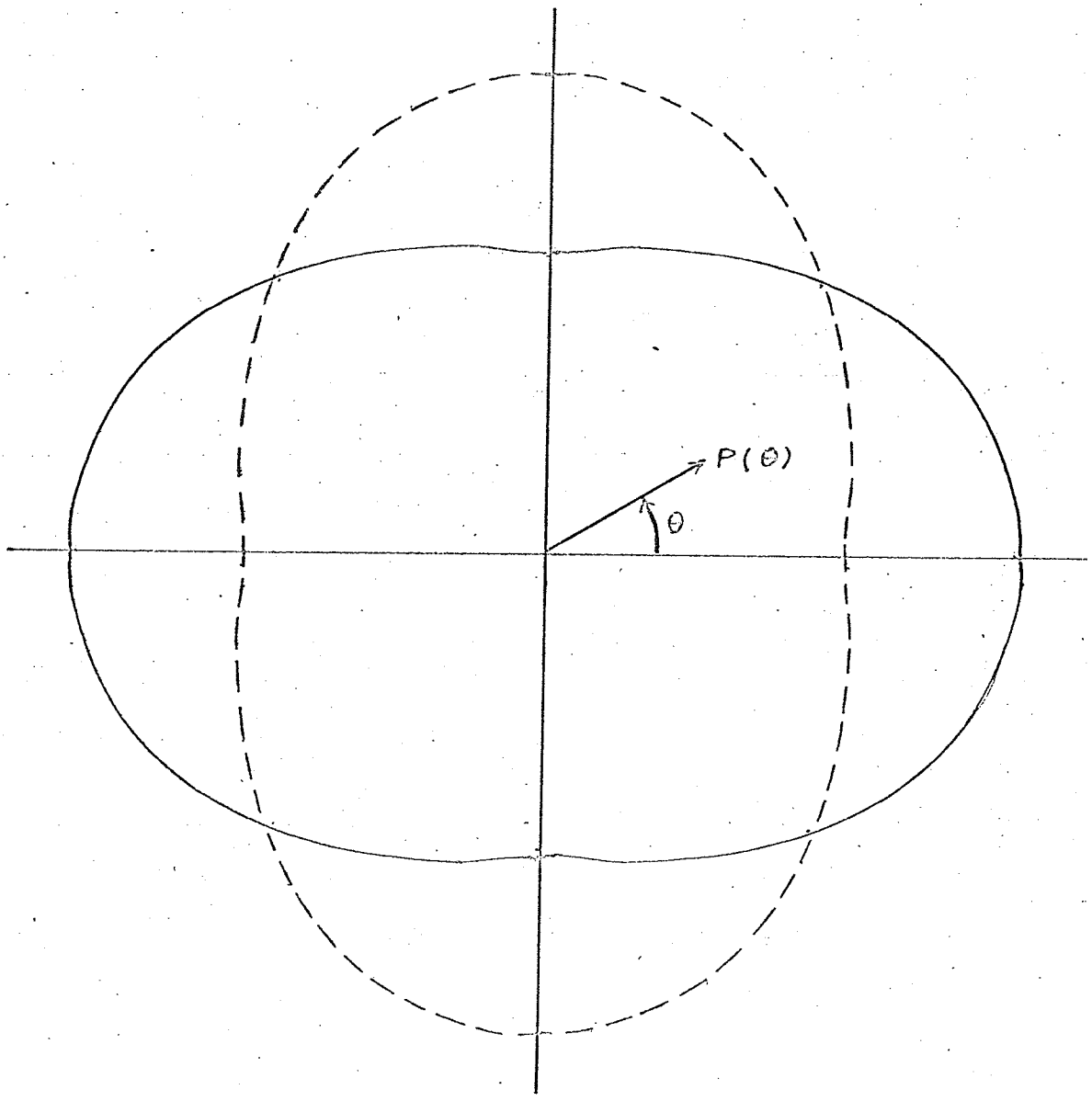

Figure 2.1 Polar plot of Peterlin's (1950) distribution function. Note how the probability for finding a molecule oriented in the x direction changes with respect to the phase of the acoustic wave. Hence, the birefringence goes positive and negative during the acoustic cycle.

where M is the molecular weight, N_A is Avogadro's number, and $\bar{\alpha}$ is the mean apparent polarizability. Then, if $\bar{\alpha}_1$ and $\bar{\alpha}_2$ denote the mean apparent polarizability along the axes a_1 and a_2 of the molecule, respectively, Peterlin concludes that

$$(n_y - n_x) = \frac{n Q \omega \tau}{(1+\omega^2\tau^2)^{1/2}} \left(\frac{2I}{\rho_0 c^3}\right)^{1/2} \sin(\omega t - kx - \phi) \qquad (2\text{-}13)$$

where

$$Q = \left[\frac{4\pi}{5} \cdot \frac{(n^2+2)^2}{9n^2} N_0 b\right] (\bar{\alpha}_1 - \bar{\alpha}_2) \qquad (2\text{-}14)$$

Comparing (2-6) and (2-14) it is noted that the term kT is missing from the latter. Jerrard (1959) has shown that in the case of pure liquids

$$M = \frac{Q}{6\eta D} \qquad (2\text{-}15)$$

where D is the rotary diffusion constant, which is a function of kT.

A comparison of (2-6) and (2-15) yields considerable disagreement. With respect to the acoustic variables, however, (2-13) is the same as (2-9). Hence, measurements of $(n_y - n_x)_{max}$ as a function of acoustic intensity or frequency would not yield information that would help decide which theory better represents the phenomenon. On the other hand, neither theory predicts an upper bound for the magnitude of the birefringence as a function of acoustic intensity despite the fact that the birefringence should

approach a maximum as the percentage of molecules aligned in the field approaches 100%.

Peterlin (1967a) has produced a theory for polymer solutions in which the molecules consist of $Z \neq 1$ beads connected by Z statistically independent non-linear elastic links (necklace model). Because of the flexibility of the molecule, the solution is assumed to behave as a pure liquid. Peterlin assumes the hydrodynamic interaction between any two beads to be that given by Rouse (1953) and the finite resistance of the molecule to rapid shape changes to be that given by Cerf (1958).

The $Z \neq 1$ links of the necklace have a root mean square length b_o and a maximum length of b_m. The hydrodynamic resistance f is concentrated in the beads. The hydrodynamic interaction is assumed to be proportional to the inverse root mean square distance between the beads under consideration. The deformation of the molecule is assumed small since the flow gradient is not very large (the Reynolds number is much less than 1). Since the deformation is small, any non-linearity of the link elasticity can be neglected. The model resists shape changes with a force proportional to the rate of deformation. The proportionality factor $\wp$ is called the inner viscosity coefficient. This viscosity associated with deformation includes the "bulk viscosity" or the resistance to the change in the molecular volume for a scalar compression of dilatation.

Peterlin then uses the calculation of Cerf (1959) to obtain the velocity vector of the beads, taking into account the hydrodynamic interaction and the forces transmitted by the chain (elastic links, inner viscosity, Brownian motion). Since the velocity of the beads has been calculated, the force F by which the molecule resists the deformation rate v is

$$F = - \Phi v \tag{2-16}$$

where Φ is the tensor of inner viscosities measuring the resistance of the molecule to deformation. The optical anisotropy of the statistical segment is proportional to the average square link length according to Kuhn and Grun (1942). Thus, the difference in the polarizability of the jth segment in the link direction γ_1, and in the direction perpendicular to it, γ_2, is given as

$$\gamma_1 - \gamma_2 = \frac{3}{5} (\alpha_1 - \alpha_2) \, b_j^2 / b_o^2 \tag{2-17}$$

where j=1,2, . . . z and α_1 and α_2 are the corresponding polarizabilities for the monomer. Peterlin then defines $(\alpha_y - \alpha_x)$ as the difference in the mean polarizability of the macromolecule and obtains

$$\frac{n_y - n_x}{n} = \left(\frac{n^2 + 2}{3n} \right)^2 \frac{2\pi N_A C}{M} (\alpha_y - \alpha_x) \tag{2-18}$$

Summing over all the polarizabilities and relaxation times associated with the segments, the final result obtained is

$$(n_y - n_x) = \frac{4\pi}{5}\left(\frac{n^2+2}{3n}\right)^2\left(\frac{2I}{\rho_0 c^3}\right)^{1/2}\frac{\eta N_A c}{M}(\alpha_1-\alpha_2)\sum_{p=1}^{z}\frac{\omega\tau_p \sin(\omega t - kx - \phi)}{(1+\omega^2\tau_p'^2)^{1/2}} \quad (2\text{-}19)$$

where

$$\tau_p = b_c^2 / 2 D_o \lambda_p$$

and

$$\tau_p' = \tau_p (1 + \nu_p \varphi_p / f)$$

τ_p is the relaxation time associated with the pth segment, τ_p' is the relaxation time of the segment modified by a factor dependent on the inner viscosity, D_o is the diffusion constant of the bead and ν_p and λ_p are eigenvalues of the interaction matrix. Equation 19 has the same form for $n_y - n_x$ as does Eq. 13, the result for a rigid ellipsoid in a viscous medium with only a single relaxation time. The phase angle by which the birefringence lags the velocity gradient is given as

$$\tan\phi = \frac{\sum \omega^2\tau_p\tau_p'/(1+\omega^2\tau_p'^2)}{\sum \omega\tau_p/(1+\omega^2\tau_p'^2)} \quad (2\text{-}20)$$

The birefringence first increases linearly with frequency, passes through a transition region whose width depends on the number of segments and the degree of permeability to the solvent, and finally approaches the saturation value

$$(n_y - n_x)_{max} = \frac{4\pi}{5}\left(\frac{n^2+2}{3n}\right)^2\left(\frac{2I}{\rho_0 c^3}\right)^{1/2}\frac{\eta N_A}{M}(\alpha_1-\alpha_2)\sum_{p=1}^{z}\left(1+\frac{\nu_p\varphi_p}{f}\right)^{-1} \quad (2\text{-}21)$$

The width of the transition region is greater for a polymer with many relaxation times than for a single relaxation time.

Despite this, the maximum phase shift is limited in Eq. (2-20) to 90°. Since the method of measurement given in the next chapter will enable measurement of this phase angle, as well as the quadrant the angle appears in (if ϕ is less than 360°), measurements of a suitable polymer over a wide frequency range would provide a good test for this aspect of Peterlin's theory.

III. APPLICATION OF THE THEORY OF ACOUSTIC DIFFRACTION OF LIGHT TO MEASUREMENT OF ACOUSTICALLY INDUCED BIREFRINGENCE

From the time Lucas (1939) first observed acoustically induced birefringence to the present, investigators have employed the same basic experimental arrangement, see Fig. 3-1. The modification by Zvetkov, et al. (1946), Badoz (1957) and Hilyard (1963) served to increase the precision. The basic assumption in all the above methods is that when a light beam passes through the test fluid, its components become separated in relative phase, and this separation can be detected with near field optical measurements. The basic measurement system is illustrated in Fig. 3-1.

The polarized light beam passes through the test fluid in the z direction perpendicular to the direction of sound propagation (x direction) with the polarization vector at 45^{o} to the x axis (Fig. 3-2a). Let the two components of the incoming light vector E be E_x and E_y. Each will have a magnitude of $E/\sqrt{2}$ and, after traversing a birefringent medium, the propagation velocity is less for one component than for the other resulting in a relative phase difference. The number of wavelengths for wave E_y in the birefringent medium is given by

$$N_1 = \frac{d n_y}{\lambda_{vac}} \qquad (3\text{-}1)$$

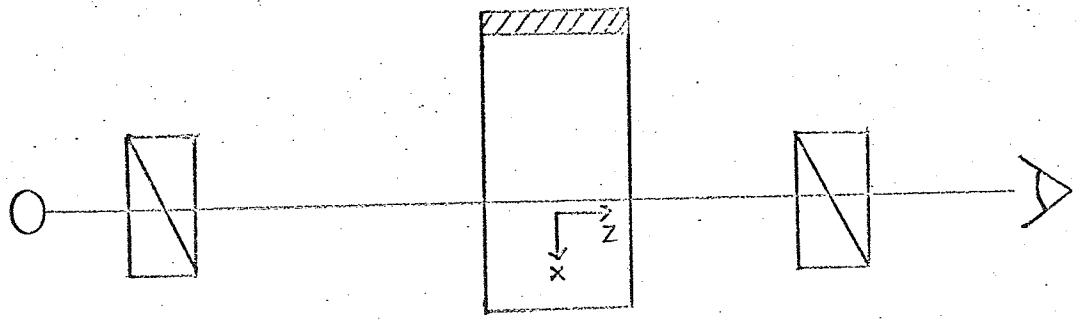

Figure 3-1. Schematic arrangement of Lucas for observing acoustic birefringence. The y direction is into the plane of the paper.

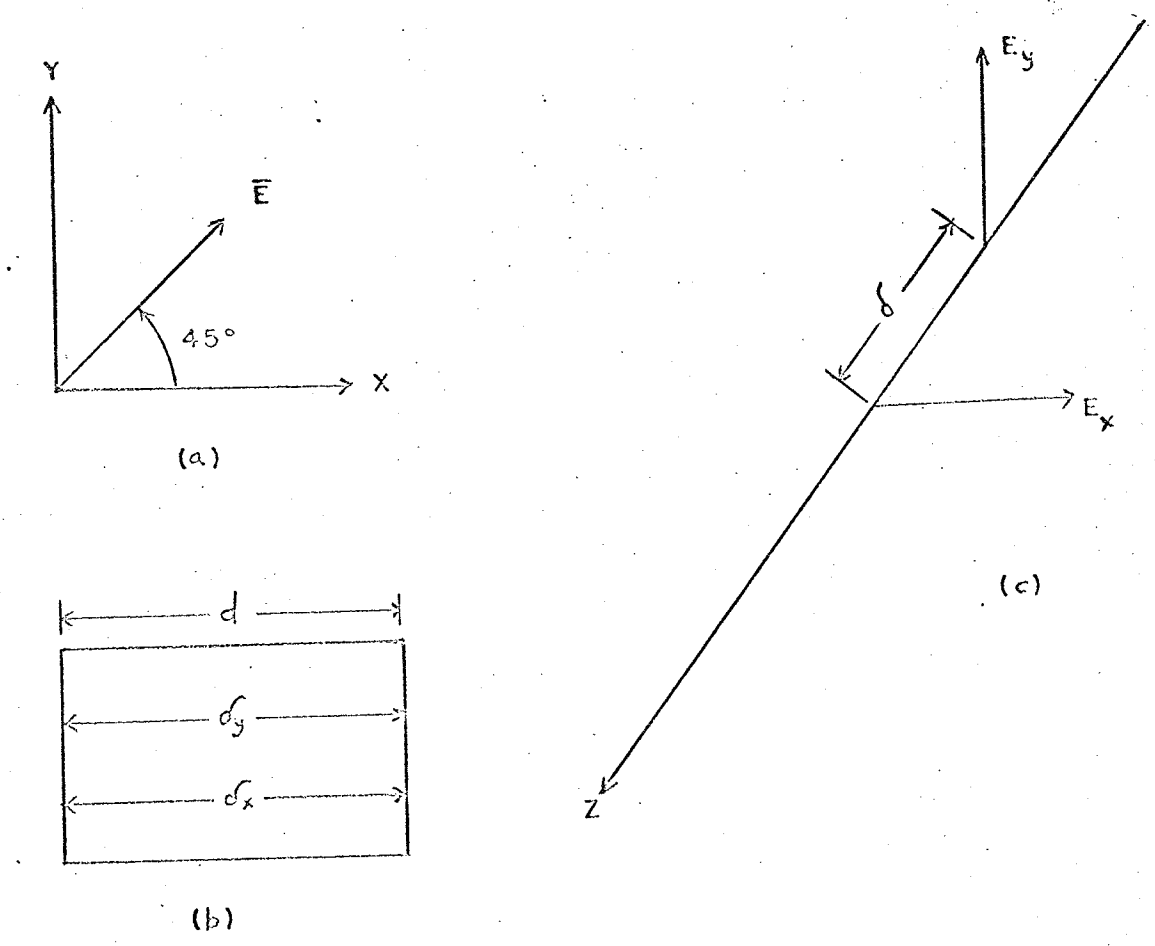

Figure 3-2. Schematic of electric vectors used to calculate photocell output.

where d is the length through the birefringent medium and n_y is the index of refraction for y polarized light. Similarly, for the x component of the electric vector,

$$N_2 = \frac{d\, n_x}{\lambda_{vac}}$$

The phase shift δ can be written as

$$\frac{\delta}{2\pi} = N_1 - N_2 = \frac{d}{\lambda_{vac}} (n_y - n_x)$$

where δ is assumed to be less than $\pi/2$ radians. Or,

$$\delta = d\, k' \tag{3-2}$$

where k' is the wave number in free space and ϵ is $n_y - n_x$. The electric vector leaving the sample medium is the vector sum of its components (Fig. 3-2c)

$$E_{exit} = \left[E_y^2 \cos^2(\omega' t - k'z - \phi) + E_x^2 \cos^2(\omega' t - k'z) \right]^{1/2} \tag{3-3}$$

having an angle to the x axis θ such that

$$\tan\theta = \frac{E_y \cos(\omega' t - k'z - \phi)}{E_x \cos(\omega' t - k'z)} \tag{3-4}$$

where w' is the angular frequency of the electric vector in free space. The analyzer prism blocks the component of E_{exit} at 45° to the x axis and passes the component at 135° (Fig. 3-3), thus,

$$E_{135°} = E_{exit} \cos(135° - \theta) \tag{3-5}$$

Substitution of Eqs. 3-3 and 3-4 into 3-5 with $E_y = E_x = E/\sqrt{2}$, yields, after some trigonometric manipulation,

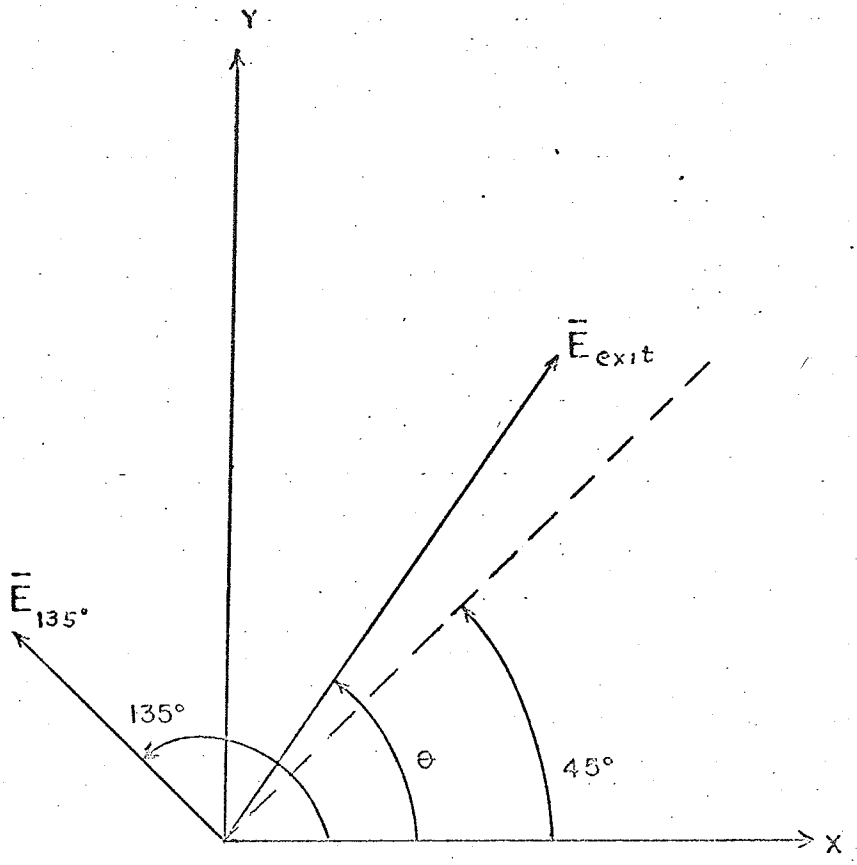

Figure 3-3. Vector diagram for calculating the light vector leaving the analyzer prism.

$$E_{135^\circ} = E \sin\left(\omega' t - k' z - \frac{\phi}{2}\right) \sin\frac{\phi}{2}$$

Or, in terms of the change in refractive index,

$$E_{135^\circ} = E \sin\left(\omega' t - k' z - \frac{\phi}{2}\right) \sin\left[\frac{d k'}{2} \epsilon\right] \qquad (3\text{-}6)$$

Since light sensitive detectors do not respond to the phase angle of the electric vector, the time varying phase shift can be neglected. Also, since the birefringence is very small, sin θ can be replaced by θ and Eq. 3-6 solved for ϵ:

$$\epsilon = \frac{E_{135^\circ}}{E} \cdot \frac{2}{k' d} \qquad (3\text{-}7)$$

If the variation of the birefringence is assumed sinusoidal in time and space, $\epsilon = \epsilon_{max} \sin(wt-kx)$ the ratio of the total intensity of light leaving the analyzer prism, I, to the total available I_o, when the analyzer and polarizer are parallel, is, after squaring Eq. 3-6

$$\frac{I}{I_o} = \frac{1}{W} \int_0^W \sin^2\left[\frac{d k'}{2} \epsilon_{max} \sin(\omega t - kx)\right] dx$$

where W is the width of the light beam. Since the expected birefringence is very small, $\sin^2\theta$ can be replaced by θ^2 and integrated, giving

$$\frac{I}{I_o} = \frac{d^2 (k')^2}{4}\left[\frac{1}{2} - \frac{\cos 2(\omega t - kW) - \cos 2\omega t}{2kW}\right] \epsilon_{max}^2$$

or

$$\frac{I}{I_o} = \frac{d^2 (k')^2}{4}\left[\frac{1}{2} - \frac{A \sin(2\omega t + 2\alpha)}{2kW}\right] \epsilon_{max}^2 \qquad (3\text{-}8)$$

where $A = \sqrt{1 - 2\cos 2kW}$ and $\tan \alpha = \cot 2kW - \operatorname{cosec} 2kW$. For the case where the light beam is much wider than the wavelength of sound in the fluid, the last term in Eq. 3-8 can be neglected yielding

$$\epsilon_{max} = \frac{2}{d k'} \sqrt{\frac{2I}{I_o}} \qquad (3\text{-}9)$$

Ward and Lein (1969) have shown that the general solution to the problem of acoustic diffraction of light can be applied to the problem of acoustic birefringence. Consider the variation of the index of refraction of the medium caused by the presence of an acoustic wave:

$$n_y = n_o + n_1 \sin(\omega t - kx) + \frac{\epsilon}{2} \cos(\omega t - kx - \phi)$$
$$n_x = n_o + n_1 \sin(\omega t - kx) - \frac{\epsilon}{2} \cos(\omega t - kx - \phi) \qquad (3\text{-}10)$$

where n_o is the undisturbed index of refraction of the medium, n_1 is the change in the index of refraction due to the scalar pressure variations caused by the acoustic wave. ϵ is the change in the index of refraction due to orientation of the molecules of the medium, and ϕ is the angle by which the birefringence lags the velocity gradient. The following assumptions have been made in obtaining Eqs. 3-10; all second order effects have been neglected, the refractive index change due to the scalar pressure field is assumed to be in phase with the pressure field, and the orientation of the molecules are assumed to occur as in Peterlin's (1950) theory. The signs of the birefringence terms were adjusted

so that if $(\omega t-kx)$ is in the first quadrant, the molecules are urged to orient themselves along the y axis resulting in an increase in the refractive index for the y polarization of the light vector and a corresponding decrease for the x polarization. A further assumption is that the changes in refractive index due to molecular alignment are small so that the contributions to the y and x polarizations can be considered equal. An additional assumption is that the velocity gradient causes the birefringence.

It is possible to combine the sine and cosine terms of Eq. 3-10, using trigonometric identities, yielding the following:

$$n_y = n_o + \sqrt{\left(n_1 + \frac{\epsilon}{2}\sin\phi\right)^2 + \left(\frac{\epsilon}{2}\cos\phi\right)^2}\ \sin\left(\omega t - kx + \delta_y\right) \tag{3-11}$$

$$n_x = n_o + \sqrt{\left(n_1 + \frac{\epsilon}{2}\sin\phi\right)^2 + \left(\frac{\epsilon}{2}\cos\phi\right)^2}\ \sin\left(\omega t - kx + \delta_x\right)$$

and

$$\tan\delta_y = \frac{\cos\phi}{\frac{2n_1}{\epsilon} + \sin\phi}$$

$$\tan\delta_x = \frac{-\cos\phi}{\frac{2n_1}{\epsilon} - \sin\phi}$$

which can be written

$$\delta_y - \delta_x = \frac{\epsilon}{n_1}\cos\phi \tag{3-12}$$

since $\frac{\epsilon}{n_1}$ is small compared to 1.

Riley and Klein (1969) have shown that starting with an index of refraction distribution whose form as that in Eq. 3-11, and solving for the amplitude of the electric vector in the nth diffraction order,

$$E_n = E\,\psi_n(v)\,e^{i(\omega' t - k' z + n(\omega t - kx + \delta) + \gamma)} \qquad (3\text{-}13)$$

where E_n is the magnitude of the electric vector in the nth order, E is the magnitude of electric vector entering the sound field, $\psi_n(v)$ is the amplitude function relating sound amplitude to the magnitude of the diffraction effect (See Appendix 1 for a computer program to evaluate this function). γ is the angle between the real and imaginary parts of the function $\psi_n(v)$ and is a function of v. v is a parameter relating sound pressure amplitude to the change in refractive index, e.g.,

$$v = k' \left(\frac{\partial n}{\partial \rho}\right)_s p\, d \qquad (3\text{-}14)$$

where p is the peak pressure amplitude and $\left(\frac{\partial n}{\partial \rho}\right)_s$ is the adiabatic piezo-optic coefficient. Riley and Klein (1967) give an empirical expression for the piezo-optic coefficient in terms of the index of refraction of the fluid

$$\left(\frac{\partial n}{\partial \rho}\right)_s = \frac{1}{\rho c^2}\left(0.639\, n_o^2 - 0.395\, n_o - .263\right) \qquad (3\text{-}15)$$

where ρ is the density of the fluid.

Ignoring common terms between the x and y components of E gives

$$E_y = \frac{E}{\sqrt{2}} \psi_n(v_y) e^{i(n\delta_y + \gamma_y)}$$

and

$$E_x = \frac{E}{\sqrt{2}} \psi_n(v_x) e^{i(n\delta_x + \gamma_x)} \qquad (3\text{-}16)$$

In the discussion of the Lucas method of measurements, the x and y components were shifted in phase but the amplitudes remained the same. Now, the amplitude variation will also be taken into account. The phase difference between the two vectors is

$$\Delta = n(\delta_y - \delta_x) + (\gamma_y - \gamma_x)$$

and the light leaving the sample cell in the nth order is

$$E_{exit} = \frac{E}{\sqrt{2}} \left(\psi_n^2(v_y) \sin^2(\omega' t + \Delta) + \psi_n^2(v_x) \sin^2 \omega' t \right)^{1/2} \qquad (3\text{-}17)$$

making an angle θ with the x axis such that

$$\tan\theta = \frac{\psi_n(v_y) \sin(\omega' t + \Delta)}{\psi_n(v_x) \sin(\omega' t)} \qquad (3\text{-}18)$$

Substituting Eq. 3-17 into Eq. 3-5 gives the following

$$E_{135°} = \frac{E}{\sqrt{2}} (1 + \tan^2\theta)^{1/2} \psi_n(v_x) \sin\omega' t \cos(135° - \theta)$$

$$E_{135°} = \frac{E}{2} \left(\psi_n(v_y) \sin(\omega' t + \Delta) - \psi_n(v_x) \sin\omega' t \right)$$

Expanding the first sine term and rearranging,

$$E_{135°} = \frac{E}{2} \left[\psi_n^2(v_y) \sin^2\Delta + \left(\psi_n(v_y) \cos\Delta - \psi_n(v_x) \right)^2 \right]^{1/2} \sin(\omega' t + A)$$

where $\tan \mathcal{L} = \dfrac{\psi_n(v_y) \sin \Delta}{\psi_n(v_y) \cos \Delta - \psi_n(v_x)}$ (3-19)

Completing the square yields

$$E_{135^\circ} = \frac{E}{2}\left[\left(\psi_n(v_y) - \psi_n(v_x)\right)^2 + 2\psi_n(v_y)\psi_n(v_x)\left(1 - \cos\Delta\right)\right]^{1/2} \sin(\omega' t + \mathcal{L}) \quad (3\text{-}20)$$

The v parameters are proportional to the corresponding quantities under the radical sign in Eqs. 3-11.

$$v_y = \left(n_1 + \frac{\epsilon \sin\phi}{2} + \frac{\epsilon^2}{8n_1}\right) k' d$$

$$v_x = \left(n_1 - \frac{\epsilon \sin\phi}{2} + \frac{\epsilon^2}{8n_1}\right) k' d$$

Let

$$v = n_1 k' d$$

and thus,

$$\frac{v_y - v_x}{v} = \frac{\Delta v}{v} = \frac{\epsilon}{n_1 \sin\phi} \quad (3\text{-}21)$$

Squaring Eq. 3-20, to obtain the photocell response,

$$\frac{I_n}{I_0} = \frac{1}{4}\left[\left(\psi_n(v_y) - \psi_n(v_x)\right)^2 + 2\psi_n(v_y)\psi_n(v_x)\left(1 - \cos\Delta\right)\right] \quad (3\text{-}22)$$

The sound pressure calibration can be accomplished by using the arrangement shown in Figure 3-4 with the analyzer set at 0° to the x axis. This provides the parameter v as a function of the voltage applied to the piezoelectric transducer. In Eq. 3-21, ϕ is independent of v at a given frequency as is the ratio ϵ/n_1, since both ϵ and n_1 are proportional to v (using the assumption of Peterlin's (1950)

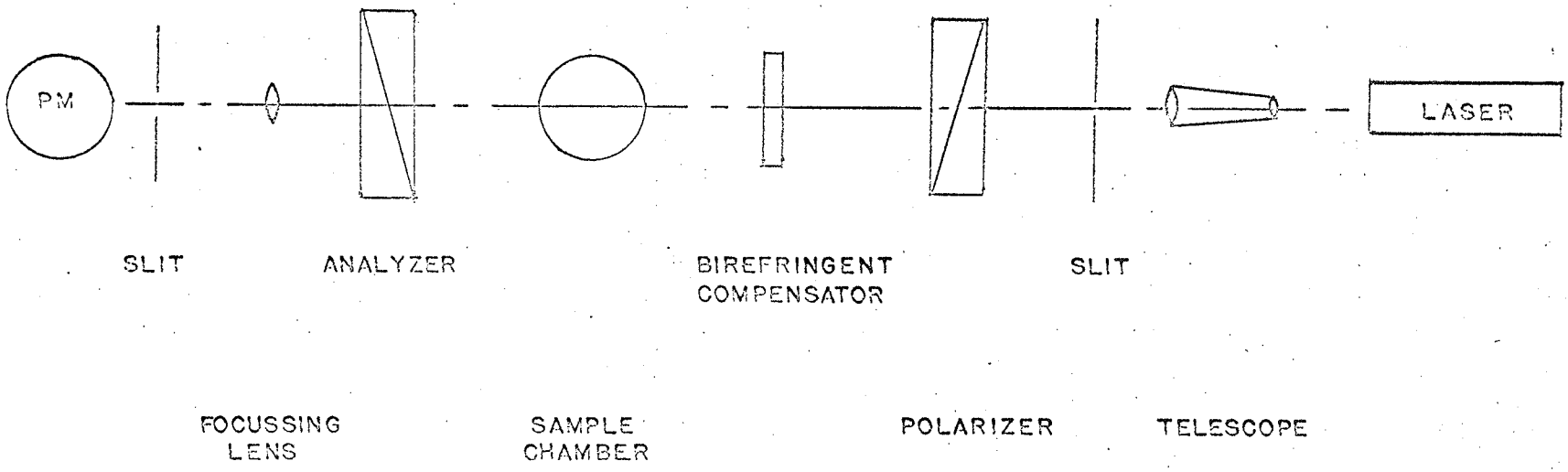

Figure 3-4. Optical arrangement for investigation of birefringence in various diffraction orders.

model). Hence $(\sigma_y - \sigma_x)/\sigma$ is also independent of σ. Similarly, $(\delta_y - \delta_x)$ is independent of σ as seen in Eq. 3-12. To obtain ϵ and ϕ, the light intensity is measured in various diffraction orders and Eq. 3-22 is solved twice to obtain $(\delta_y - \delta_x)$ and $(\sigma_y - \sigma_x)/\sigma$. In the zero order, however, Eq. 3-22 can only be used to find $(\sigma_y - \sigma_x)/\sigma$. The function $\psi_n(\sigma)$ is calculated by numerical methods to obtain not only the magnitude but also the phase angle η (the program is given in Appendix 1). Then

$$\tan \phi = \frac{(\sigma_y - \sigma_x)}{\sigma (\delta_y - \delta_x)} \tag{3-23}$$

and

$$\epsilon = \frac{\eta_1 \, (\delta_y - \delta_x)}{\cos \phi} \tag{3-24}$$

A second method of measuring birefringence in the various diffraction orders (Riley and Klein (1969)) takes advantage of the fact that the phase differences and amplitude changes measured are independent of time. The phase difference Δ can be compensated for by a Babinet-Soleil compensator and the ratio of the two amplitudes $\psi_n(\sigma_y)/\psi_n(\sigma_x)$ can be measured by rotating the analyzer prism. The procedure is exactly the same as that required to analyze elliptically polarized light. The photocell output is observed and the two adjustments made until the light exiting from the analyzer prism is extinguished. Then Δ is just the negative of the value of the compensator setting and,

if β is the rotation of the analyzer, then

$$\psi_n(\nu_y) = \tan\beta \;\; \psi_n(\nu_x) \tag{3-25}$$

where β is measured with respect to the x axis and is considered positive if the rotation is toward the y axis. Evaluation of the data is straight forward, i.e., $\psi_n(\bar{\nu}_x)$ and η_x are calculated from the experimental value of $\bar{\nu}_x$. $\bar{\nu}_y$ is determined from $\psi_n(\bar{\nu}_y)$ by taking the inverse of the function (a trial and error procedure). η_y is then determined and

$$\delta_y - \delta_x = \Delta - (\eta_y - \eta_x) \tag{3-26}$$

The birefringence information is then evaluated using Eqs. 3-23 and 3-24.

In order to get $\delta_y - \delta_x$ and $(\bar{\nu}_y - \bar{\nu}_x)/\bar{\nu}$ from Eq. 3-22, the incident light intensity I_o must remain constant so that the ratio of I_n/I_o can be calculated. However, the laser light source used did not have sufficient long term stability to get accurate results. Further, variations in the optical path due to manual adjustments or thermal gradients can cause the overall light transmission to be different from time to time. The method proposed by Riley and Klein (1969) eliminates the incident intensity as a parameter and $\delta_y - \delta_x$ and $\bar{\nu}_y - \bar{\nu}_x$ can be calculated from Eqs. 3-25 and 3-26. However, the sensitivity is limited to values of about 0.01 for both $\delta_y - \delta_x$ and $\bar{\nu}_y - \bar{\nu}_x/\bar{\nu}$.

A method which has a sensitivity of about .001 and minimizes the effect of varying incident light intensity can be obtained by measuring the photocurrent for two orientations of the analyzing prism. For the crossed position, Eq. 3-22 can be used. However, consider the situation wherein the analyzer is rotated a small angle χ. Then, the vector leaving the analyzer is given as

$$E_{(135^\circ+\chi)} = E_{exit} \cos(135^\circ + \chi - \theta) \tag{3-27}$$

Substituting Eq. 3-17 into 3-27 gives the following:

$$E_{(135^\circ+\chi)} = \frac{E}{\sqrt{2}} \psi_n(v_x) \left[1 + \tan^2\theta\right]^{1/2} \sin\omega' t \cos(135^\circ + \chi - \theta)$$

where $\tan\theta$ is given by Eq. 3-18.

$$E_{135^\circ+\chi} = \frac{E}{\sqrt{2}} \psi_n(v_x) \sin\omega' t \left[\cos(135^\circ+\chi) + (\sin(135^\circ+\chi)\tan\theta\right]$$

$$E_{135^\circ+\chi} = \frac{E}{\sqrt{2}} \left[\psi_n(v_x) \sin\omega' t \cos(135^\circ+\chi) + \psi_n(v_y) \sin(\omega' t + \Delta) \sin(135^\circ+\chi)\right]$$

Dividing by $\sin(135^\circ + \chi)$ and expanding the second sine term we get

$$E_{135^\circ+\chi} = \frac{E}{\sqrt{2}} \cos(45^\circ+\chi) \left[\left\{\psi_n(v_y)\cos\Delta - \psi_n(v_x)\tan(45^\circ+\chi)\right\}^2 + \psi_n^2(v_y)\sin^2\Delta\right]^{1/2} \sin(\omega' t + \Lambda)$$

where

$$\tan\Lambda = \frac{\psi_n(v_y)\sin\Delta}{\psi_n(v_y)\cos\Delta - \psi_n(v_x)\tan(45^\circ+\chi)}$$

Completing the square yields

$$H = \psi_n(v_x)\tan(45^\circ + \chi)$$

$$J = 1 - \cos\Delta$$

$$E_{135^\circ+\chi} = \frac{E\cos(45^\circ+\chi)}{\sqrt{2}}\left[\left\{\psi_n(v_y) - H\right\}^2 + 2\psi_n(v_y)\cdot H\cdot J\right]^{1/2} \qquad (3\text{-}28)$$

If $\chi = 0$, then Eq. 3-28 reduces to Eq. 3-20. The ratio of the photocell response for $\chi = 0$ to the response for $\chi \neq 0$ is

$$\frac{I_n}{I_{n\chi}} = \frac{\left[\left\{\psi_n(v_y) - \psi_n(v_x)\right\}^2 + 2\psi_n(v_y)\psi_n(v_x)\cdot J\right]}{2\cos(45^\circ+\chi)\left[\left\{\psi_n(v_y) - H\right\}^2 + 2\psi_n(v_y)\cdot H\cdot J\right]} \qquad (3\text{-}29)$$

The incident intensity does not appear in Eq. 3-29 so that the light source need only be stable long enough to obtain 2 photocell readings. Also, χ can have any value up to $\pm 45^\circ$, which would be equivalent to measuring just I_n in the nth diffraction order. A χ of 0.5 degrees was chosen to obtain current ratios of approximately 10^4 in the zero order. The quantity $(v_y - v_x)/v$ is obtained from measurements in the zero order using Eq. 3-29 and is used in the other orders to obtain $(\delta_y - \delta_x)$. ε and ϕ may then be found using Eqs. 3-23 and 3-24. Eq. 4-7 is used to evaluate the experimental data since it takes into account the leakage of light through crossed polarizing prisms.

IV. LIMITATIONS ON SENSITIVITY

The photomultiplier tube used as a light detector has two fundamental limitations. One is the shot noise current i_{sn} which limits the preciseness with which the anode current can be measured. The other is the dark current i_d, i.e., the anode current present when no light impinges on the photocathode. This current limits the smallest light level which can be detected. Yariv (1971) states that the shot noise current is

$$\overline{i_{sn}^2} = 2Ge(\bar{i}_c + i_d)B \qquad (4\text{-}1)$$

where G is the current gain in the photomultiplier, e is the charge on an electron, $\bar{i}_c$ is the average value of the output current due to light impinging on the photocathode, and B is the bandwidth of the detection circuit. The manufacturer's data sheet shows a typical value of G is about 2×10^6. The measured value of dark current is about 2 na. Assuming that no light falls on the phototube and that the bandwidth of the detection circuit is about 1 kHz, then from Eq. 4-1 the shot noise current is about 1 na.

If an optical signal impinges on the phototube, then not only will the anode current increase, but, according to Eq. 4-1, the noise level will increase too. If the signal consists of a large, steady background with a small varying component, then the shot noise generated will swamp out the small variations. This fact makes it necessary to minimize

the amount of stray light falling on the tube when attempting to measure acoustically induced birefringence. Some of the steps employed to minimize stray light are turning off room lights, removing or covering all pilot lights, and use of an aluminum foil baffle around the phototube and the focusing lens. By restricting the bandwidth of the output circuit to about 8 Hz, the dark current could be measured and was found to be the same with the slit open as with the slit closed. This observation was made with the laser off. When the laser is turned on, the steady output current increased to about 5 na for slit openings corresponding to those used during data taking. This increase was due to light leaking through the crossed polarizing prisms. This problem is discussed in detail below.

For signals that are large compared to the dark current, the shot noise increases as the square root of the signal level and hence the signal to noise ratio is higher for larger signals. The noise level can be traded off against the bandwidth of the measuring circuit so that when the signals produced by the acoustically induced birefringence are large, short acoustic pulses may be used. For example, when castor oil is used as the sample fluid, signals as large as 1 μa can be obtained. With a bandwidth of 2 kHz, the shot noise component, as calculated from Eq. 4-1, is about 10 na so acoustic pulses as short as 1 ms could be used. For small signals, longer acoustic pulses were necessary to maintain the low noise levels.

The range over which the acoustic pulse width can be varied is limited. Pulses could not be made much shorter than 1 ms due to rise time limitations on the tuned circuits in the rf amplifier system. On the other hand, although very long pulses could be generated, self heating of the sample fluid resulted from pulses longer than about 0.5 sec. For this reason, pulses longer than about 0.1 sec were not used, except for very low intensity pulses. However, with a pulse width of 0.1 sec and a detector bandwidth of 8 Hz, the shot noise level (from Eq. 4-1) is about 0.1 na. When this is compared to the leakage current of 5 na due to the finite extinction ratio of the prisms, it can be seen that the noise level of the phototube does not limit the maximum sensitivity of the system.

If the signal level were to fall below the dark current of the phototube, three methods exist for measuring the signal level. First, the phototube can be replaced with another device which has a greater sensitivity to the laser wavelength. For example, the 1P28 used here could be replaced with a much more expensive RCA 7625 photomultiplier tube which has 50 times greater sensitivity. Another possibility is to use a more intense laser. Although a 1 mw laser was used here, 50 mw lasers are currently available. A third possibility, although not as effective as the previous methods, is to work at higher sound intensities. The factors which limit the maximum intensity used are heating

of the sample, cavitation, and the appearance of the second order effects. In the present work, the limiting factor was heating of the sample due to the high acoustic absorption of the samples used.

The factor most responsible for the inability of the system to distinguish very small signals generated by acoustically induced birefringence in the sample fluid is the light which leaks through the crossed polarizers. This steady light was adjusted by means of a slit on the front of the phototube housing so that the anode current was about 5 na. It must be emphasized that the 5 na current is set by the experimenter and, even if the above methods of increasing the detector sensitivity were employed, it would be necessary to reduce the slit width to bring the background level back to about 5 na. This level was chosen to bring the currents generated at different polarizer orientations within the dynamic range of the oscilloscope and yet still be larger than the dark current of the phototube.

By definition, the ratio of the light transmitted by a pair of aligned polarizers to the light transmitted by the same polarizers in the crossed position is called the extinction ratio. The polarizers used in these experiments had an extinction ratio of about 10^7 to 1. With a 1 mw laser and a phototube sensitivity of about 5 a/mw, the expected background level would be about 500 na. However, with the beam expanding telescope and the height limiting slit in

in place, the measured background was about 30 na with the phototube slit wide open. As the laser aged, its output decreased, so that it was necessary to open the slit wider to maintain the 5 na background.

The primary mode of detection is observing a change in the output current of the phototube when an acoustic pulse interrupts the light beam. In the previous chapters, the change in current is presumed to be due to acoustically induced birefringence. However, the leakage through the prisms follows the same optical path as the main beam, so it is also diffracted, causing a change in the phototube current. The cause of the finite extinction ratio is not known. If it were, the sensitivity limit would be decreased by about a factor of ten. The sensitivity would then be limited by the difficulty in observing the difference between two numbers of almost equal magnitude.

A number of items were considered in an attempt to determine the cause of the finite extinction ratio. Even if a means were not found to increase the ratio, at least a proper correction could be found to account for the presence of the leakage. One possibility is that strain birefringence in the prisms would cause a relative phase shift in the components of the polarized light. This hypothesis was checked by means of a birefringent compensator. Adjusting the compensator to obtain a null in the output current did not improve the extinction ratio. In addition, it did not

degrade the extinction ratio, so its use in compensating for strain birefringence does not degrade the system performance.

By use of an aperture placed immediately after the analyzing prism, light rays travelling off axis to the laser beam could be eliminated. However, this procedure had no effect on the extinction ratio. This meant that the light comprising the leakage light had to be co-axial with the laser beam. A check with a third polarizer placed just after the analyzing prism showed that the leakage light was polarized in the easy direction implying that stacking several polarizers would not improve the extinction ratio. Also, inserting a polarizer just after the laser, so that the light entering the system was already polarized, had no effect. The prisms were also rotated on their vertical axis to establish that the extinction ratio was independent of the alignment for angles less than about 10^{o}.

The presence of small scratches on the prisms could cause some depolarization due to scattering. Moving the relative position of the light beam in the prism aperture should cause the number of scratches present in the beam to vary and hence change the extinction ratio. The ratio did not change during movement of either prism.

When the sample cell is placed in the system, the observed extinction ratio is reduced. The degradation is due to strain birefringence, however, and can be compensated for by the mica compensator. If the windows are inserted

too tightly, the strain becomes non-linear and cannot be completely compensated. Water placed in sample cell produces no change in the extinction ratio while oleic acid in the sample cell produces a definite degradation to the ratio to about 2×10^6. The degradation seems to be due to scattering of the light beam and the resulting partial depolarization. Diluting the sample in a suitable solvent reduces the scattering, as well as reducing the birefringence by much more than a proportionate amount.

For liquids that scatter an appreciable amount of light, the system described in the previous chapter is sufficiently sensitive to measure any birefringence not masked by the scattered light. For liquids that do not scatter light, the items that need the most improvement are the polarizing prisms. Suppliers of optical devices report that although the extinction ratio may be guaranteed to be better than 10^5 to 1 for high quality prisms, it is unlikely that a prism set would exhibit a ratio greater than 10^8 to 1. Hence, the prisms used in the current system are near the limit of available extinction ratios.

In order to obtain birefringence data when the signal is the same order of magnitude as the background leakage current, a correction based on the definition of extinction ratio was developed. Let the square root of the extinction

ratio be Z. Then, if the incident electric vector is E, the electric vector leaving the prism has a magnitude E/Z. This idea can be incorporated into Eq. 3-5 so that the light leaving the analyzer can be written

$$E_{135^\circ} = E_{exit}\left[\cos(135^\circ - \theta) + \frac{1}{Z}\right] \tag{4-2}$$

If Eqs. 3-17 and 3-18 are now substituted into 4-2, we get, after some calculation,

$$E_{135^\circ} = \frac{E}{2} e^{\delta}\left[\left\{C - D(1-\sqrt{2}B)\right\}^2 + 2CD(1-\cos\Delta)(1-\sqrt{2}B)\right]^{1/2} \tag{4-3}$$

Repeating these steps for the case when the analyzer is rotated by a small angle χ, we obtain for Eq. 3-27

$$E_{135^\circ+\chi} = E_{exit}\left[\cos(135^\circ+\chi-\theta) + \frac{\cos\chi}{Z}\right] \tag{4-4}$$

with the result

$$E_{135^\circ+\chi} = E e^{\delta}\frac{A}{\sqrt{2}}\left[\left\{C - D\left(\tan(45^\circ+\chi) - \frac{B}{A}\right)\right\}^2 + 2CD(1-\cos\Delta)\cdot \left(\tan(45^\circ+\chi) - \frac{B}{A}\right)\right]^{1/2} \tag{4-5}$$

with $A = \cos(45^\circ+\chi)$ $\qquad C = \psi_n(v_y)$

$B = \frac{1}{Z\cos\theta}$ $\qquad D = \psi_n(v_x)$

The ratio of the intensity in the nth diffraction order for $\chi = 0$ to the intensity when $\chi \neq 0$ is then given by

$$\frac{I_n}{I_{nk}} = \frac{1}{\sqrt{2}\,A} \cdot \frac{\left[\left\{C - D\left(1-\sqrt{2}\,B\right)\right\}^2 + 2CD\left(1-\cos\Delta\right)\left(1-\sqrt{2}\,B\right)\right]}{\left[\left\{C - D\left(\tan\left(45°+x\right) - \frac{B}{A}\right)\right\}^2 + 2CD\left(1-\cos\Delta\right)\left(\tan\left(45°+x\right) - \frac{B}{A}\right)\right]} \qquad (4-7)$$

Eq. 4-7 can be used to find $\sigma_y - \sigma_x$ and $\sqrt{\sigma_y} - \sqrt{\sigma_x}$ by trial and error. However, the measured currents must have the dark current and any undiffracted background currents subtracted from them before forming the current ratio.

V. EQUIPMENT

The instrumentation employed in the experimental study consists of pulse and synchronizing generators, an rf generator and power amplifier, an electro-acoustic transducer and sample chamber, temperature control apparatus, and the optical system. Each of the five stages are discussed separately.

The pulse and synchronizing generators consist of a group of Tektronix model 160 series components shown in Fig. 5-1. A type 160A power supply furnishes power for all units. The first model 162 waveform generator provides all the necessary synchronizing functions. With the operating mode switch in the triggered position with a 6.3 volt, 60 Hz signal derived from a filament transformer (Stancor P6466) connected to the trigger input terminal, the synchronizing pulses available from the model 162 are synchronized to the power line. This is an advantage since the 120 cycle ripple from the power supply to the rf power amplifier causes a variation in rf amplitude. By synchronizing the pulse and the oscilloscope sweep to the power line, an acoustic pulse is generated whose amplitude is free from rapid fluctuations. When medium length pulses (0.017 sec. to 1 sec.) are employed, the waveform duration is set to provide properly spaced synchronizing pulses. For example, if 0.02 sec. pulses are needed at 0.1 sec. intervals, the waveform duration is set to 0.09 sec. so that only every 6th

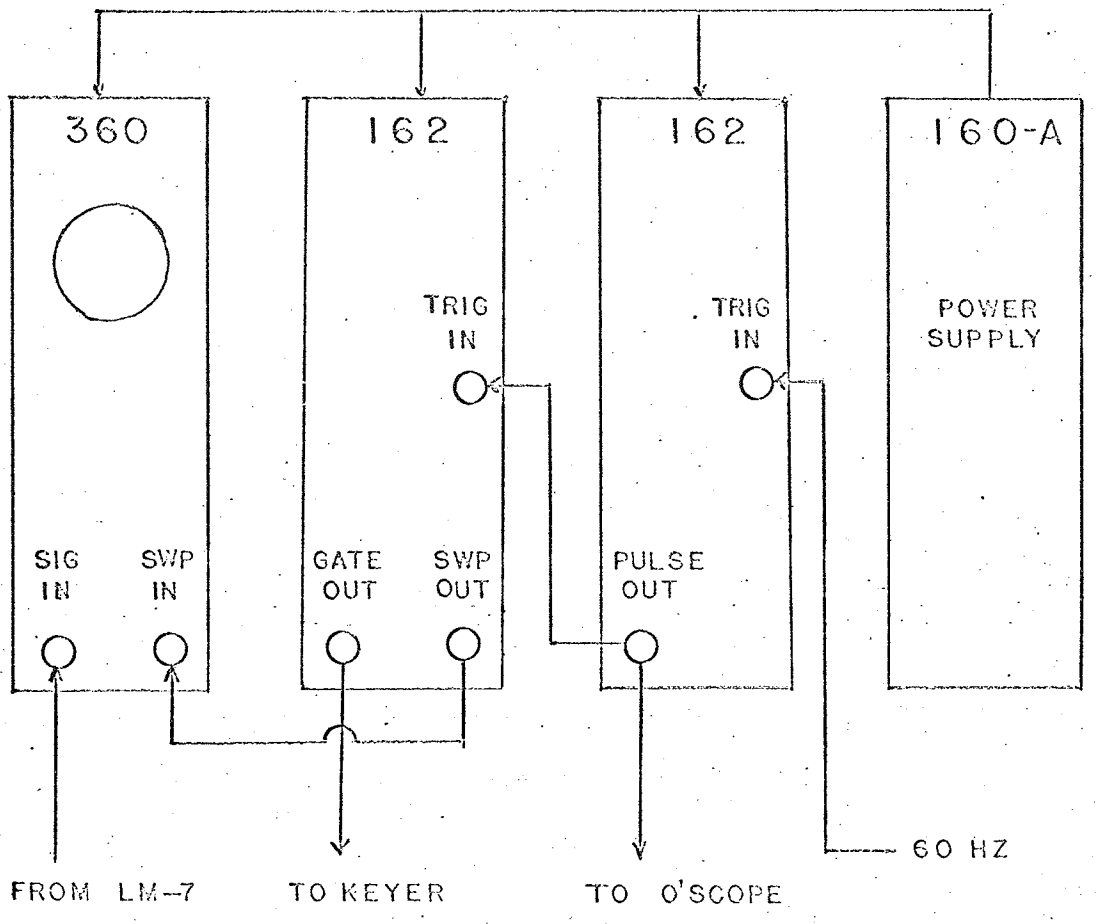

Figure 5-1. Pulse and synchronizing generator wiring diagram.

power line pulse results in a synchronizing pulse being generated.

The second waveform generator is used to provide a pulse to gate the rf generator. The amplitude of the gating pulse is fixed by the equipment, but the gate width can be varied from 0.1 ms to 10 sec. Trigger pulses to drive this unit are obtained from the first unit. Care must be taken during experiments so that the time between trigger pulses are always greater than the gate time. When high power levels are used, the ratio of trigger interval to gate interval is never less than 10 and for very low power levels the ratio is never less than 2. The reason for the high ratios is to keep the total power dissipation in the test fluid as low as possible.

A Ferris Model 22-c signal generator is used as a source for the nominal frequencies of 1, 3, 5, 7, and 9 MHz. The precise frequency is determined at the time data was being taken, since efficient conversion of electrical energy to acoustical energy occurs at the resonant frequency and is influenced by the nature and temperature of the fluid in the sample cell. The frequency drift of the signal generator is less than 1 part in 10^4 per hr. after about 2 hrs. warmup.

The frequency of operation is adjusted for maximum acoustical power transfer to the sample and is then determined with a calibrator unit-model LM-7 aircraft frequency measuring device. The accuracy of this unit was 0.05% when compared with a Systron-Donner Model 1037 electronic

frequency counter. The calibrator is permanently connected to the signal generator since loading its output causes the signal generator to shift frequency.

A Tektronix model 360 indicator is used as a detector of the zero beat between the rf signal generator and the calibrator's internal oscillator. Since the LM-7 is a heterodyne type of frequency meter, it is necessary to know the approximate value of the frequency so that the appropriate harmonics of the calibrator oscillator could be chosen. This is easily accomplished by utilizing the dial of the rf generator which can be read to about 2%.

The output of the signal generator is fed into the chassis housing the keying stage, the preamplifier stages and the driver stage. The keying stage (Fig. 5-4) functions as an electronic switch. The rf signal is applied to the cathode and the gate pulse is applied to the grid of the keyer tube. A 22.5 volt battery is used to keep the tube biased in the cutoff state. Hence under quiescent conditions, the tube will not amplify the rf signal. When a gate pulse is applied, the bias on the tube changes and the tube amplifies in the grounded grid mode. Buffering for the signal generator is provided by a cathode follower and an emitter follower. As the keying stage is turned on and off, a large variation in input impedance occurs. The frequency of the rf generator is measured during the quiescent state but must be known during the rf pulse. The buffer stage

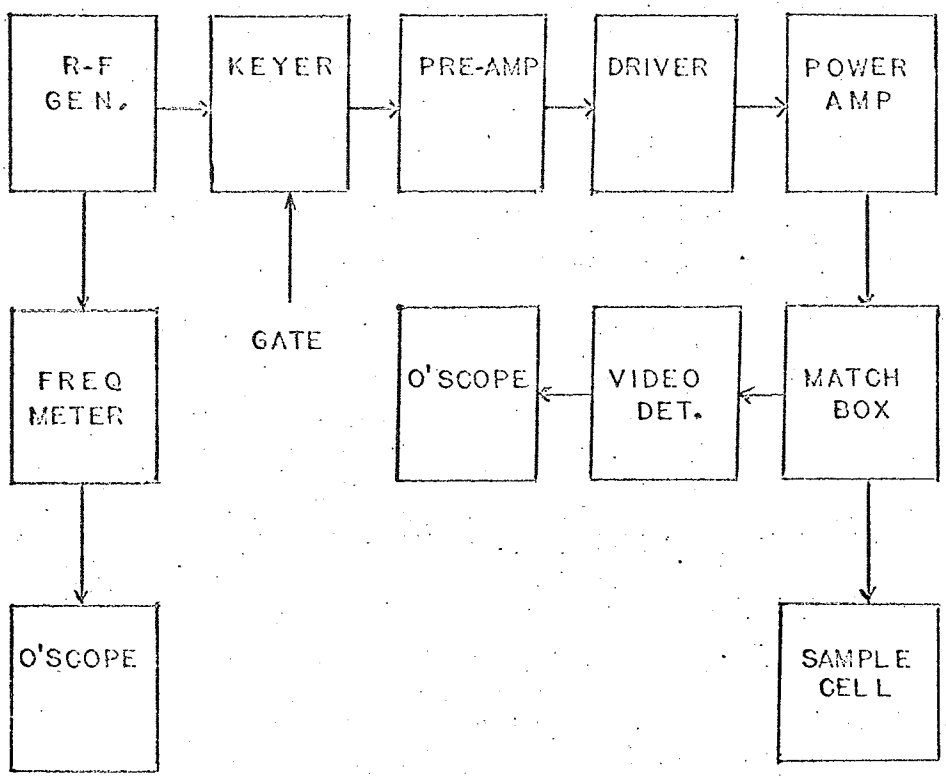

Figure 5-2. Path of flow for the rf signal.

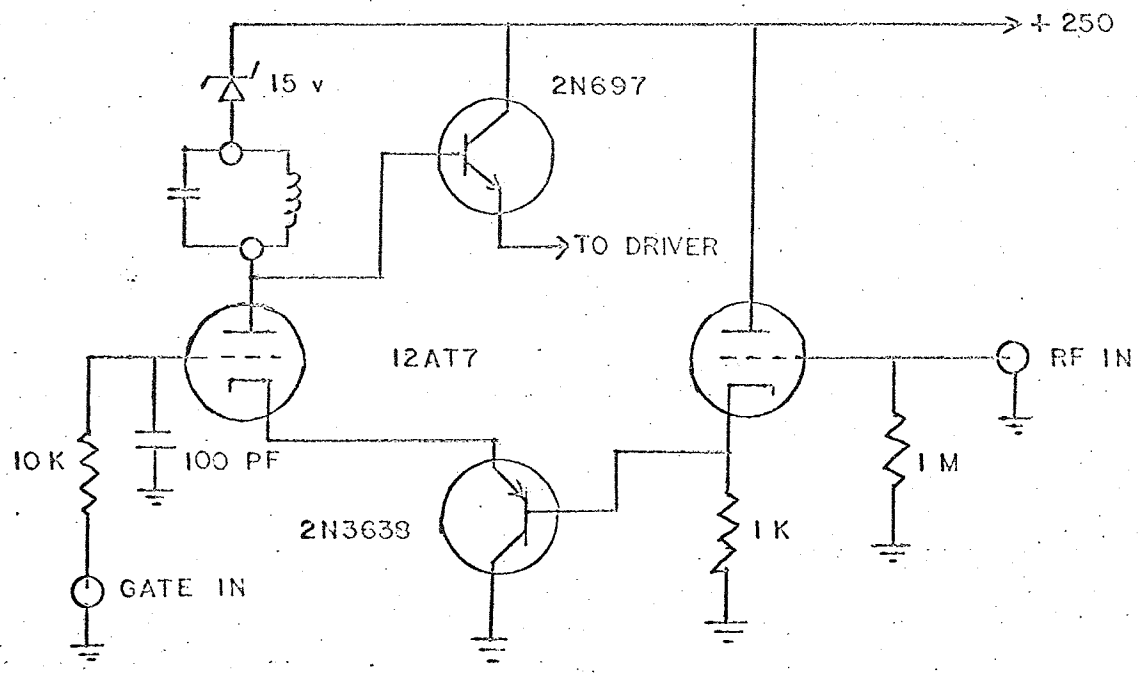

Figure 5-3. Schematic diagram of the buffer stage and keying stage.

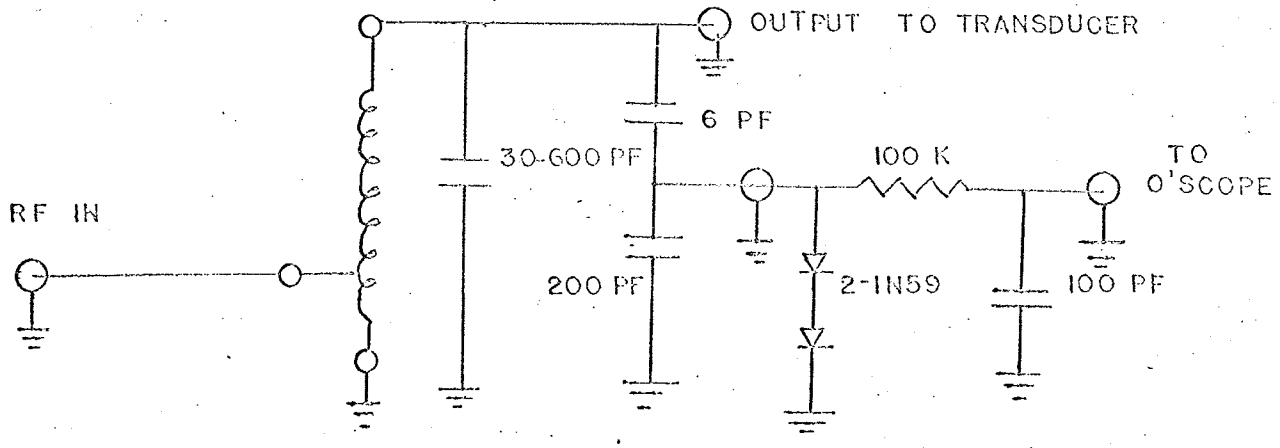

Figure 5-4. Network used to match the transducer to the 50 ohm output of the final amp.

eliminates the loading change, and hence, the frequency shift that would occur without it.

The driver stage is a standard tuned grid-tuned plate rf amplifier capable of delivering 30 watts to a 50 ohm load at 1 MHz. At 9 MHz, the driver can deliver only about 3 watts. The final output stage is also a tuned grid-tuned plate amplifier. The power supply for the final stage uses mercury arc rectifiers to obtain a high voltage and a high current capability. A pi L - C filter is used to reduce the ripple. However, a small amount of ripple remains, and, in order to obtain a stable pattern on the oscilloscope, it is necessary to synchronize the pulses to the power line.

The rf voltage is fed to a matching network, basically a tuned autotransformer, (Figure 5-4) to obtain maximum power transfer to the electro-acoustic transducer. In parallel with the tuning capacitor is a voltage divider arrangement which makes it possible to obtain a voltage proportional to that applied to the transducer, independent of tuning the main tuning capacitor and at a level low enough to prevent damage to the oscilloscope.

The transducer is an x-cut quartz plate having a nominal resonant frequency of 1 MHz. The mounting arrangement shown in Fig. 5-5, retains the transducer by clamping at the edge. The front is exposed directly to the sample fluid while the back is exposed to air. The edge of the transducer is

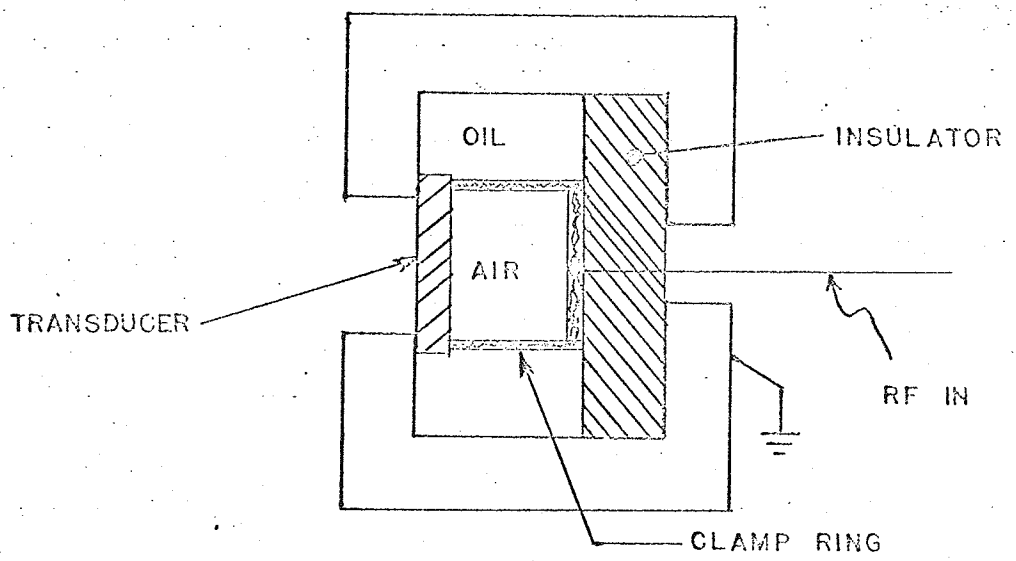

Figure 5-5. Schematic of the transducer mounting.

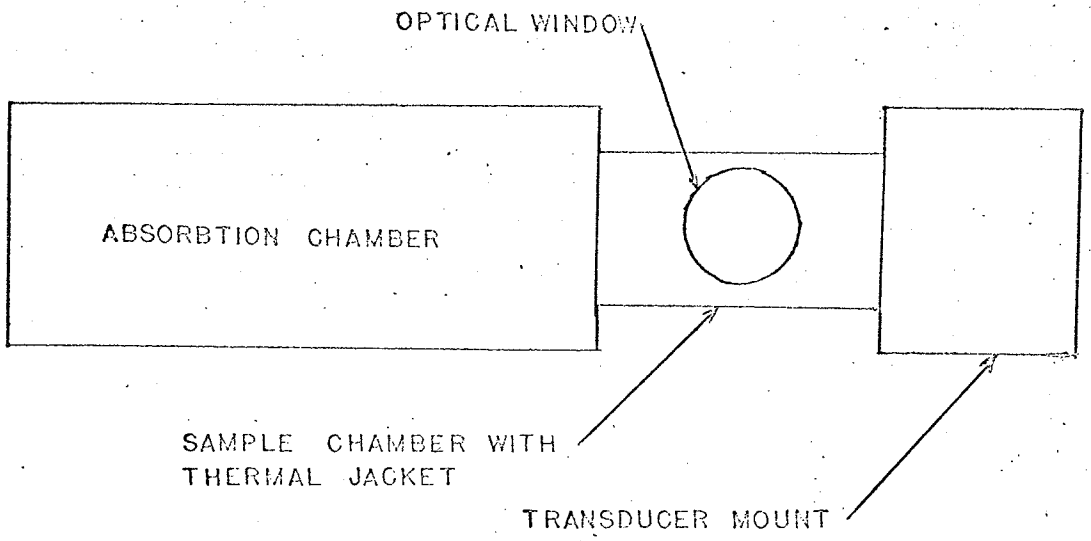

Figure 5-6. Construction of the sample chamber.

enclosed by a chamber containing Dow-Corning type 720 silicon oil whose purpose is to increase the dielectric strength about the edge, since arcing will occur around the edge in air which has a lower dielectric breakdown than the oil.

The sample chamber is sandwiched between the acoustic absorption chamber and the transducer (see Fig. 5-6). The walls of the chamber are hollow permitting fluid to be pumped through in order to maintain a pre-determined constant temperature. A 5/16" diameter hole in the top of the chamber permits filling and withdrawing of samples and insertion of the temperature control probe during the experiments. Two 1" diameter holes bored into the sides of the chamber provide for mounting the optical windows. The holes are threaded so that the window and a teflon gasket may be secured in place by means of a threaded ring (see Fig. 5-7). When assembled, the chamber has a capacity of about 20 cc.

The windows were formed from No. 1 coverslip glass, 25 mm in diameter. The use of thinner windows resulted in bowing of the glass coverslips, due to internal pressure of the sample fluid, which acted like a fluid filled lens disturbing the optical beam and making the diffraction pattern difficult to obtain. On the other hand, the use of thicker glass for the windows resulted in the appearance of excessive strain birefringence which could not be compensated. Even with the No. 1 glass employed, excessive tightening of the threaded ring would produce excessive strain birefringence.

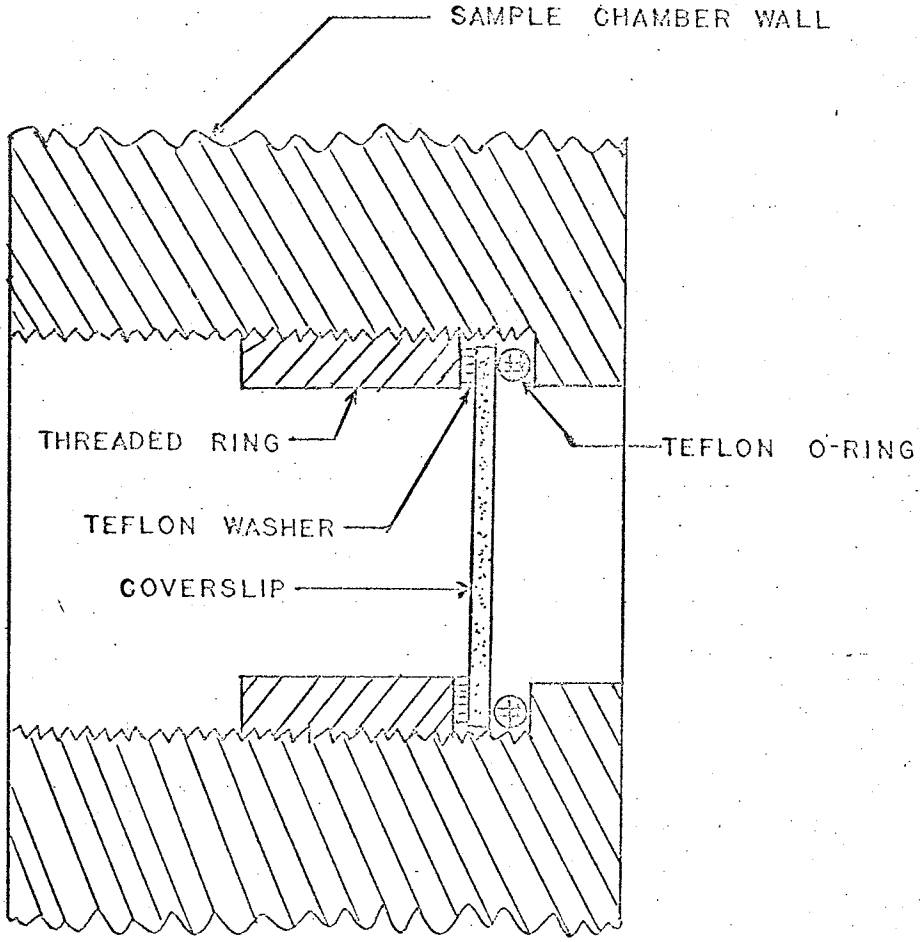

Figure 5-7. Mounting of the optical windows.

The acoustic absorption chamber is filled with the sample fluid to assure that a traveling wave field was maintained. The effectiveness of the chamber could be tested readily by observing the sharpness of the nulls obtained when the intensity of light in a particular diffraction order was plotted against acoustic pressure. At 3 MHz, less than 1% of the incident energy was reflected into the sample chamber. At higher frequencies the reflection was very much less owing to the greater absorption in the sample fluid. A neoprene gasket sealed the chamber assuring that the sample did not leak outside the chamber.

The temperature control system consists of a main water tank and circulating pump, an auxiliary cold water tank and circulating pump, and an electric heater (see Fig. 5-8). The main water bath tank is heated or cooled by means of the electric heating element or by the cold water circulating through a copper coil. The power to the heating element and to the cold water circulating pump is controlled by a Cenco electronic relay. The relay is operated by a mercury bulb temperature control element in which the mercury would rise and fall in a capillary tube making or breaking electrical contact with a wire inserted in the capillary. Control is sufficiently sensitive so that the main bath could be maintained at constant temperature to within $\pm$ 0.05^{o}C. A Cole-Palmer proportional controller is used to control the circulating pump delivering water

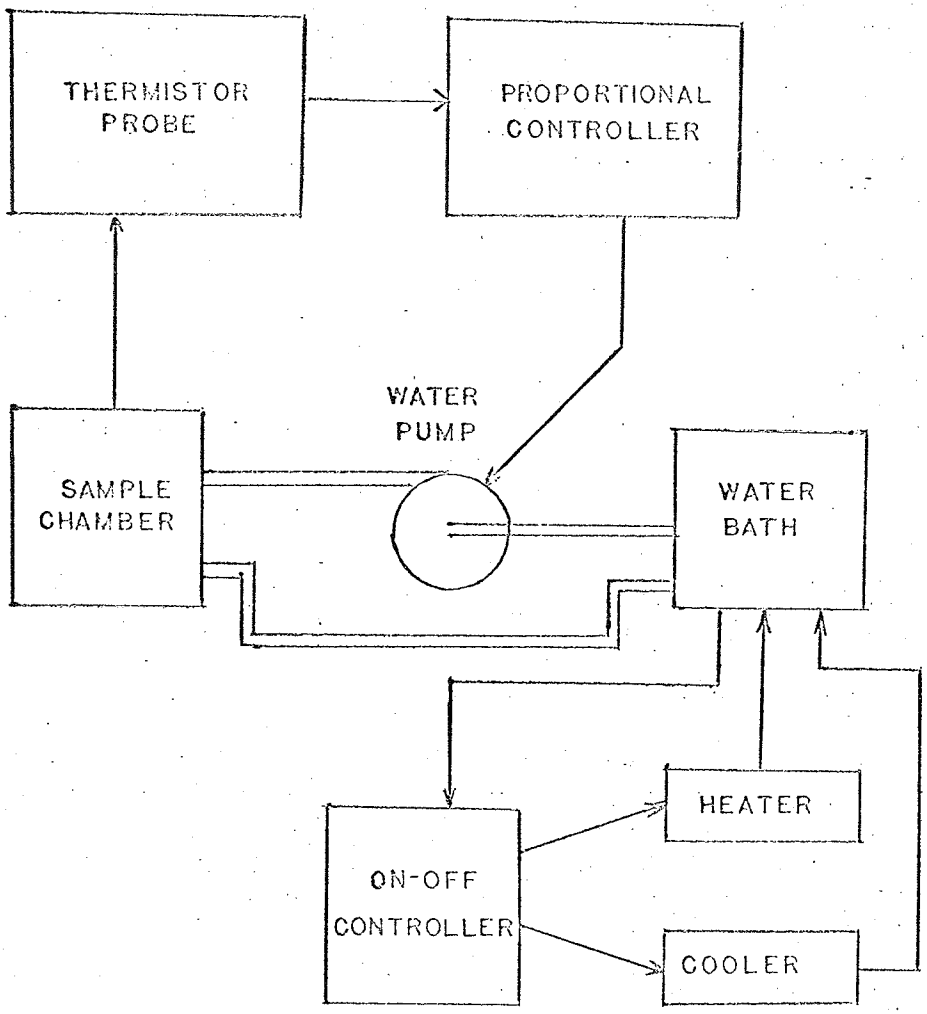

Figure 5-8. Temperature control system.

from the main bath to the sample chamber when temperatures above room temperature are used. The main bath is approximately 1°C warmer than the desired temperature. A temperature sensitive resistor is placed in the sample chamber out of the path of the acoustic wave. Thus, as the temperature in the chamber varies, the resistance changes resulting in a change in the speed of the circulating pump. The auxiliary coolant pump is operated in an on-off manner, while on the other hand the main circulating pump runs continuously, with the pumping rate varying proportionately to offset thermal losses to the surroundings. It is estimated that the temperature variation in the sample chamber was no more than 0.5°C. Better control of the sample chamber temperature could not be obtained since there is considerable heat loss to the surroundings. The optical windows, the acoustic transducer and the absorption chamber are not thermally jacketed and hence represents paths for heat loss that could not be controlled by fluid flowing in the sample chamber jacket above.

The optical system is mounted on a 2 m Gaertner double rod optical bench supported at both ends and at the center. All the components are mounted on carriages designed for use with this bench, and can be positioned along the axis of the bench and secured in place at the desired position. Carriages with transverse motion attachments are used for the laser, the sample chamber mounting, and the photomultiplier

housing. These items are attached firmly to 19 mm rods which fit the carriages. All other components except the optical lenses are mounted on 13 mm rods and adapters are used to fit them to the carriages. The lenses are mounted in Gaertner lens holders which in turn are mounted on 9 mm rods and adapters are used to fit them to the 19 mm holes in the carriages. Fig. 3-4 shows the optical arrangement.

A Spectra-Physics model 130-B helium-neon laser is used as the light source and is capable of emitting 1 mw of monochromatic polarized conherent light at 632.8 nm wavelength. The output amplitude has less than 2% peak to peak noise at high frequencies (greater than 1 Hz). On the other hand, the long term stability is poor. The amplitude could often fall by 40% after 8 hours continuous use although it would recover overnight.

The laser beam is too narrow to use directly, thus a telescope is used to expand the beam approximately 3 times in diamter. The telescope consists of two double convex lenses, one 29 mm f. l. and the other 90 mm f. l., the beam enters the shorter focal length lens and exits from the longer. The telescope alignment procedure is started by marking the spot on the wall opposite the optical bench where the undisturbed laser beam falls. Then, place a target at the approximate position where the focal point of the short f. l. lens should be on the optical bench and marking on it the position of the laser beam, the short lens is mounted

in its holder and oriented so the beam is focused at the center of the target mark. The target is removed and the long f. l. lens is mounted and oriented so that the center of the beam falls on the wall marking and so the diameter of the beam remained constant along its entire length.

A slit is placed in front of the telescope to limit the height of the expanded laser beam. The slit is opened just enough to minimize the diffraction of the beam (about 0.2 to 0.5 mm). The polarizing prisms used are Glan-Thompson prisms with 5.5 mm clear aperture. When crossed, the extinction ratio is about 2×10^6. When the electric vector entered the prisms parallel to the diagonal of the face, it is either extinguished or maximally transmitted. Light reflecting from most non-metallic surfaces is almost completely polarized with the electric vector perpendicular to the plane of incidence when the indicent angle satisfies Brewster's Law:

$$\tan \theta_i = n \qquad (5\text{-}1)$$

where n is the refractive index of the surface and θ_i is the angle of incidence. By examining reflected light through the prism, the principle axis can be determined when the reflection disappears. (By a similar procedure, it was found that the laser emitted light whose electric vector was horizontal.) The 45° direction is established by observing a vertical bar through the prism with a telescope, rotating

the prism until its side is parallel to the side of the bar (all components are mounted on the optical bench). The prisms are mounted by Crystal Optics Co. in a 4.4 cm diameter ring with a potting compound. The ring is fitted in a divided circle, which can be read to 0.1° by means of a vernier. A Zeiss birefringent mica rotary compensator (an accessory to their polarizing microscope) is used to compensate for the strain birefringence in the optical windows of the sample cell. It is also used to determine the sign of $(\sigma_y - \sigma_x)$. However, the compensator does not quite replace the Babinet-Soleil compensator since, to obtain variable phase delay between the x and y components of the electric vector, the mica plate must be rotated, which also changes the amplitude of the x and y vectors. The theory of this device is discussed in Appendix 3. The nominal retardation is given as 18° for the sodium D line but when calibrated at the laser wavelength, the maximum phase shift is found to be $15.26 \pm 0.17^{\circ}$. A 189 mm f. l. lens is used to focus the light emerging from the analyzer prism on a slit mounted on the front of the photomultiplier housing. Positioning the lens is critical when 1 MHz acoustic waves are used, else the different diffraction orders cannot be separated. Since the sample chamber behaves optically like a fluid filled lens of long focal length, always double convex due to hydrostatic pressure, it is necessary to check the lens position whenever the sample fluid temperature is changed or whenever a different fluid is inserted in the chamber.

The photomultiplier used to detect the light leaving the analyzer is an RCA 1P28 mounted in a brass housing. A mu-metal shield with a 1" square hole for light to enter is placed over the top of the tube to protect it from stray magnetic fields. A Keithley model 240 high voltage regulated supply is used to provide the 800 v needed by the photomultiplier circuit. It is estimated from data supplied by the manufacturer that a 0.01% change in the applied voltage results in a change of 0.1% in the current output of the photomultiplier for a constant light intensity, hence the need for a very stable power supply. The 800 v bias is chosen to provide the best signal to noise ratio, which is somewhat dependent on the bias level.

A neutral density filter is used to reduce the laser output by a factor of about 100 when the laser intensity was being calibrated. Although the nominal value of the transmission coefficient is 2%, calibration resulted in a transmission coefficient of $1.174 \pm 0.003\%$ at 632.8 nm. The calibration was performed by measuring the phototube output current with an accurate ammeter with and without the filter in place.

VI. EXPERIMENTAL PROCEDURE

The experimental procedure starts with the alignment of the double rod optical bench. Using three carriages, one with transverse motion, a telescope, and two 9 mm diameter rods, the following procedure enables the alignment of the three support brackets so that torsional strain in the rods is minimized. First, with no carriages on the optical bench, the supports are adjusted while sighting along the rods to minimize any obvious torsion. Then a 9 mm rod is mounted on one end of the bench, the second in the center, and the telescope on the other end, in a carriage with transverse motion. The telescope is adjusted so that the two rods can be seen simultaneously. The center support is adjusted so that the sides of the rods are parallel to each other. Then the telescope and rod are interchanged and the end support is adjusted until the two rods are parallel.

The laser is mounted on the optical bench using a transverse motion carriage such that the laser beam was about 8 in. above the optical bench. The laser is rotated in a horizontal plane until the laser beam falls on the center of a rod at the other end of the bench. A rod is then mounted at the center and the laser moved transversely to bring the beam to the center of the rod. The procedure is repeated several times until alignment is obtained. The two 9 mm rods are then removed from the bench since the laser beam now provides a visible optical axis.

The beam expanding telescope is mounted on the bench, the alignment of which is discussed in the previous chapter. The remaining components can then be mounted on the optical bench as shown in Fig. 3-4, and each is aligned by adjusting its height until the laser beam passes through the optical center and secured in that position. The component can now be rotated in a horizontal plane until the laser beam reflects back upon itself and the carriage thumb screw tightened to hold the adapter in place. The polarizing prism is aligned at 45°, as described in Chapter V. The distances between the optical components are not critical except for that between the diffraction image forming lens and the slit on the photomultiplier housing. This adjustment is made during the course of the experiments.

About 50 cc of the sample fluid is withdrawn from its storage container, by means of a syringe, and transferred to the sample chamber. This is repeated until the chamber is filled. All the following calibrations are performed with the sample fluid in the chamber. The fluid is allowed to stand for at least one-half hour before taking data to allow temperature equilibrium to occur and to allow any bubbles formed in the filling process to disappear.

The main temperature control bath is controlled independently of the sample chamber $1^{\circ}C$ above or below the desired sample chamber temperature, depending on the temperature of the room. Thus, the rate of flow of water to the

sample chamber will determine the temperature of the sample since a thermal balance occurs between the heat obtained from the main bath by circulation of water and heat loss to the surroundings. While a temperature gradient is set up by this arrangement, which is greater than would occur if the rate of water flow were constant, the temperature can be sensed in the sample chamber by the thermistor connected to the proportional controller and maintained to within $\pm$ 0.1°C at the point where the optical beam traverses the acoustic beam. If the constant flow arrangement is used, the temperature could change by as much as $\pm$ 0.5°C due to changes in ambient temperature coupled with poor thermal jacketing of the sample chamber. An attempt to sense the temperature in the sample chamber and to use this to control the main bath temperature, while a constant flow of water was maintained between them, resulted in unstable operation.

The following procedure is used to calibrate the laser intensity and to establish the correct setting of the analyzer and polarizer combination. The slit on the photomultiplier housing is closed, the analyzer prism is rotated to obtain maximum transmission of light through the system. The room lights are then turned out and the 800 v bias is applied to the photomultiplier circuit. The photomultiplier assembly is moved transversely until the maximum deflection of the oscilloscope trace is obtained. Leakage of the light through the closed slit was great enough so that 5 to 10 μa

output could be obtained from the photomultiplier. Care must be taken so that the current does not exceed 40 μa, since the oscilloscope input impedence is 1 megohm and the linear range of the photomultiplier output extends only to 40 v between the anode and ground. The analyzer prism is then rotated until a null is obtained, the neutral density filter mounted on the optical bench, the analyzer rotated about 6°, and the slit opened until an output reading of about 10 μa was obtained. The analyzer prism angle is read on the divided circle, and the photomultiplier current read on the oscilloscope, and all values are recorded. The analyzer is then returned to the crossed position, the neutral density filter is removed, and the null established more precisely and the resulting angle recorded. Since the intensity of the light passing through the polarizer and analyzer combination is proportional to $\sin^2 \theta$, where θ is the angle of rotation of the analyzer and is zero degrees at null, the photocurrent that can flow when the polarizer and analyzer axes are parallel, can now be calculated as

$$i_{90°} = i_{\theta} / (\sin^2 \theta \cdot 0.1174)$$

The index of refraction is measured by means of the Wollaston refractometer assembly mounted directly on the sample chamber in such a manner that the refractometer could be positioned in the sample fluid in the center of the laser beam. The neutral density filter should be installed and the height restricting slit closed as a safety precaution.

A telescope with an eyepiece mounted at right angles to the optical axis is used to view the laser beam. The slit is opened just enough to let sufficient light through for the index of refraction measurement. The assembly is rotated until perfect reflection is observed and this angular position recorded. The assembly is rotated in the opposite direction until perfect reflection occurred once more. The total change in angle Θ_c thus measured is just twice the critical angle, so

$$n_0 = 1/\sin(\Theta_c/2) \qquad (6\text{-}1)$$

The rf and gate pulse systems are arranged as shown in Figs. 5-1 and 5-2. Each time the frequency is changed during the course of experiments, the rf system has to be re-tuned, i.e., adjust all the resonant circuits to resonance. As a precaution against high power dissipation or large transient voltage, the gate pulse width used should be 2 ms with a repetition rate of 20 pps and the plate voltage on the final amplifier is set to 200 volts. All tuning capacitors are adjusted for maximum amplitude of the output pulse starting from the matchbox tuning capacitor and working back to the driver grid tuning capacitor, while the output pulse is observed on an oscilloscope. When the tune-up procedure is complete, the rf signal generator output voltage is returned to zero and the final plate voltage increased to 2000 v, or if maximum power is required, to 3000 v.

For the frequency range considered in these experiments, the calibration of the sound intensity can be made by reverse interpolation in the tables of acoustic diffraction function values generated by the computer program in Appendix 1. The polarizing prism is rotated to 0^{o} and the neutral density filter inserted to eliminate the effect of AIB on the calibration. The calibration is carried out by increasing the rf generator output and recording the central order photo-current with the sound on and with the sound off for a series of rf voltages. V values up to 6 can be used and the ratio V/v determined, where v is the voltage applied to the transducer. The average ratio is then taken as the calibration constant. In order to obtain the average intensity of the acoustic wave integrated over its width, the method of Klein and Cook (1967) is used giving

$$I_{avg} = \frac{V^2}{2k^2 d^2 \rho_o^2 \left(\frac{\partial n}{\partial \rho}\right)_s^2} \qquad (6\text{-}2)$$

with Eq. 3-15 used to evaluate $(\partial n/\partial \rho)_s$. The ratio V/v is plotted for several frequencies near the nominal frequency and the frequency where the ratio was maximum is used in obtaining the birefringence data. The LM-7 frequency measuring device is used to determine the frequency of operation accurately. The tuning of the rf amplifier is then further adjusted to provide maximum output at the operating frequency.

Just prior to taking birefringence data on the sample fluid, the analyzer and the rotary mica compensator are adjusted for null. If strain birefringence in the sample cell optical windows is present, but not too large, the rotary mica compensator can cancel completely the optical phase shift thus produced by the windows. For the case where the strain birefringence is relatively large, the amount of optical phase shift varied across the width of the laser beam and can only be partially compensated for.

When the analyzer is adjusted to the cross position and the rotary mica compensator is adjusted to cancel the strain birefringence in the optical windows, a small amount of light still passed through the analyzer. Careful inspection of various parts of the optical system revealed that the polarizer and analyzer prism combination limits the depth of the null. The pair of prisms have an extinction ratio of 2×10^6 at the laser wavelength which, while quite good, is the main limiting factor in determining the birefringence of the liquid sample. The effect of this light leakage is to cause a small current to flow in the photomultiplier circuit at zero sound level. For this condition, the measurement of AIB consists of determining the change in this background current, which changes due to acoustically induced diffraction of light, as well as due to acoustically induced birefringence. When measuring the effect in castor oil, the induced birefringence causes such large changes in the light output, that the background level can be

ignored. For most other fluids, the background level shift had to be taken into account. It should be noted that in the side orders, no light leakage occurs with the acoustic level at zero, but the leakage light is diffracted when the acoustic wave occurs resulting in the appearance of light even if the induced birefringence is zero.

In order to make measurements at such low light levels, it is necessary to restrict the bandwidth of the photomultiplier output circuit to minimize the noise level. This is done by placing a capacitor in parallel with the input to the oscilloscope. Values used were 200 pf, 1000 pf, 0.005 μf and 0.02 μf. The capacitance associated with the input of the oscilloscope, the connecting cable, and the output of the photomultiplier totals 50 pf.

VII. EXPERIMENTAL RESULTS

Castor oil and oleic acid were investigated over a wide range of conditions in order to establish the validity of Eq. 4-7. These liquids exhibit a relatively large birefringence so that imperfections in the optical system did not significantly effect the data. Both liquids have high viscosity which limited the maximum acoustic intensity obtainable at the point of measurement. As the frequency of operation increased, this effect became more pronounced. For example, at 9 MHz, the acoustic absorption was so high that data could not be obtained. Since the oleic acid absorption is not as great, measurements at 9 MHz were possible.

The phototube current ratio predicted by Eq. 4-7 varies over a wide range of magnitudes. In Fig. 7-1, Eq. 4-7 is plotted for castor oil at 3 MHz for a value of $\Delta\nu/\nu$ which gave a best fit to the data. Although the ratios varied by more than three orders of magnitude, the experimental data varied in the same way. When taking the phototube current ratio data, the ratios are difficult to reproduce to within the precision with which they can be read on the oscilloscope (3%), when the acoustic intensity is brought to zero and then returned to some fixed level. The very steep slopes present on the curve in Fig. 7-1 indicate that a variation in ν would result in a very much larger variation in the current ratio. The circles shown in the figure represent the experimental data and their radius represents an

Figure 7-1. A plot of the 0 order current ratios for from 0.4 to 6.0. Castor oil at 31°C and 3 MHz.

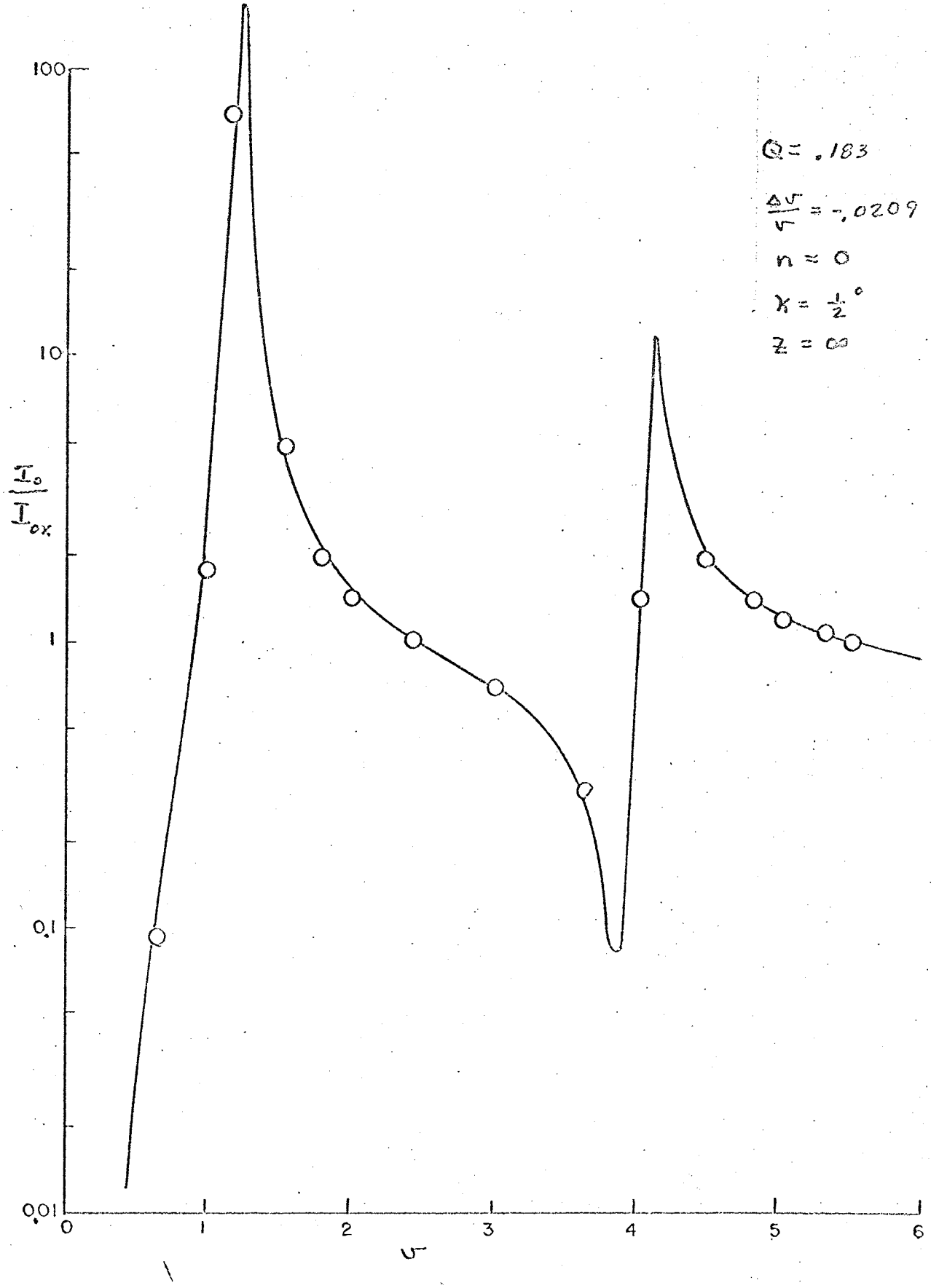
100
10
1
0.1
0.01
$\frac{I_o}{I_{ox}}$
0
1
2
3
4
5
6
ν
Q = .183
$\frac{\Delta\nu}{\nu}$ = -.0209
n = 0
$\chi = \frac{1}{2}°$
z = ∞

error tolerance of about five percent in the magnitude of the current ratio. However, an error of $\pm$ 50% in the current ratio would still result in the circle touching the theoretical curve at a σ value of 1.0.

When attempting to find a value for $\Delta\sigma/\sigma$ which best fits the experimental data, the error in the magnitude of the current ratio does not provide an acceptable criterion. Even the logarithm of the current ratio is not a good test since the curves are still quite steep on a semi-log plot such as Fig. 7-1. The criterion for best fit is to minimize the average of errors in the acoustic intensity required to obtain the observed current ratios. This procedure showed that the average error in the acoustic intensity for an experimental run such as that shown in Fig. 7-1, is often smaller than the error in reading the oscilloscope, which, in this case, the average error is about 1.2%. However, one difficulty with this procedure is that ratios measured when the curve is fairly flat (such as the region about σ of 3.0 in Fig. 7-1) exhibit large errors in σ. This is exactly the opposite of the problem occurring when the slopes of the curve are very steep. No satisfactory procedure was found that would incorporate the best aspects of both error minimizing methods.

Figure 7-2 extends the comparison between theory and experiment to the fourth order. The curves become smoother as the order increases so that the accuracy of the comparison depends more and more on the accuracy of the

Figure 7-2. The phototube output current ratios for various diffraction orders. Castor oil at 37°C and 3 MHz.

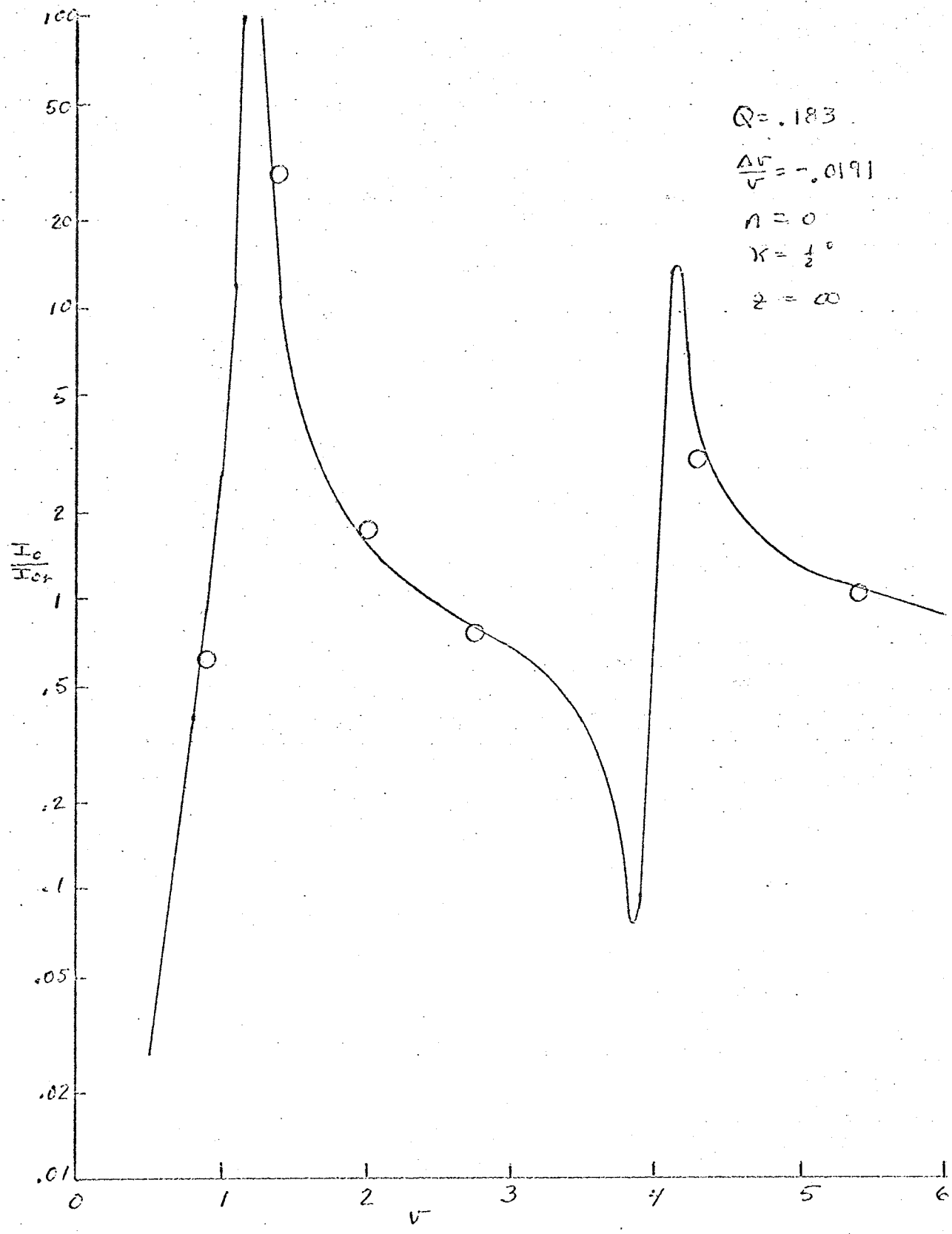
Q = .183
Δν/ν = -.0191
n = 0
κ = ½°
z = ∞
100
50
20
10
5
2
1
.5
.2
.1
.05
.02
.01
Ic/Ico
0
1
2
3
4
5
6
ν

Fig. 7-2a.

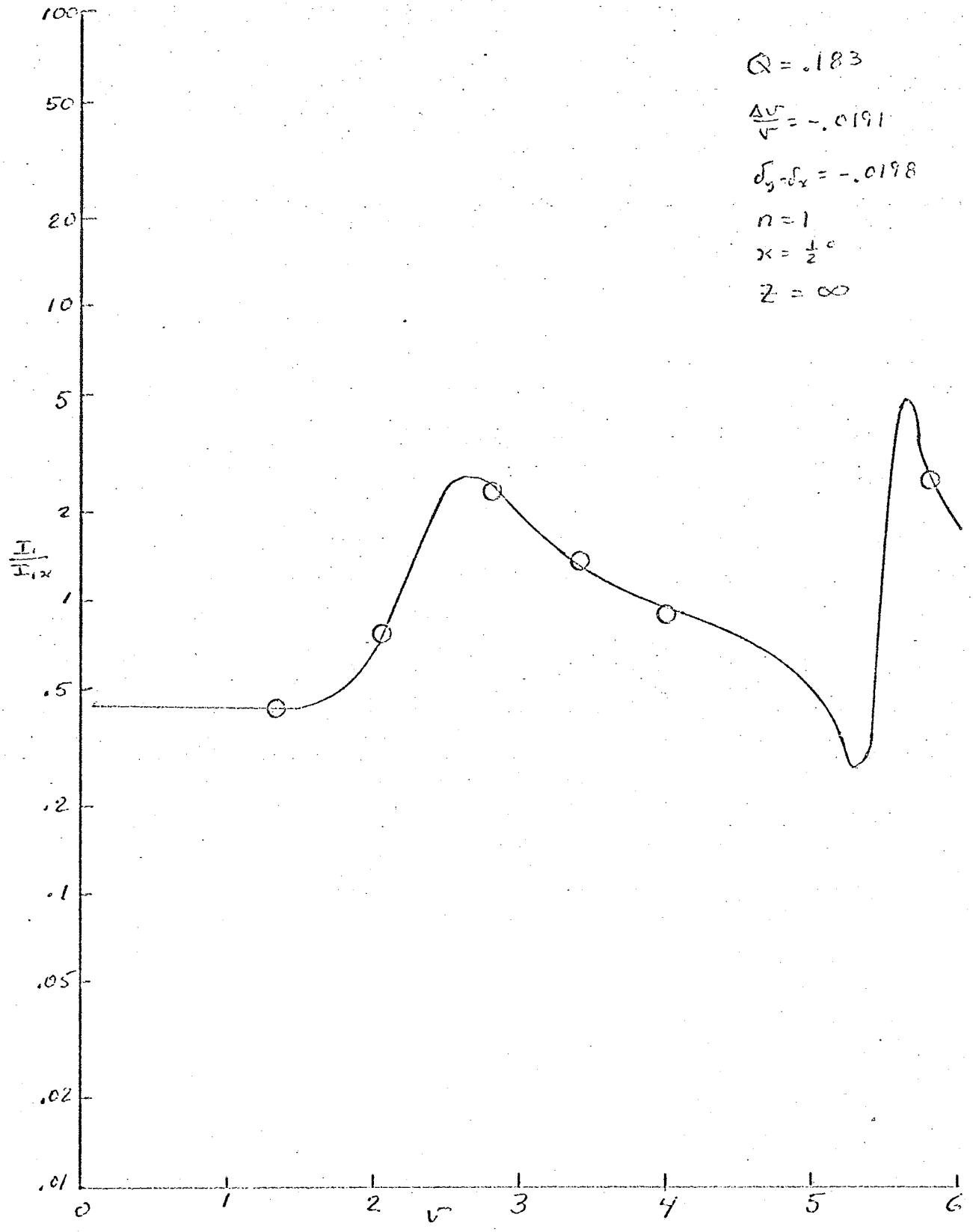
Q = .183
Δν/ν = -.0191
δy - δx = -.0198
n = 1
x = ½ c
Z = ∞
100
50
20
10
5
2
1
.5
.2
.1
.05
.02
.01
I1/I1x
0
1
2
3
4
5
6
ν

Fig. 7-2b.

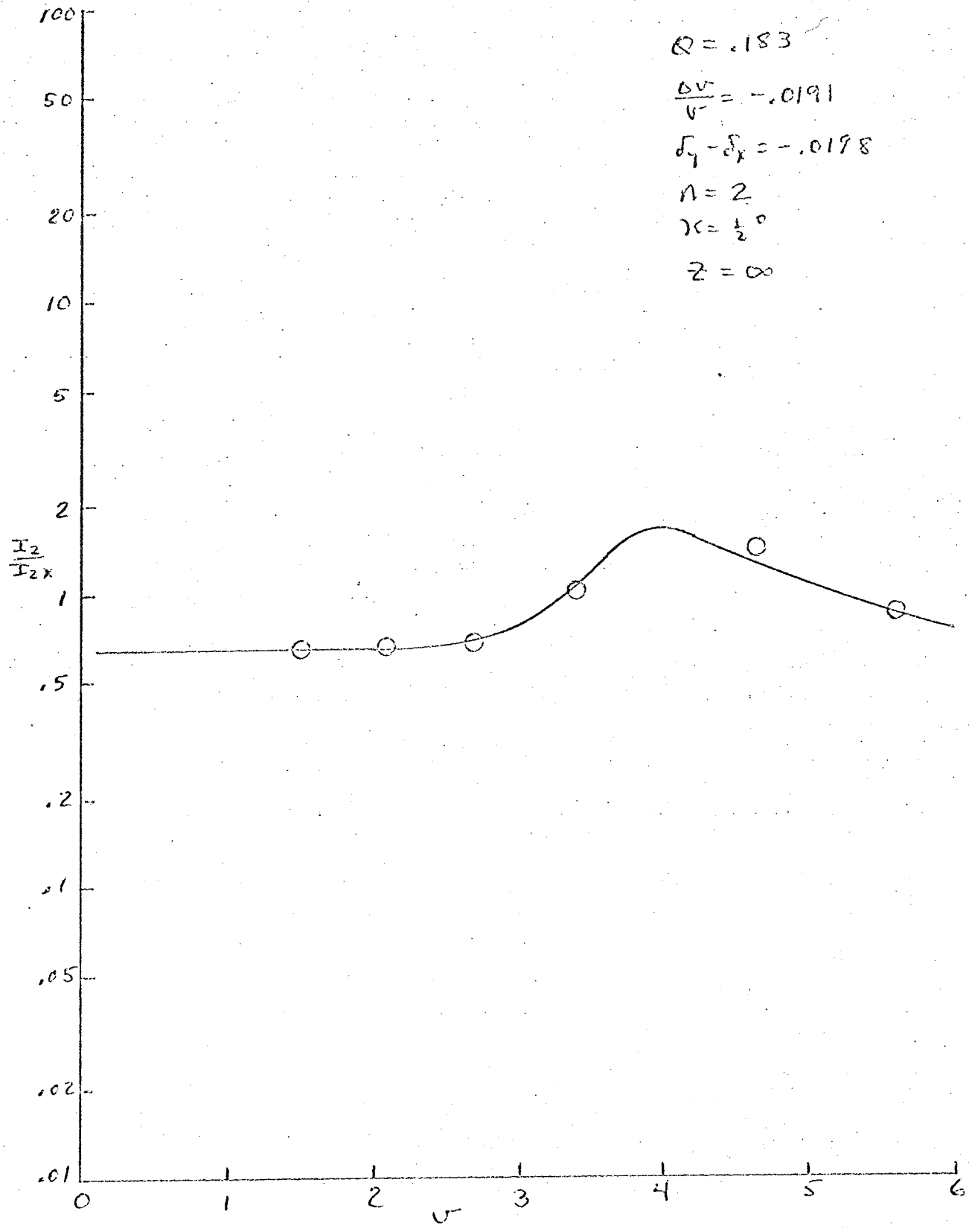
Q = .183
ΔV/V = -.0191
δ1 - δx = -.0178
n = 2
x = 1/2°
Z = ∞
100
50
20
10
5
2
1
.5
.2
.1
.05
.02
.01
I2/I2x
0
1
2
3
4
5
6
V

Fig. 7-2c.

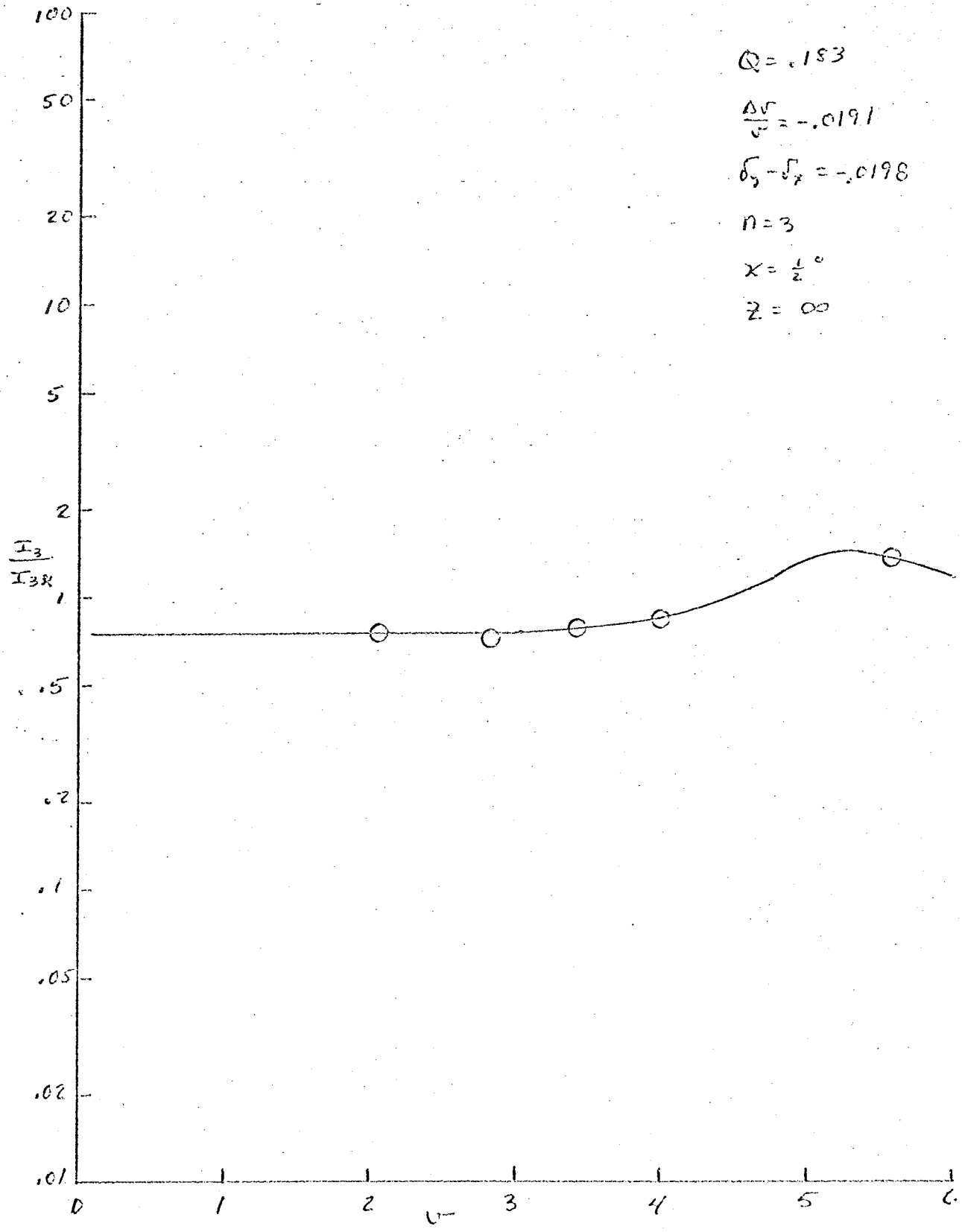
Q = .153
Δv/v = -.0191
δy - δx = -.0198
n = 3
x = 1/2
Z = ∞
I3/I3R
100
50
20
10
5
2
1
.5
.2
.1
.05
.02
.01
0
1
2
3
4
5
6
U

Fig. 7-2d.

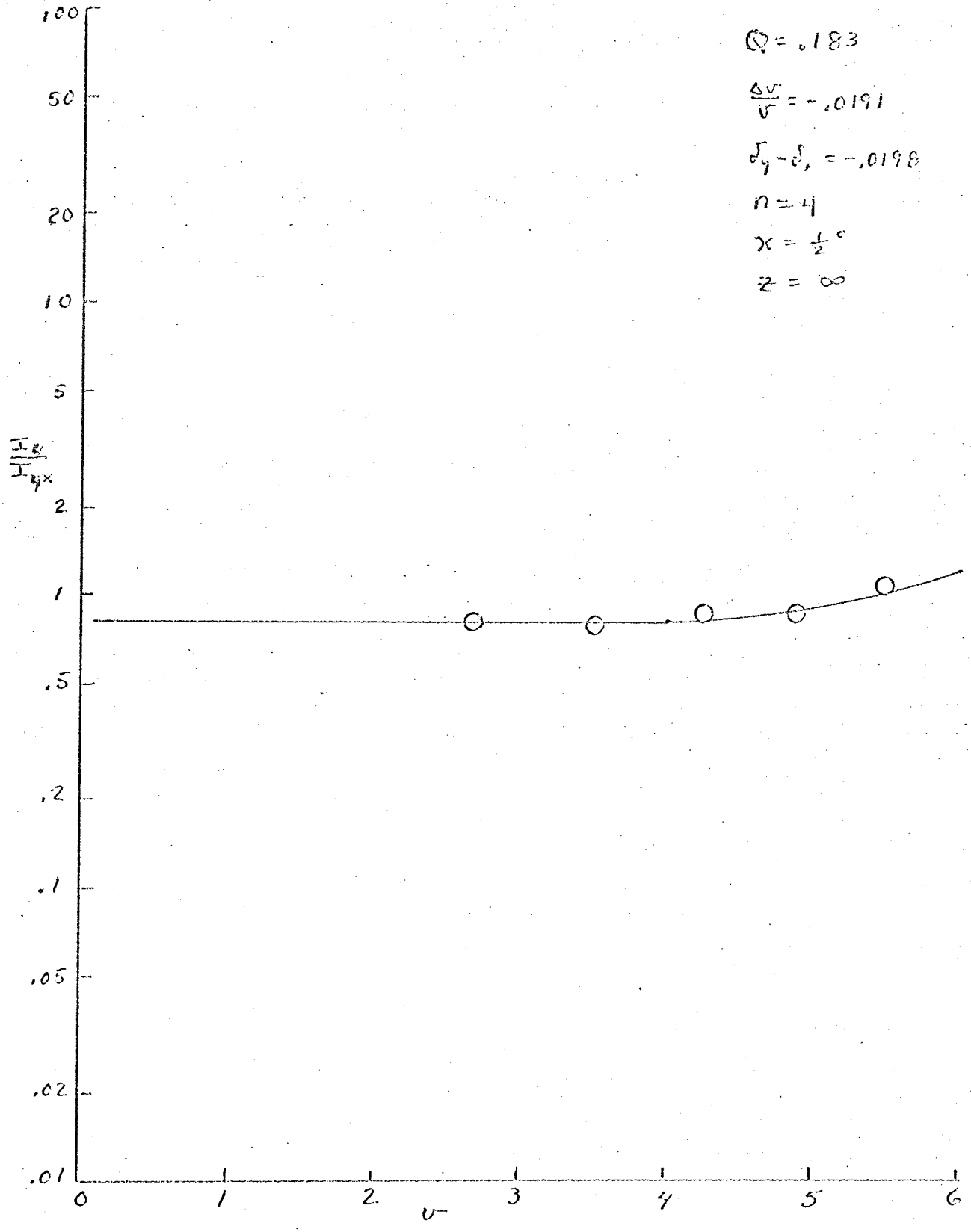
Q = .183
Δv/v = -.0191
δ1 - δ0 = -.0198
n = 4
x = 1/2°
z = ∞
100
50
20
10
5
2
1
.5
.2
.1
.05
.02
.01
Ie/Iex
0
1
2
3
4
5
6
v

Fig. 7-2e.

current ratio measurements. However, the curves demonstrate that there is good agreement between the various orders for a fixed value of $\delta_y - \delta_n$, though the data in the first order suffer from the same evaluation problem found in the zero order, i.e., some areas have a shallow slope and require an evaluation on the basis of accuracy in the current ratio and other areas have such a steep slope that they require an evaluation on the basis of accuracy in the ν values.

The results discussed above are all for 3 MHz. Additional runs were made at 5 MHz in castor oil and 9 MHz in oleic acid. As the frequency increases, the amount of light in the various diffraction orders change resulting in a change in the shape of the current curves. The most obvious changes are the position and the sharpness of the maxima and minima (Figs. 7-3 and 7-4). It is seen that with increasing frequency, the zero order data exhibit a gradual smoothing of the current ratio curves. Surprisingly, the higher order curves are gradually becoming more peaked. Because the acoustic intensity levels used at high frequencies were kept low, to avoid heating the sample, measurements were not made at the maxima and minima to verify their presence. The zero order maximum at 5 MHz could be reached, however, and agreement with the theoretical shape remained good. The curves are extended to a ν of 5.5 for ease in comparing the high frequency curves with those at low frequencies. The small amplitude of the peak on the zero order curve in Fig. 7-4 is not only due to

Figure 7-3. The phototube output current ratios for various diffraction orders. Castor oil at 31°C and 5 MHz.

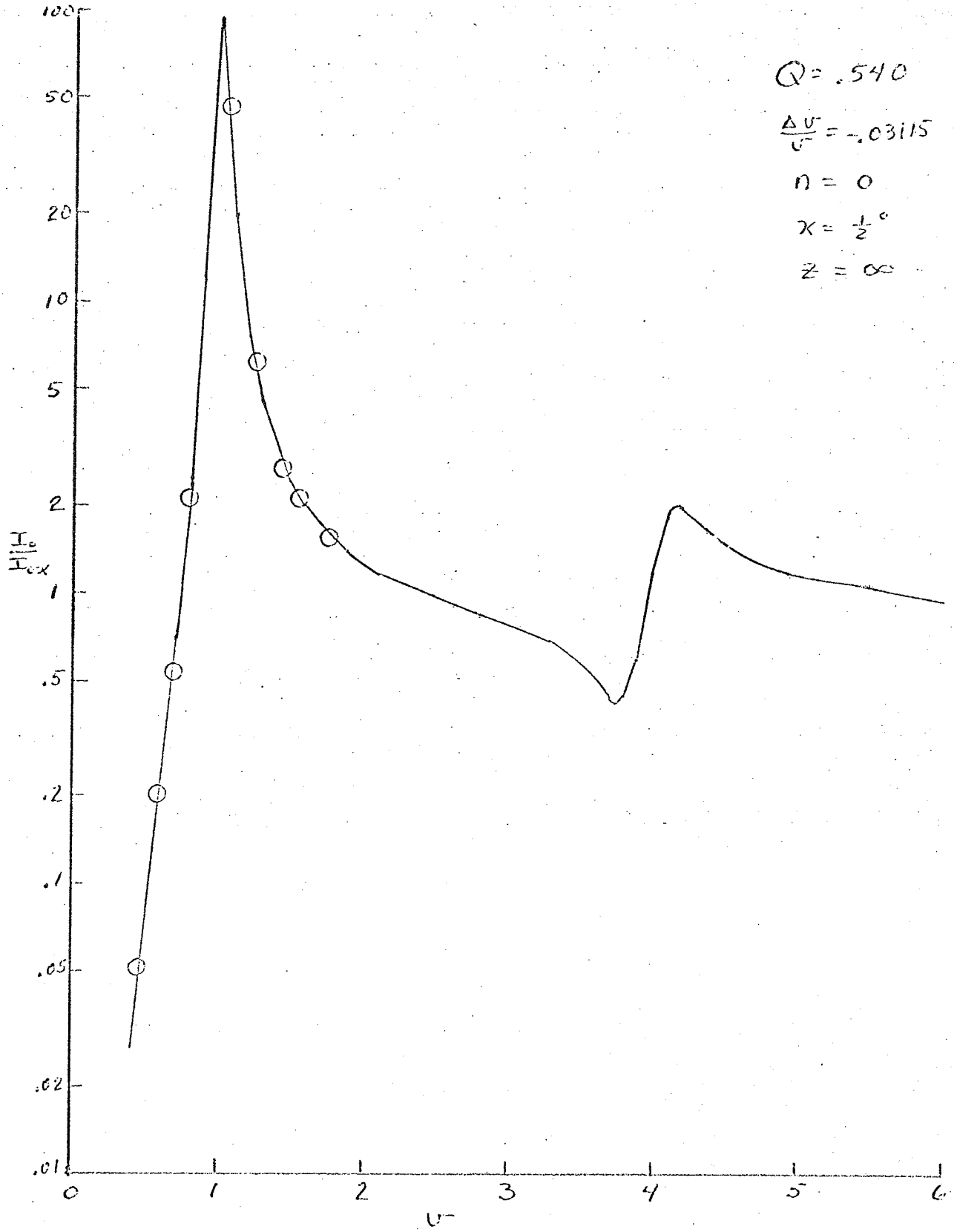
Q = .540
Δv/v = -.03115
n = 0
x = 1/2
z = ∞
100
50
20
10
5
2
1
.5
.2
.1
.05
.02
.01
I_e/I_ex
0
1
2
3
4
5
6
v

Fig. 7-3a.

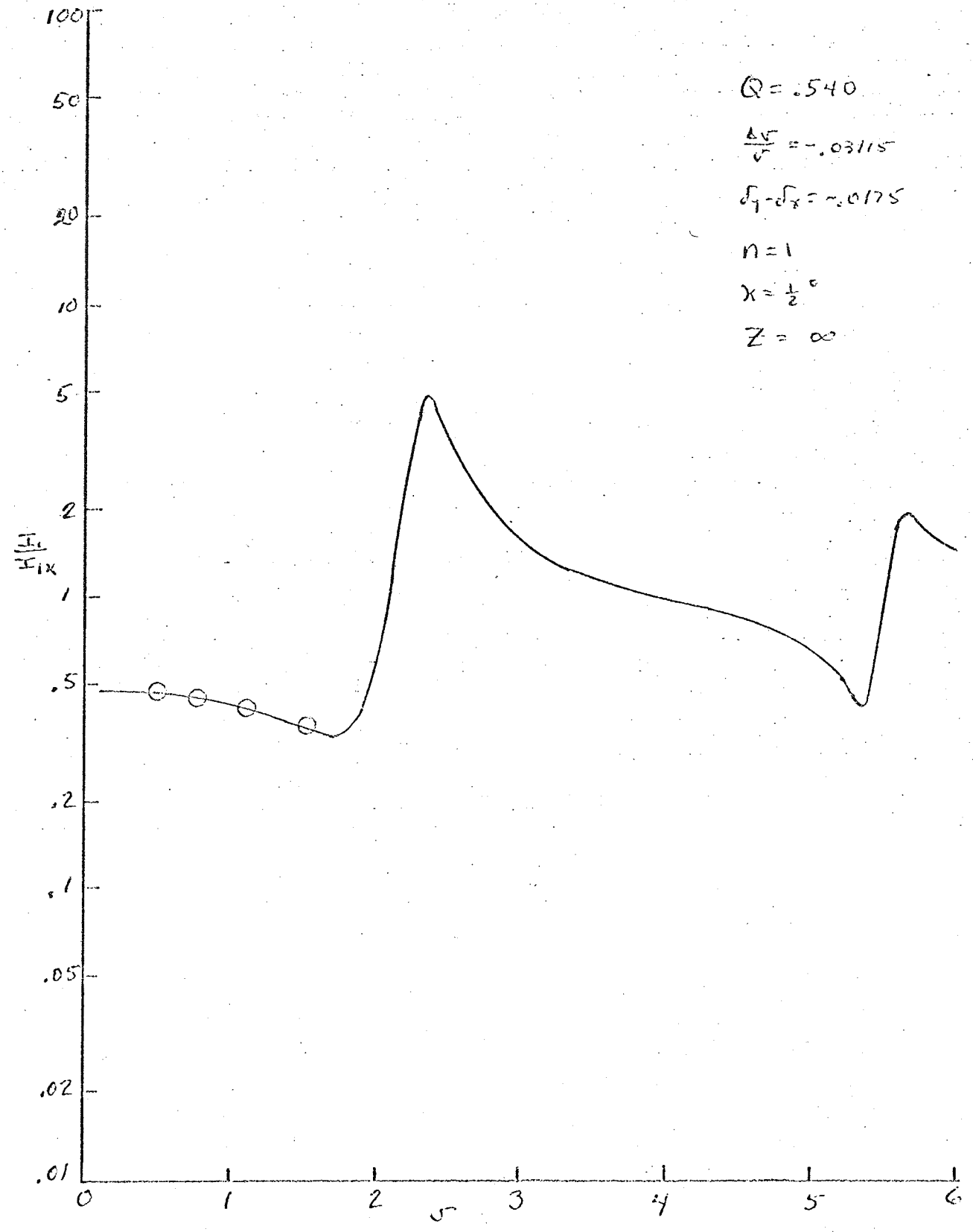
Q = .540
Δν/ν = -.03115
δ1 - δ2 = -.0175
n = 1
χ = ½°
Z = ∞
100
50
20
10
5
2
1
.5
.2
.1
.05
.02
.01
H_L / H_iχ
0
1
2
3
4
5
6
s

Fig. 7-3b.

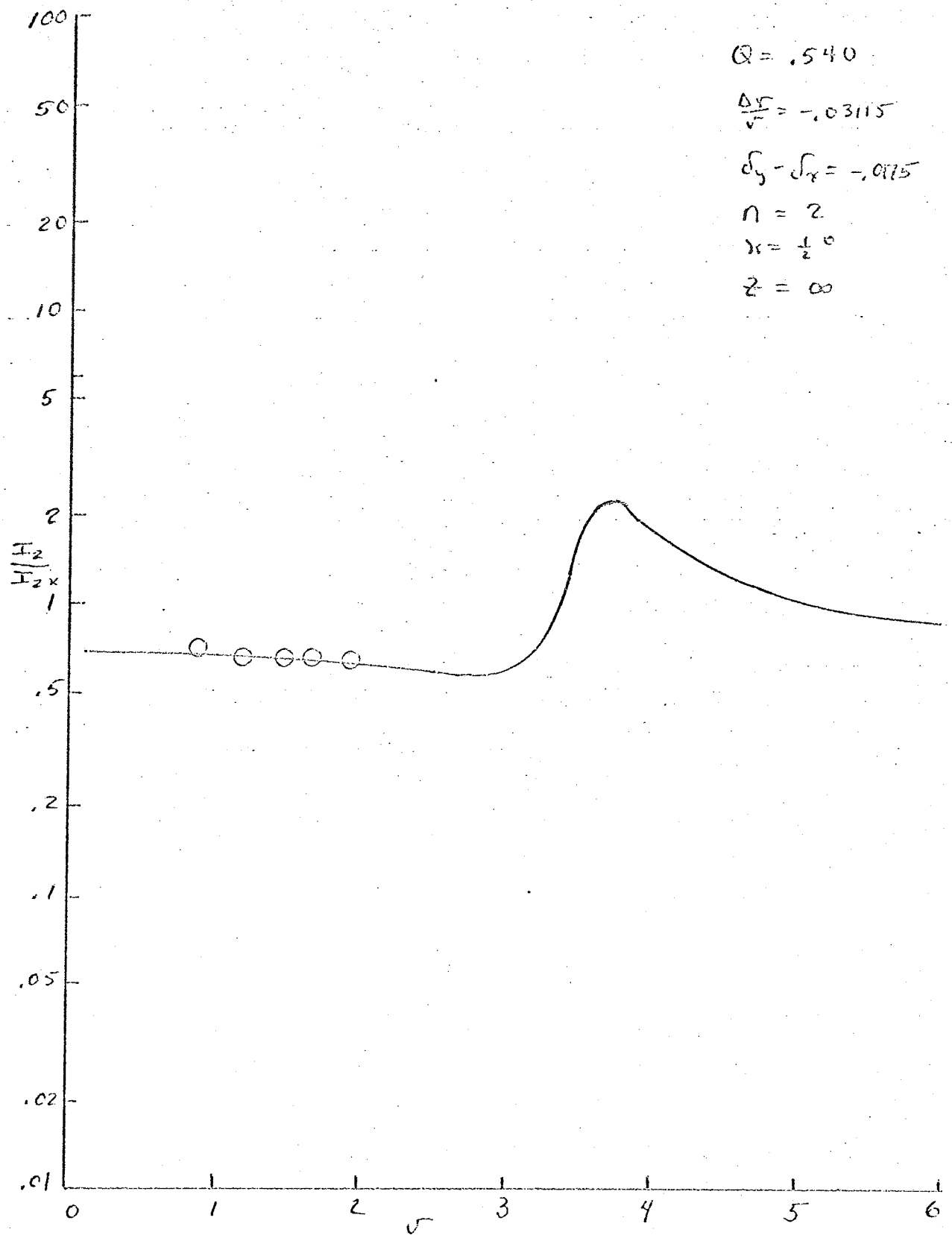
Q = .540
Δr/r = -.03115
δy - δx = -.0775
n = 2
x = 1/2
z = ∞
100
50
20
10
5
2
1
.5
.2
.1
.05
.02
.01
Hz / Hz x
0
1
2
3
4
5
6
r

Fig. 7-3c.

Figure 7-4. The phototube output current ratios for various diffraction orders. Oleic acid at 15°C and 9 MHz.

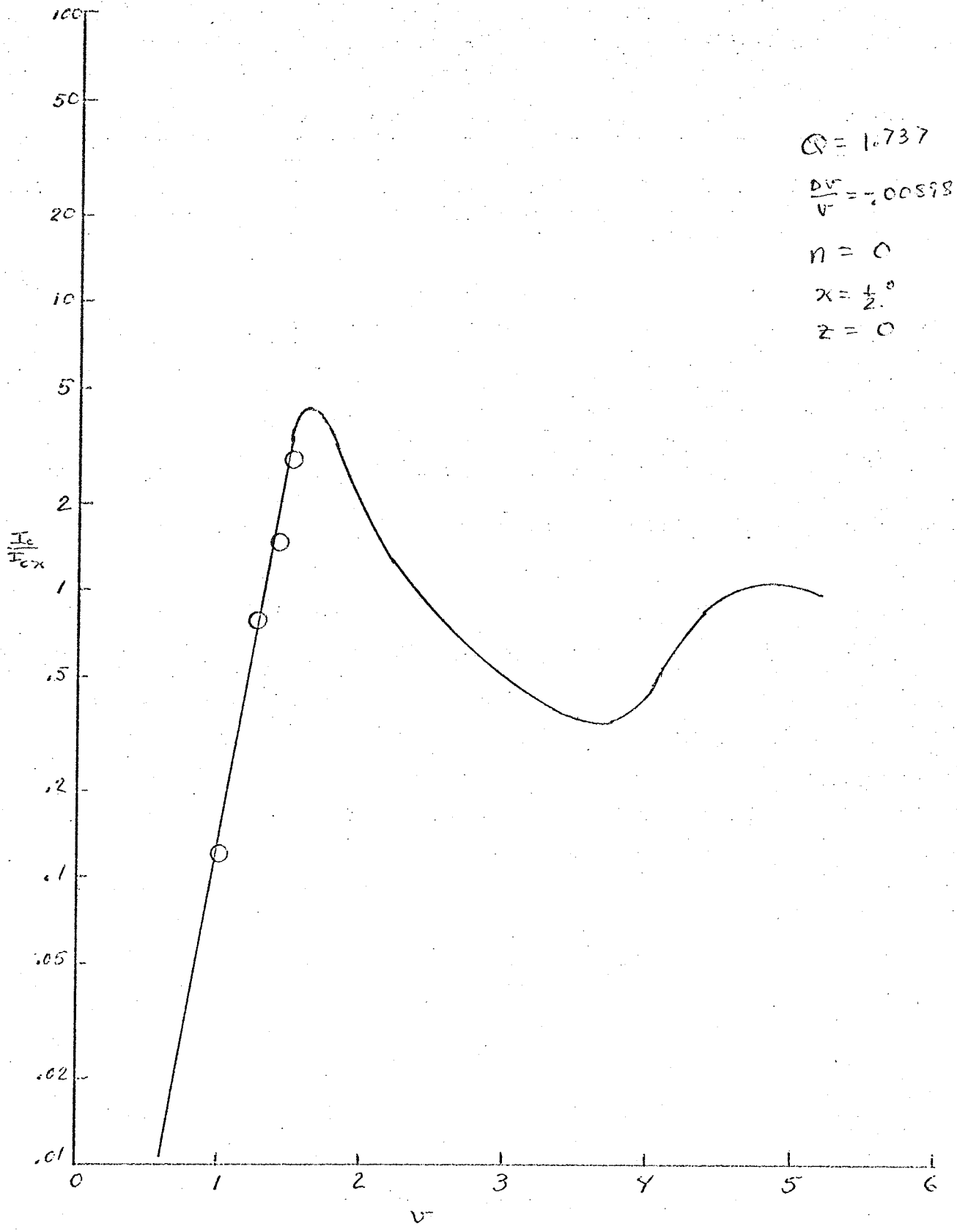
100
50
20
10
5
2
1
.5
.2
.1
.05
.02
.01
$\frac{I_e}{I_{ex}}$
0
1
2
3
4
5
6
v^-
Q = 1.737
$\frac{\Delta v^-}{v^-} = .00598$
n = 0
$\alpha = \frac{1}{2}°$
z = 0

Fig. 7-4a.

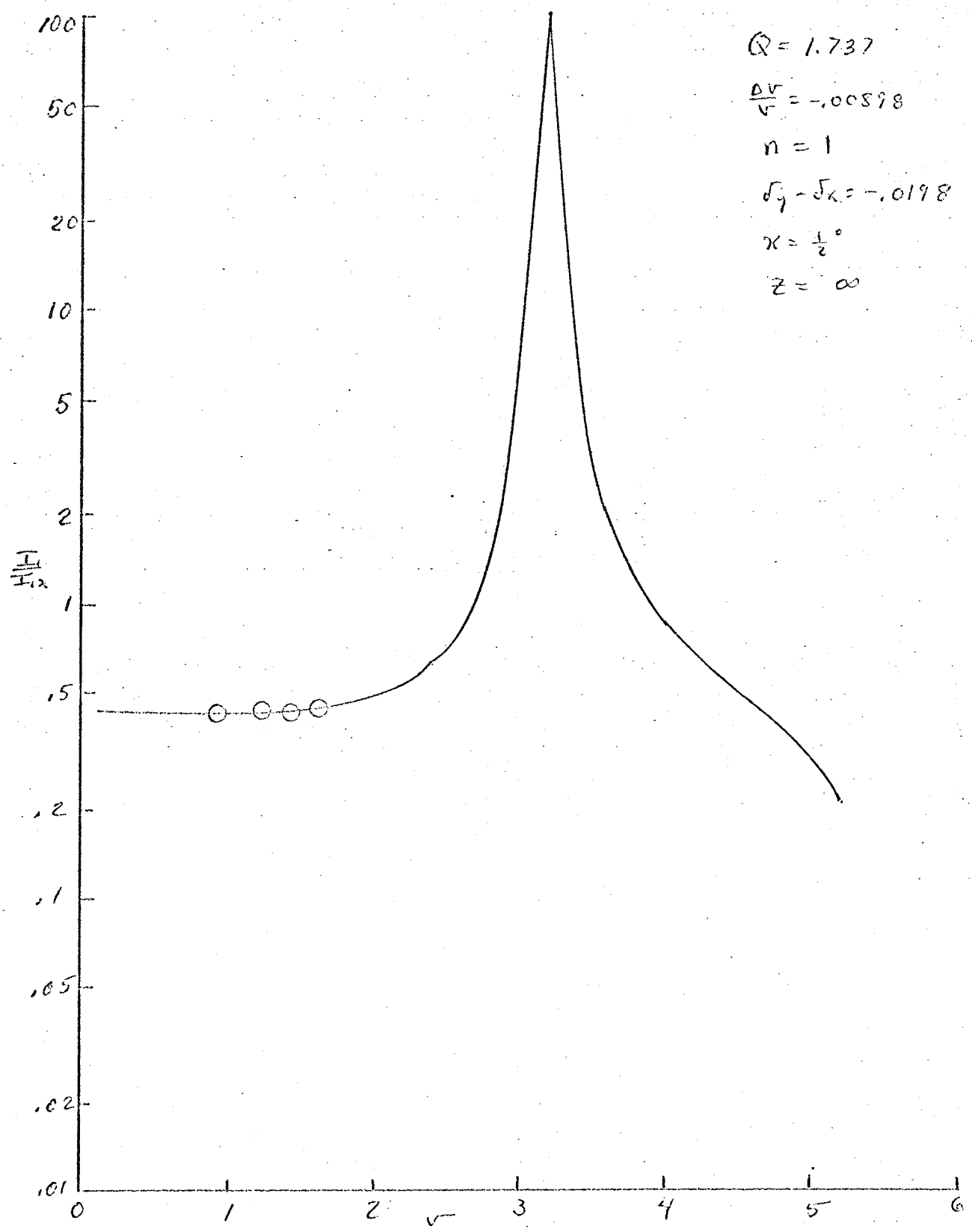
Q = 1.737
Δv/v = -.00598
n = 1
δ_y - δ_x = -.0198
x = 1/2°
z = ∞
100
50
20
10
5
2
1
.5
.2
.1
.05
.02
.01
I/I_12
0
1
2
3
4
5
6
v

Fig. 7-4b.

the low value of $\Delta\sigma/\sigma$, exhibited by the oleic acid, i.e., using 0.031 for the value of $\Delta\sigma/\sigma$ the curve shape differed only slightly so that the changes in shape appear to be due to the increase in Q.

The maxima and minima for the current ratios do not correspond to the maxima and minima of the phototube output current when the analyzer is oriented at 0^{o}. For the data plotted in Fig. 7-1, the first maximum occurs at a σ of 2.3. For fluids that exhibit only a small birefringence, the correspondence becomes better. The point at which the current becomes a maximum then, is not the best point to evaluate the birefringence data. When attempting to measure weakly birefringent liquids, the best point at which to obtain and evaluate the data is just prior to the first maximum. Data may also be obtained just after the first maximum or near any of the other maxima, but the scatter in the current magnitudes increases due to the extreme sensitivity of the current ratio to the amplitude of the sound. This restriction applies to all orders.

Another point that was investigated concerned whether or not there is an optimum diffraction order for evaluating $\delta_y - \delta_x$. The point in all diffraction orders where the sensitivity is high and the amplitude of the current ratio is not greatly dependent on the acoustic amplitude is the point where the current ratio curve begins to rise toward the first maximum. The amplitude of the current ratio is nearly constant

from zero to the inflection point and, for the sake of comparison, the current ratio, as the acoustic intensity is reduced to zero, is plotted in Fig. 7-5 for the first five diffraction orders. For small values of $\delta_y - \delta_x$, the limiting value increases rapidly as a function of order number and, even though the available light is decreasing, it is advantageous to work in the highest order in which sufficient acoustical power can be generated to reach the inflection point. On the other hand, when $\delta_y - \delta_x$ is larger than -0.01, the curves begin to flatten out and the low orders, where more light is available, yield more consistent results.

When measuring fluids with very low birefringence, a correction must be made for the leakage of light through the prisms, otherwise the data appear to show a pronounced amplitude effect. Figure 7-6 shows some attempts at fitting a value of Z such that the value of $\Delta V/V$ is independent of V. The ratio of the phototube currents was calculated by first subtracting any background current due to electrical leakage and scattering and then taking a ratio. The presence of background due to leakage of light through the crossed polarizers was not subtracted out. If Eq. 4-7 contains the correct form of the correction, then the leakage will be automatically taken into account. The best fit was obtained for a Z equal to -5×10^3. The measured extinction ratio is about 10^7 so the expected value of Z is about 3.1×10^3. The negative sign associated with the Z which gave

Figure 7-5. The limit of the current ratio as the acoustic intensity goes to zero for the first five orders and various values of $\sigma_y - \sigma_x$.

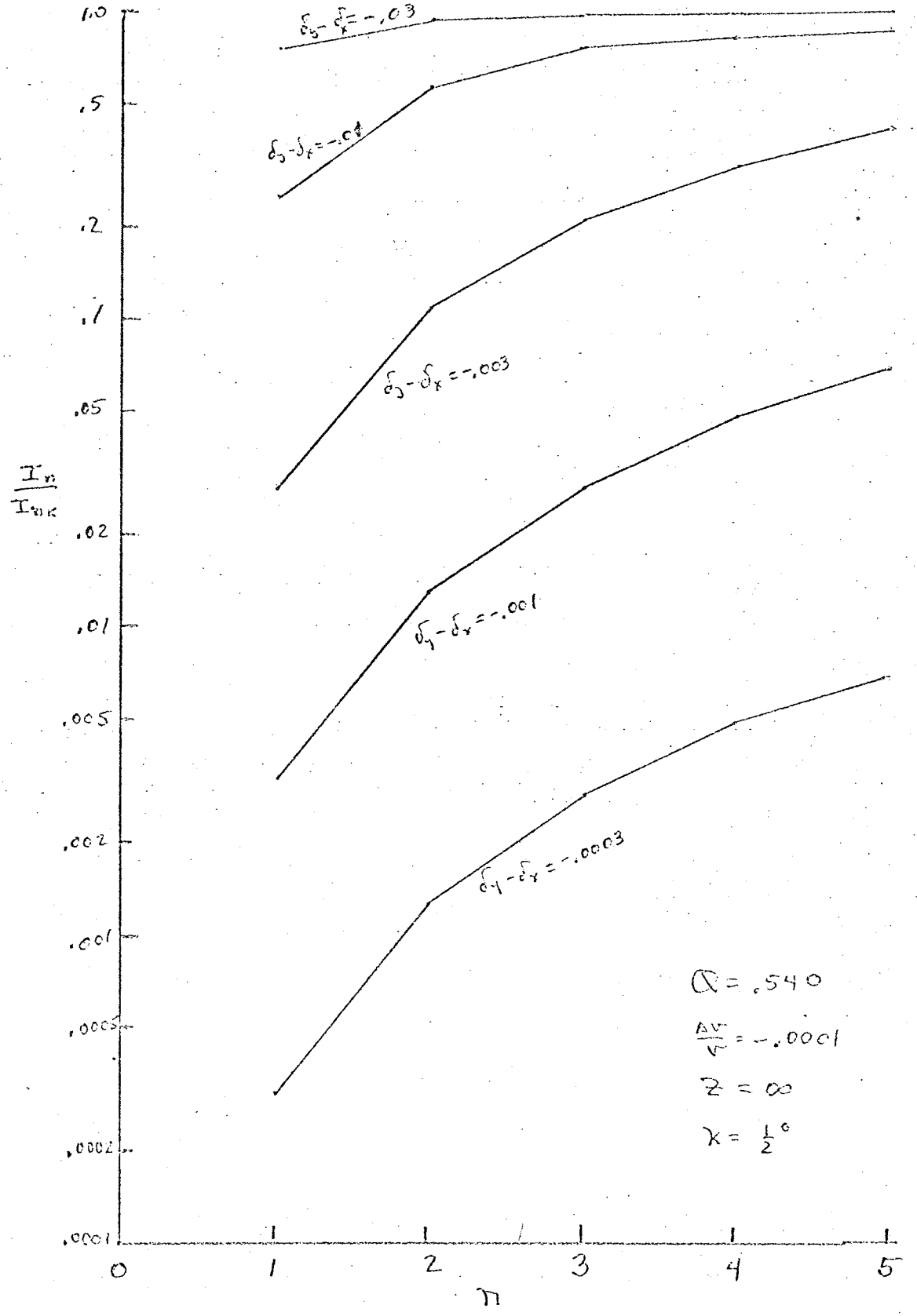
1.0
.5
.2
.1
.05
.02
.01
.005
.002
.001
.0005
.0002
.0001
$\frac{I_n}{I_{n=1}}$
$\delta_3 - \delta_x = -.03$
$\delta_2 - \delta_x = -.01$
$\delta_3 - \delta_x = -.003$
$\delta_4 - \delta_x = -.001$
$\delta_4 - \delta_x = -.0003$
$\Omega = .540$
$\frac{\Delta V}{V} = -.0001$
$Z = \infty$
$\chi = \frac{1}{2}°$
0
1
2
3
4
5
n

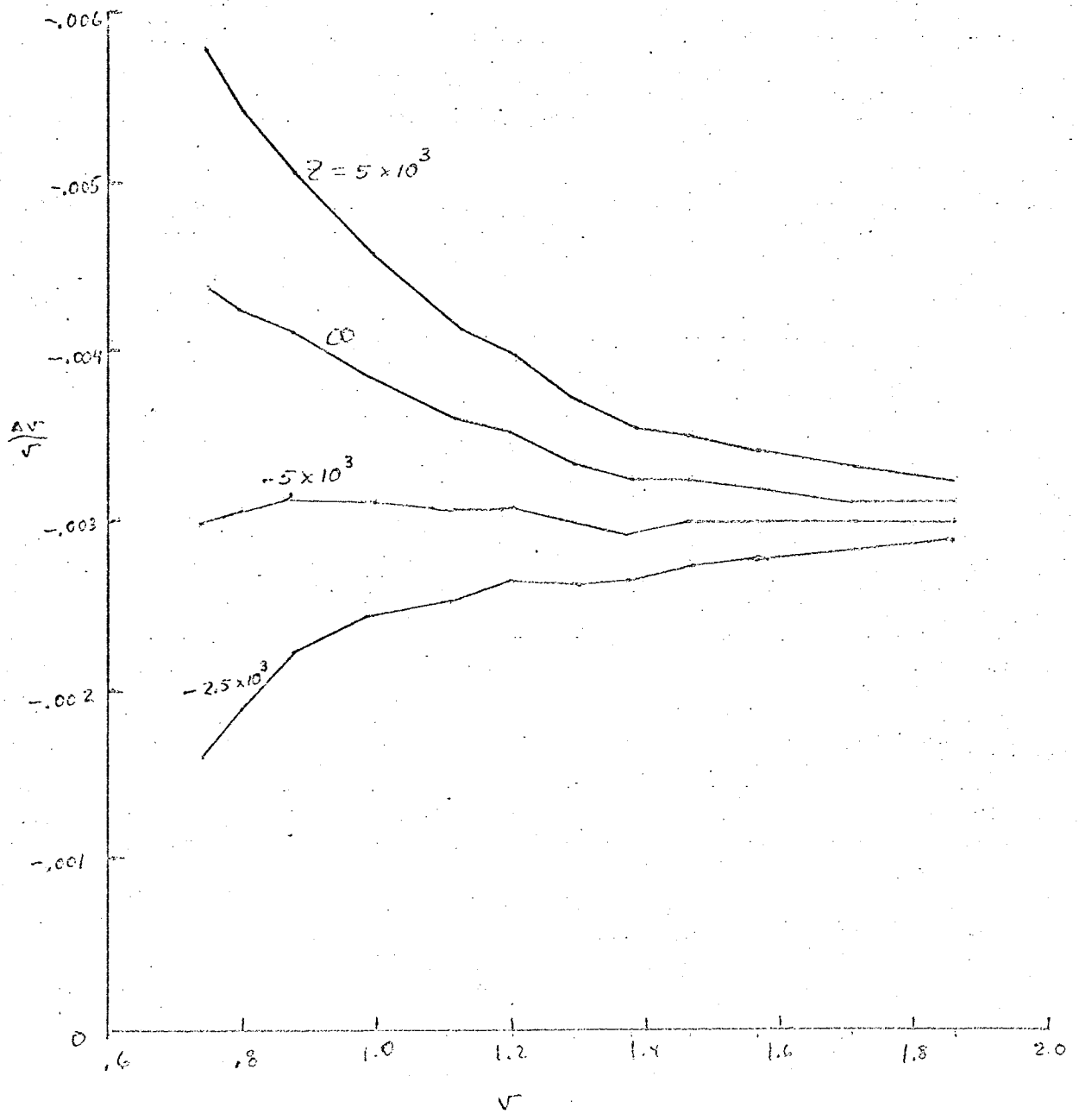

Fig. 7-6. This graph shows the effect of different values of extinction ratio when evaluating very small $\Delta V/V$. The value of Z yielding the flattest curve is taken as the apparent extinction ratio. The data is taken from one run of polyethylene glycol at 24° and 5 MHz. (40% aqueous solution)

the best fit was unexpected. Since Z^2 is the extinction ratio and, since the magnitude is about the expected value, the fact that a negative sign appears means only that the electric vector representing the leakage light has the opposite phase than originally postulated.

Figure 7-7 summarizes the acoustically induced birefringence data. Figure 7-7a shows the normalized birefringence calculated from Eq. 3-24. According to the theories of the effect discussed in Chapter II, the birefringence is proportional to frequency below the relaxation frequency and independent of frequency above relaxation. The curves are separated by a small but definite amount which indicates that the relaxation frequency is near the measurement frequency over the temperature range shown. The phase angle by which the birefringence lags the velocity gradient is shown in Fig. 7-7b. Most of the phase angles measured are greater than $\pi/4$ so that the measurement frequencies were above the relaxation frequency in most cases. The relaxation times calculated from the phase information are shown in Fig. 7-7c. Each relaxation time was calculated from a single frequency measurement, an impossibility for near field measurements. Since the relaxation times measured at two frequencies are in agreement, probably there is only a single process, also an impossible inference when near field measurements are made.

Figure 7-7. Summary of data obtained for Castor Oil.
a. The normalized birefringence.
b. The phase angle by which the birefringence lags the velocity gradient.
c. The rotary relaxation time.
d. The constant G for castor oil.

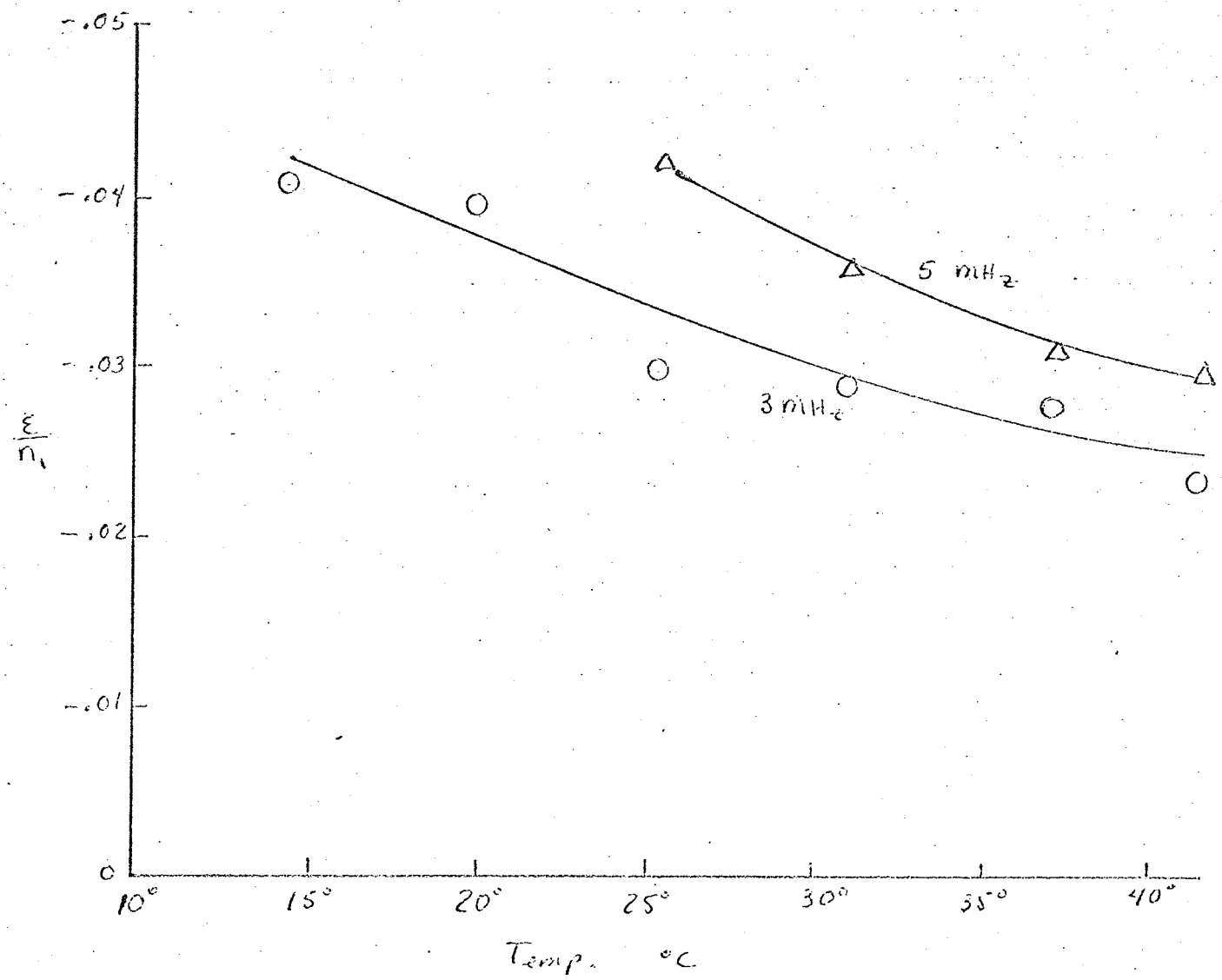
-.05
-.04
-.03
-.02
-.01
0
$\frac{\varepsilon}{n_1}$
5 mH₂
3 mH₂
10°
15°
20°
25°
30°
35°
40°
Temp. °C

Fig. 7-7a.

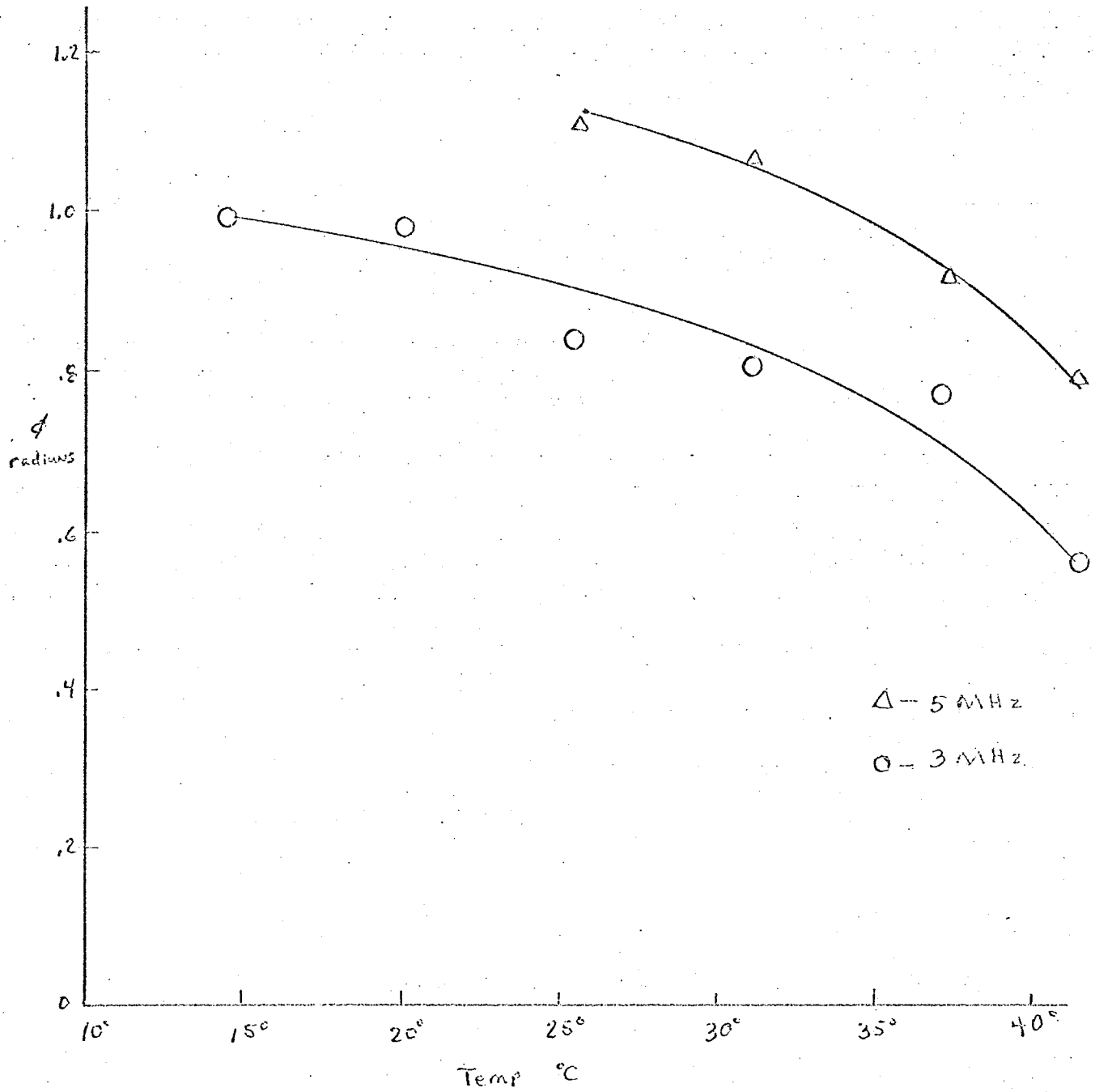

Fig. 7-7b.

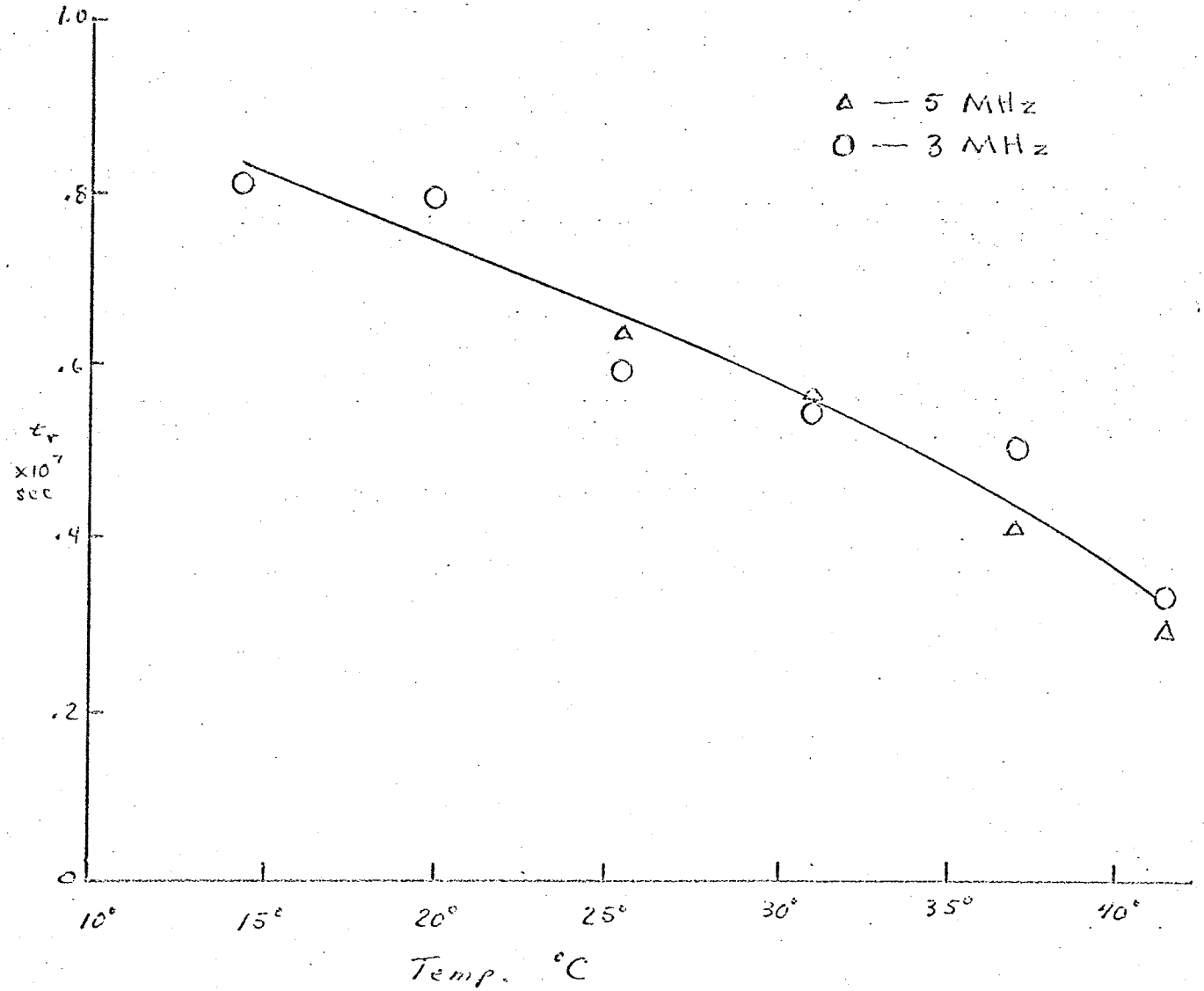

Fig. 7-7c.

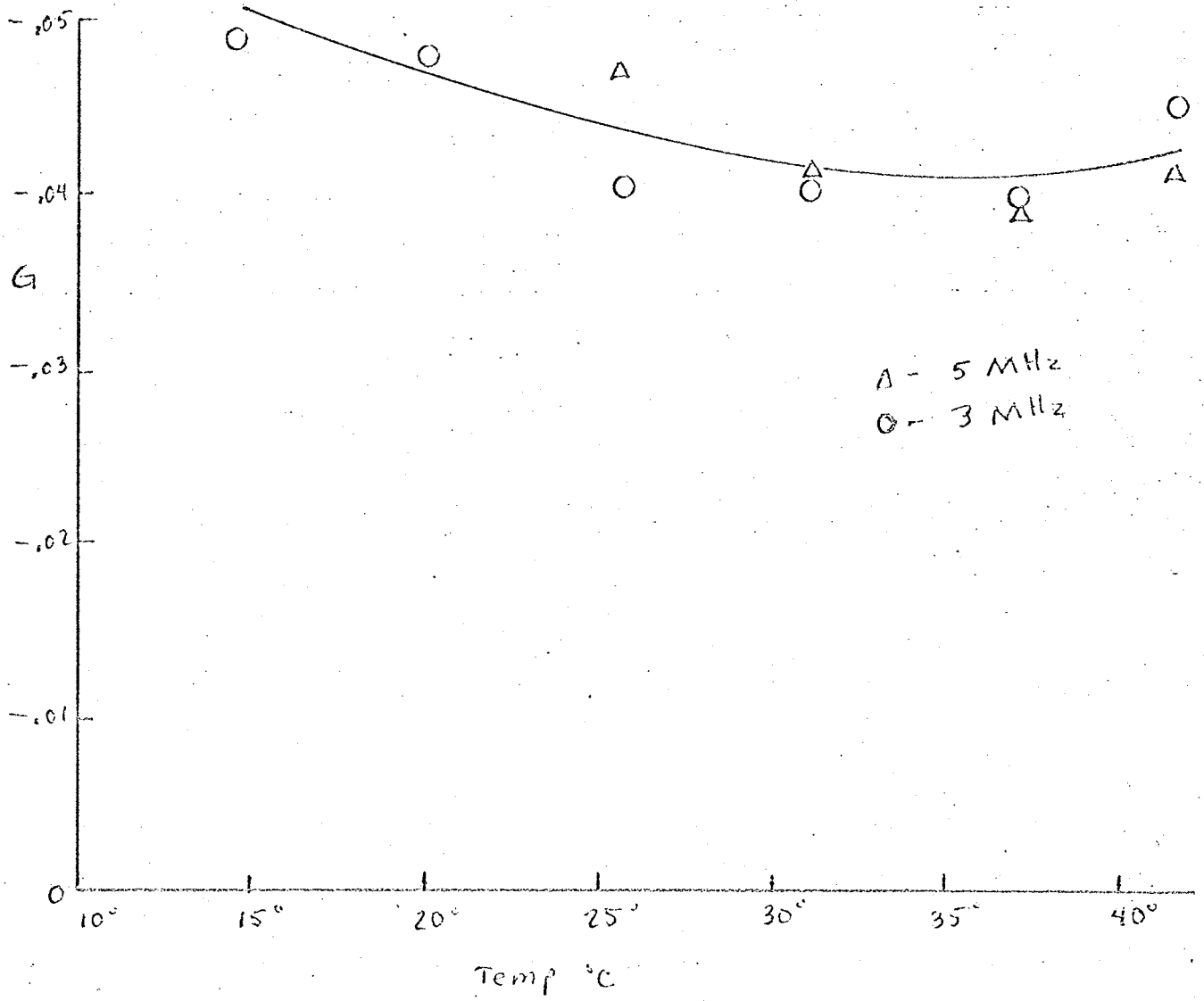

Fig. 7-7d.

Both the acoustically induced birefringence and the relaxation time depend on the viscosity of the fluid. As the temperature is increased, the viscosity falls by nearly a factor of ten over the temperature range of 15 to 41°C. (Handbook of Chemistry and Physics, 1968). Neither the birefringence nor the relaxation time vary by such a large amount and this implies that the Maxwell constant changes by nearly a factor of ten over the measured temperature range. G, which is defined by Riley and Klein (1969) as a characteristic of the fluid being studied is proportional to η M. When G is plotted as a function of temperature as in Fig. 7-7d, only a small temperature coefficient is found. This is a more direct indication that the Maxwell constant changes in almost inverse proportion to the viscosity.

The corresponding summary data for oleic acid is shown in Fig. 7-8. The induced birefringence is noticeably smaller than for castor oil. Also, the phase angles are small, indicating that the relaxation frequency is well above the measuring frequency. The magnitude of the phase indicates that oleic acid has a relaxation frequency of 26 MHz at 25°C. At 35°C, this figure rises to about 50 MHz. The oleic acid scatters the incident light causing a substantial background current in the phototube output circuit. Although sufficient signal currents were available in the adjacent diffraction orders to obtain a fairly consistant data for the induced birefringence, the available signal in the zero order was smaller than the

Figure 7-8. Summary of data obtained for Oleic Acid.
a. The normalized birefringence.
b. The phase angle by which the birefrigence lags the velocity gradient.
c. The rotary relaxation time.
d. The constant G for oleic acid.

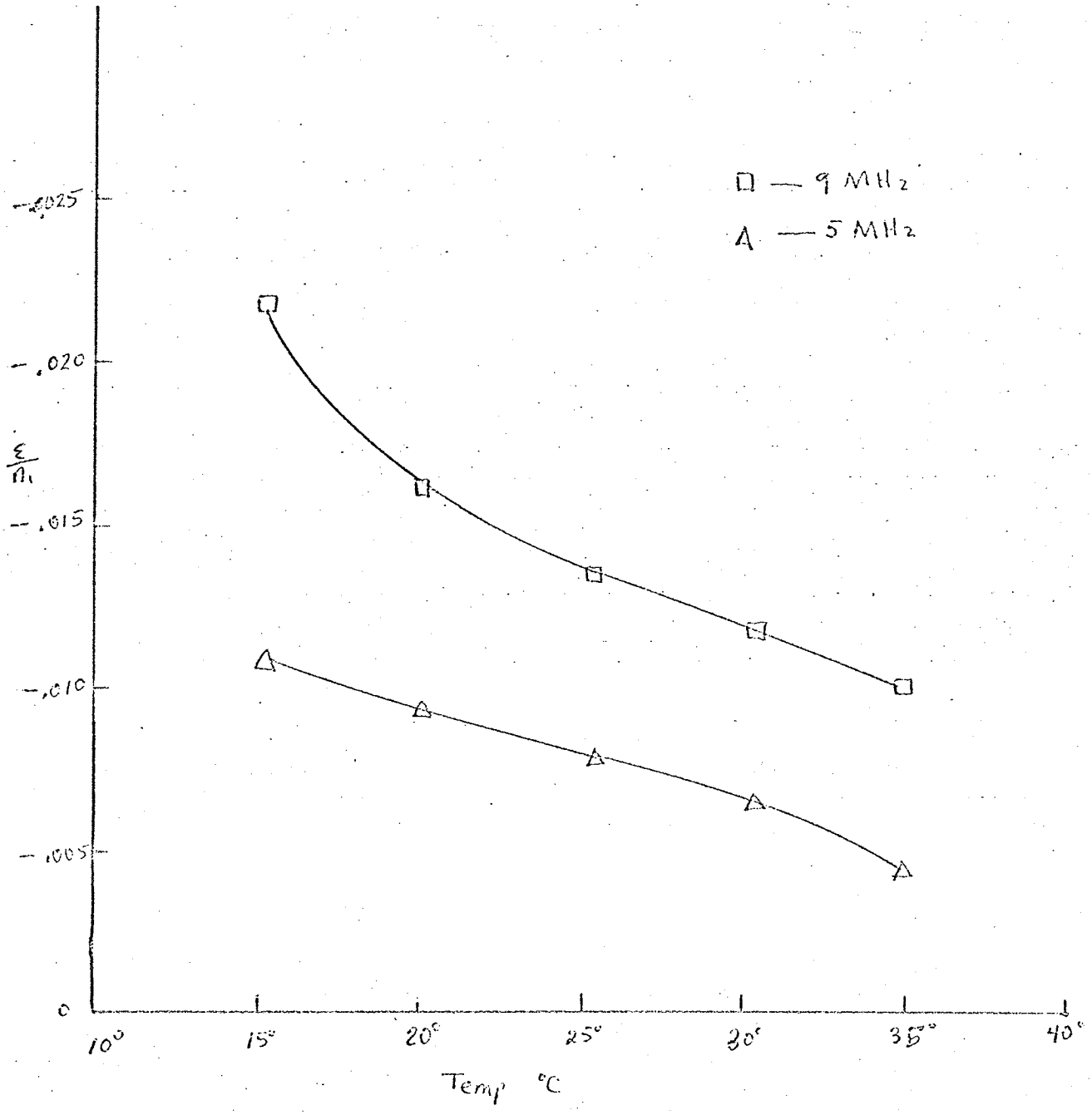

Fig. 7-8a.

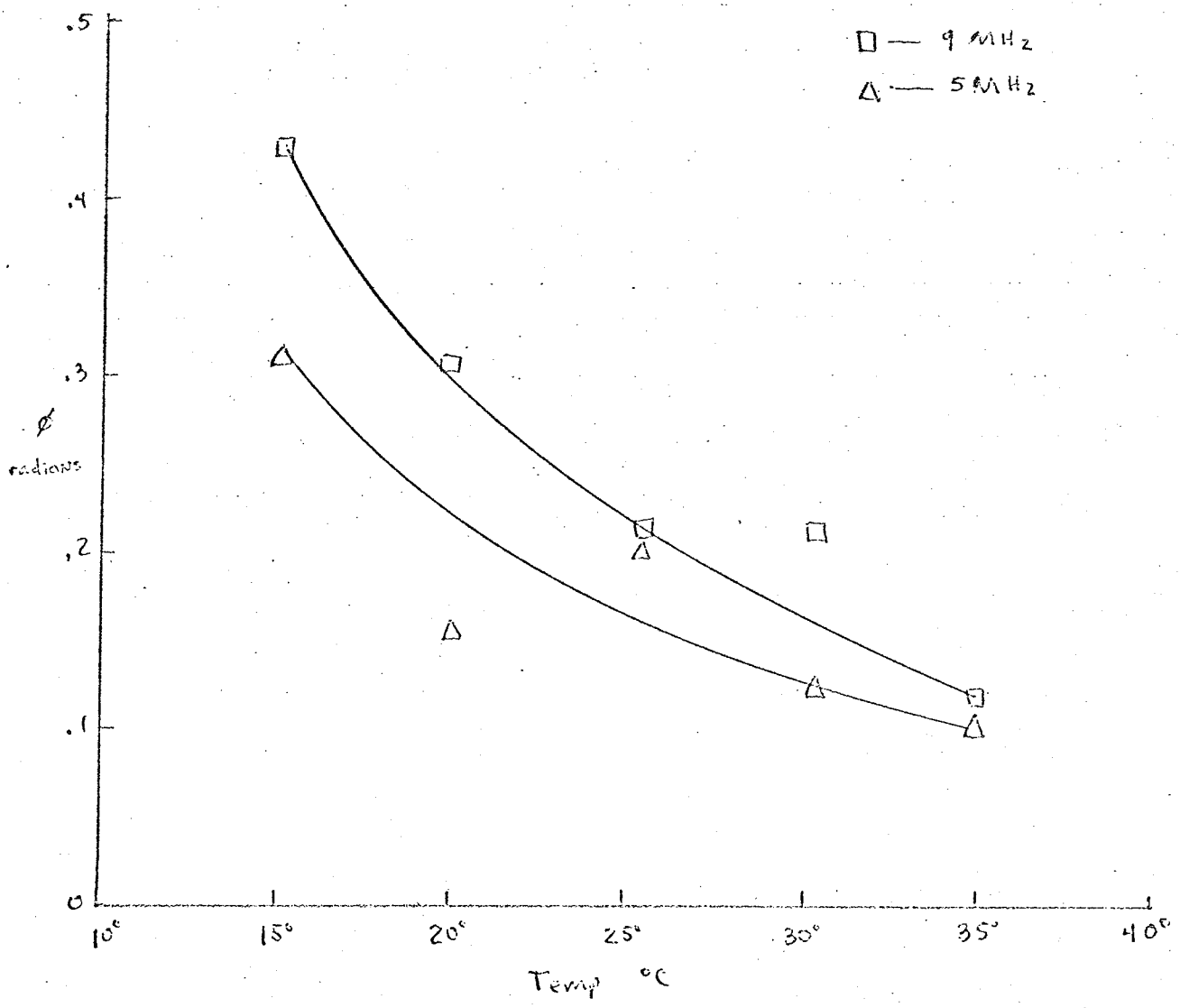

Fig. 7-8b.

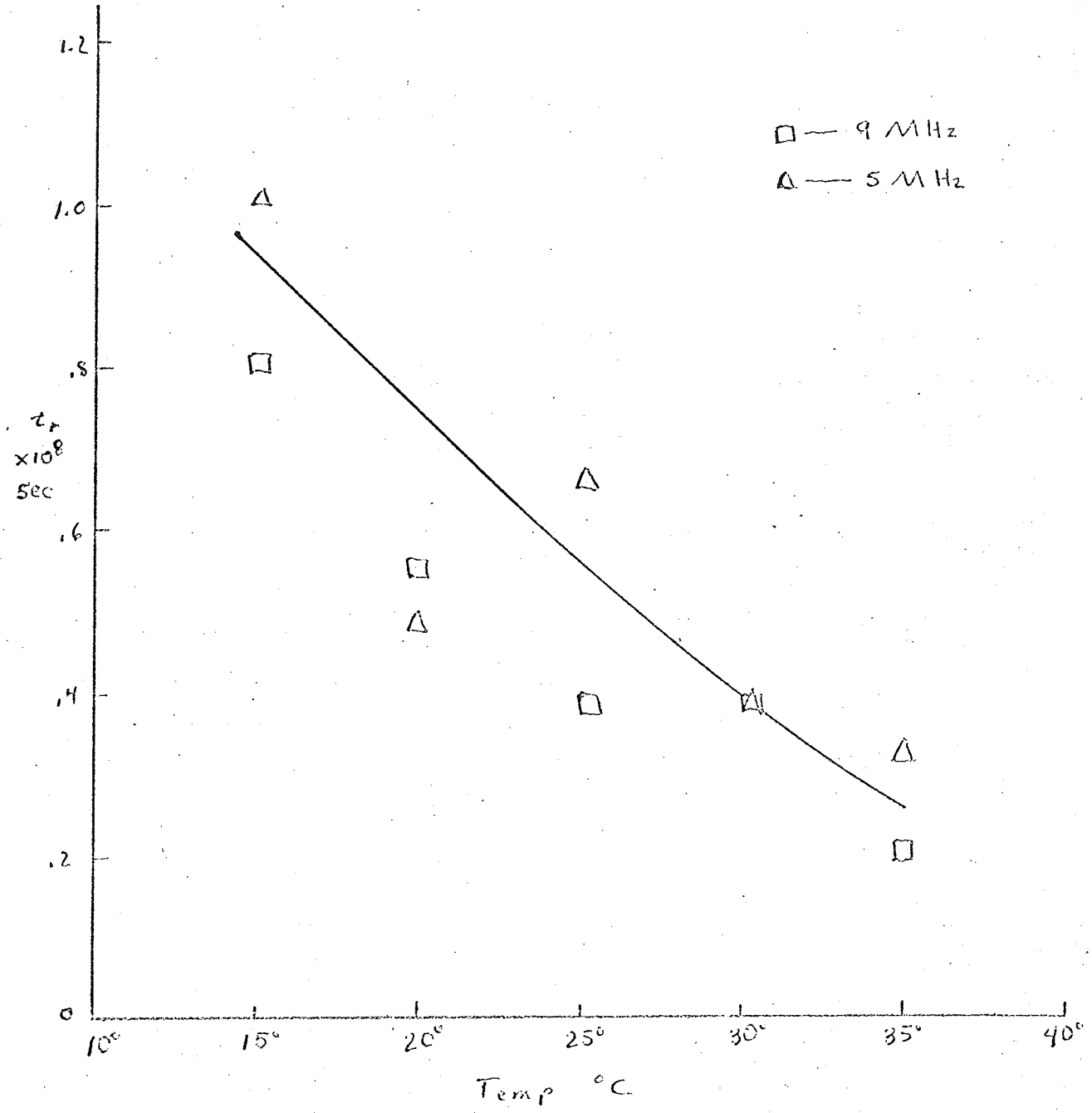
1.2
1.0
.8
.6
.4
.2
0
t_r $\times 10^8$ Sec
□ — 9 MHz
Δ — 5 MHz
10°
15°
20°
25°
30°
35°
40°
Temp °C

Fig. 7-8c.

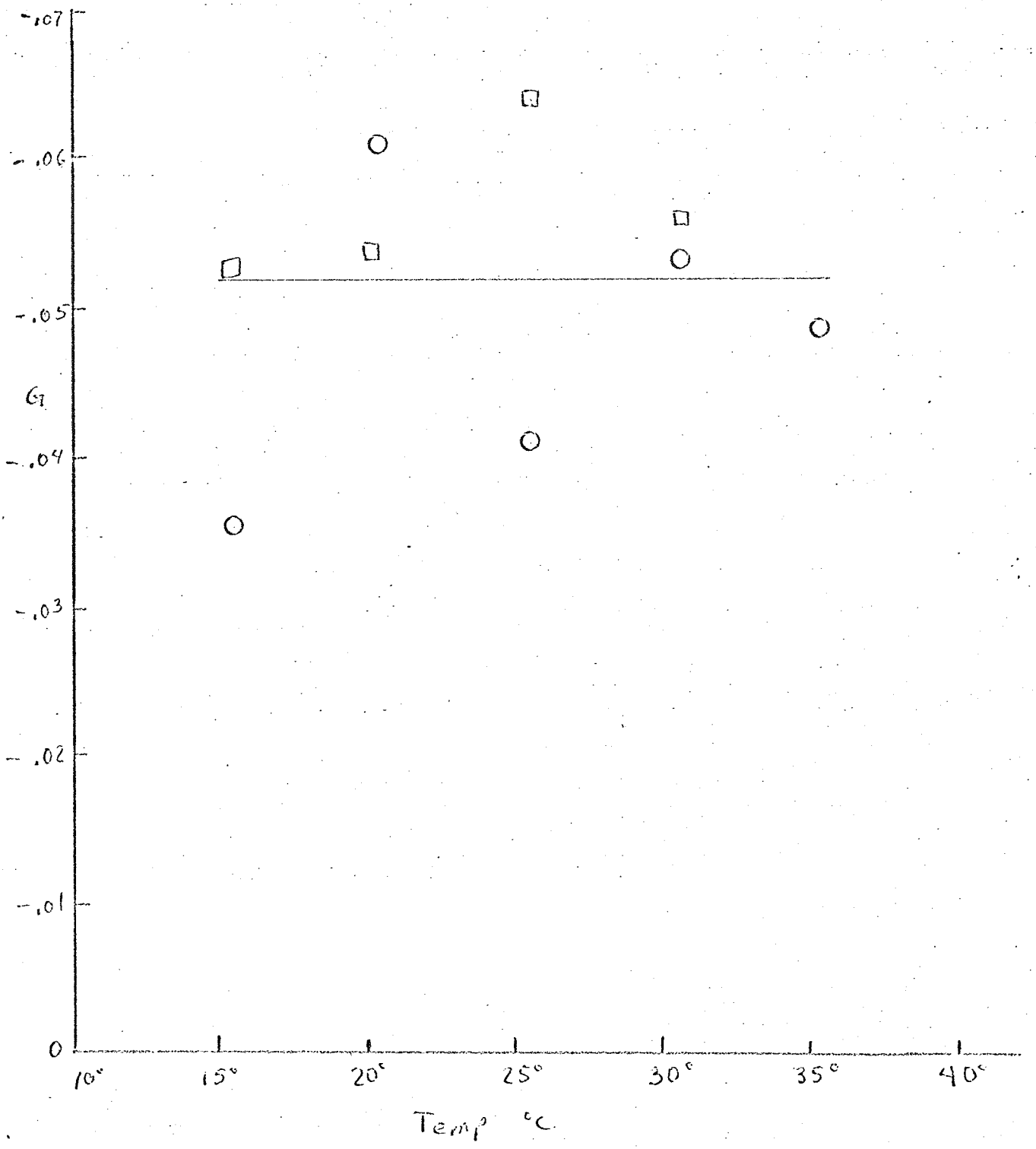

Fig. 7-8d.

background resulting in considerable scatter in both the relaxation time and the G coefficient. Surprisingly, the value of G found is nearly the same as for castor oil. Since the coefficient of viscosity for oleic acid is smaller than castor oil by nearly 2.5 times (Keffler and McLean, 1935), then the Maxwell constant for oleic acid must be correspondingly larger than that of castor oil.

When investigating the properties of polyethylene glycol (PEG), a modification to the definition of G must be made to account for the differences in the concentration of various samples. In order to compare the results of the birefringence measurements in PEG solutions with the pure fluids investigated earlier, the concentration is defined as the number of grams of PEG in one gram of solution. This definition, then, leads to a number which is the value $[G]_{sp}$ and represents the value of G at 100% concentration or a pure liquid, even though the material may not, in fact, be a liquid at the temperature used. This procedure differs markedly from the usual one in organic chemistry where the properties of a material are investigated as the concentration goes to zero.

The data obtained for PEG (20,000 molecular weight dissolved in water) is summarized in Table 7-1. The values for $[G]_{sp}$ are lower than the values for castor oil and oleic acid by about a factor of 4. However, the apparent relaxation times and phase angles fall between them. Additional

Table 7-1. Summary of data obtained for Poly Ethylene Glycol (PEG) 20k M.W. dissolved in water and Ethyl Cinnamate (EC).

	c	T	f	ϵ/n_1	ϕ	t	$[G]_{sp}$
	g/g	°C	MHz		rad	$x10^{-8}$ sec	g/g
PEG	0.5	20	5	-0.0058	0.82	3.3	-0.013
PEG	0.4	20	5	-0.0036	0.68	2.5	-0.014
PEG	0.4	24	5	-0.0037	0.89	3.9	-0.012
PEG	0.4	24	9	-0.0048	0.84	2.0	-0.015
EC		15	9	-0.005			

differences are the positive temperature coefficient of the phase angle, the relative independence of the phase angle, when frequency is varied, and the variation of relaxation times with frequency. The slowly varying phase as a function of frequency and the variation in relaxation times as a function of frequency both indicate the presence of more than one relaxation frequency in the PEG solution. The number of frequencies at which data was obtained is too limited to determine the number and position of the relaxation frequencies. In theory, if one could make measurements on a wide variety of molecular weights, the size of the subunit involved could be obtained when the number of relaxations is reduced to one. Such a study was attempted but the birefringence of the lower molecular weights was too small to be measured.

The data on ethyl cinnamate (EC) was limited by the very small signals occurring during measurement. The birefringence noted in Table 7-1 is smaller than oleic acid.

Further, the relaxation frequency must be much greater than 9 MHz since no signal current was observed in the zero order. This would place the relaxation frequency above 100 MHz and place a lower limit on G of about -0.05, the value which is observed for castor oil and oleic acid, though there is no reason to expect the value to be the same.

VIII. DISCUSSION AND CONCLUSIONS

The initial experiments were undertaken to verify that taking the ratio of the phototube output currents for two orientations of the analyzing prism would allow determination of the birefringence induced by the passage of sound waves through the sample fluid. The necessity for taking a ratio results from the requirement, in a photoelectric detection method, for taking into account the variation in the intensity of the light source and in the transmission characteristics of the optical system. The results shown in the previous chapter show that excellent agreement is obtained between the experimental and theoretical values of the current ratio over a wide range of conditions. Although the magnitude of the acoustically induced birefringence could not be predicted in advance, once the birefringence has been measured for a particular set of conditions, then for variation of the acoustic amplitude, the different diffraction order, and for liquids exhibiting a single relaxation time, the acoustic frequency, the resultant changes in the magnitude of the current ratios could be predicted to within experimental accuracy. The agreement between theory and experiment is reasonably clear for castor oil but is less clear with the other fluids examined due to the increased experimental scatter accompanying the small birefringence exhibited by other fluids.

The small scatter in the castor oil birefringence data allows a partial comparison of the modified theory of Lucas (Eq. 2-5) and the theory of Peterlin (Eq. 2-13). Although both theories have the same dependence of the birefringence on the acoustic intensity and the same variation when the measuring frequency is near or above the relaxation frequency, they differ in their description of the optical parameters of the fluid and has, in addition, a viscosity term. Comparison of Fig. 7-7a with 7-7c indicates that the birefringence decreases at about the same rate as the relaxation time which, if the optical parameters do not change appreciably over the temperature range, is predicted by Eq. 2-13. However, in Eq. 2-5, the measured birefringence should decrease much faster due to the presence of the viscosity term. The viscosity of castor oil decreases by nearly a factor of ten over the temperature range in which measurements were made (14.4^{o} to 41.3^{o} at 3 MHz). It would appear then, that Eq. 2-13 more closely predicts the acoustically induced birefringence when the temperature of the fluid is varied than does Eq. 2-5. Similar conclusions can be made by comparison of Figs. 7-8a and 7-8c which show the results for oleic acid. The birefringence at 9 MHz decreases nearly the same rate as the relaxation time over the temperature range of 15.3^{o} to 35.0^{o}. However, the viscosity is decreasing by a factor of 3 so that the same discrepancy between Eqs. 2-5 and 2-13 still exists.

Zvetkov et al. (1946) measured the birefringence of castor oil as a function of temperature for both flow birefringence and near field acoustic birefringence methods and found that the Maxwell constant had a negative temperature coefficient for flow birefringence and a positive temperature coefficient for the acoustic birefringence at 2.8 MHz. If the ordinates of Fig. 7-72 are divided by the viscosity of the castor oil for each temperature, the resulting curve has a slope similar to the curve obtained by Zvetkov et al. They argued that the difference in slopes was due to the occurence of different mechanisms causing the birefringence in each case. They noted that the values of M for castor oil exceeded by several times the values determined for pure, aromatic liquids with highly anisotropic molecules and they attributed this fact to the presence of complexes of associated molecules which are themselves isotropic but, under the influence of a gradient field, become anisotropic due to the photoelastic effect. However, they cautioned that an exact molecular picture could not be given for such a complicated system as a viscous organic oil. The presence of associated complexes of molecules would help to explain the anomalous result of Hilyard (1963) who found that the relaxation time for n-dodecanol (a 12 carbon compound) was longer than that of oleic acid and linseed oil (18 carbon compounds). The size of the complexes formed in each liquid may not bear any relationship to the number of carbons in the molecule.

The frequencies at which measurements were made in the present study covered the range of 3 to 9 MHz. In this range, the use of Bessel functions to calculate the intensity of the electric vector in a given diffraction order would introduce substantial errors in the evaluation process. The current ratio variation as a function of frequency is shown in Figs. 7-2 through 7-4. The substantial changes in the shape of these curves do not occur when the Bessel function is used. The Bessel function is the same as the diffraction function for the special case of the geometry factor, Q equal to zero. Therefore, the use of the acoustic diffraction function to evaluate the data is essential to prevent erroneous results. Q does not have to be known very accurately in this frequency range in order to obtain accurate results, e.g., an error of 10% in Q would change the calculated value of $\Delta\sigma/\sigma$ less than 1%. For this reason only one Q was used for each frequency despite the variations in the velocity of sound with temperature and for different fluids. As the frequency of operation is increased, however, the value of Q must be known with increasingly better accuracy to maintain the 1% error in the evaluation of $\delta_y - \delta_x$ and $\Delta\sigma/\sigma$.

Some of the data in Chapter VII can be compared with data obtained by others. Riley and Klein (1969) give a value of G for castor oil of 0.048 at an unspecified temperature. This value agrees very well with the curve drawn in Fig. 7-7d for temperatures around room temperature. Unlike Fig. 7-7d, they noted that their data at 5 MHz did not agree with

the data obtained below 3 MHz and cited the use of Bessel functions in their data evaluation procedure as the possible cause.

Hilyard (1963) and Zvetkov et al. (1946) express their results in the form of the Sadron constant S

$$S = \varepsilon/g \tag{8-1}$$

where g is the velocity gradient. The results given in Chapter VII can be converted to this form by using

$$S = \left(\frac{\varepsilon}{n_1}\right) \frac{0.639\, n_o^2 - 0.395\, n_o - .263}{\omega} \tag{8-2}$$

Hilyard obtains a Sadron constant for oleic acid near field case of 12.0×10^{-11} at 20°C. Using data from Fig. 7-8a, we get 14.1×10^{-11} in the far field. Although the data for ethyl cinnamate cannot be compared directly since Hilyard's data is at 20° and the data listed in Table 7-1 is at 15°, the ratio of the birefringence obtained for oleic acid to the birefringence obtained for ethyl cinnamate is 4.5 at 20° for Hilyard and 4.2 at 15° for the data in Chapter VII. Although the near field and the far field data for oleic acid agree fairly closely, Hilyard was unable to determine the relaxation time since the measurements were taken at an acoustic frequency much less than the relaxation frequency. The far field data was taken in the same frequency range and yet, the relaxation time could be measured. This demonstrates the advantage of far field measurements.

The results for polyethylene glycol shown in the previous chapter, along with the results of Hilyard (1963) and

Zvetkov et al. (1946) for polyisobutylene and polystyrene, indicate that the birefringence exhibited by these polymers is less than those exhibted by the viscous oils. In addition, the variation of the birefringence with frequency indicates that there exists more than one relaxation time. Zvetkov et al. point out that both the polyisobutylene and the polystyrene solutions exhibit appreciable flow birefringence and that the low value of acoustic birefringence observed is due to the inability of the polymers to follow the rapid variations of the acoustic wave.

According to the theory of Peterlin (1967a), a polymer composed of many subunits connected as a flexible chain exhibits a very broad transition region as the measuring frequency is increased from below to above the relaxation frequency. He notes that methods of measuring acoustic birefringence up to that time did not yield phase information. He derives the frequency variation for both the amplitude and the phase of the birefringence for several models of polymer solutions. By taking measurements over a wide frequency range, some indication of the molecular structure can be obtained as well as the number of subunits in the chain. The polyethylene glycol data shown in Table 7-1 did not cover sufficiently wide range to provide much information about its structure, but because the phase angle did not change appreciably between the two measuring frequencies, implies that a fairly large number of subunits must be present. Clearly, a very wide range of frequencies must be used, perhaps 3 orders of magnitude.

Solutions of polymers exhibit considerably less birefringence than do viscous oils such that attempts at such measurements over a wide band of frequencies are fraught with difficulties. At the lower frequencies, the birefringence is simply too small to be measured. At the higher frequencies, birefringence measurements are difficult since the high absorption of sound in the sufficiently concentrated solutions restricts appreciably the range of intensity in which measurements can be made. An obvious solution is that of developing even more sensitive measuring instrumentation. The apparatus described in Chapter V is limited in sensitivity by the extinction ratio of the polarizing prisms used and methods to increase the extinction ratio were discussed. Because the detection regime is quadratic, the extinction ratio must be increased by two orders of magnitude in order to obtain one order of magnitude improvement in the sensitivity and prisms with such high extinction ratio are not available at present. The technique for accounting for the leakage of light through the prisms is only an approximation and more detailed information must be obtained, such as the source of the leakage, before a more complete correction methodology emerges, or a more improved prism design can result. Until improved sensitivity becomes available, by whatever means, it may not be possible to obtain details of configuration and structure of molecules in solution by acoustically induced birefringence methods.

REFERENCES

Abramovitz, M. and Stegun, I. 1964. National Bureau of Standards Publication AMS 55, "Handbook of Mathematical functions".

Badoz, J. 1957. Thesis, University of Paris.

Barnard, J. W., Fry, W. J., Fry, F. J. and Brennan, J. 1956. Arch. Neurol. Psychiat., 75, 15.

Born, M. 1918. Ann. Physik, 55, 177.

Cairns, J. 1961. J. Mol. Biol. 3, 756.

Cerf, R. 1958. J. Phys. Radium, 19, 122; Adv. in Polym. Science, 1959, 1, 382.

Dunn, F. 1958. Am. J. of Phys. Med., 37, 148.

Dunn, F. 1965. Acoustic Absorption by Biological Materials. Proc. Third Symposium Ultrasound in Biology and Medicine, ed. E. Kelley, p. 51.

Frenkel, J. 1944. Acta Physiochim, U.R.S.S., 19, 51.

Frenkel, J. 1946. Kinetic Theory of Liquids. Oxford: Clarendon Press, p. 292.

Fry, W. J. 1958. Use of Intense Ultrasound in Neurological Research, Am. J. Phys. Med. 37, 143-147.

Hall, L. 1948. Physical Rev. 73, 775.

Hawley, S. A., Macleod, R. M., and Dunn, F. 1963. J. Acoust. Soc. Am. 35, 1285.

Henrici, P. 1962. "Discrete Variable Methods in Ordinary Differential Equations," New York: McGraw Hill.

Hilyard, N. C., and Jerrard, H. G. 1962. J. Appl. Phys., 33, 3470.

Hilyard, N. 1963. Thesis, University of Southampton.

Jeffery, G. B. 1922. Proc. Roy. Soc. (London), A102, 161.

Jerrard, H. G. 1959. Chem. Revs., 59, 345.

Keffler, A., and McLean, D. 1935. J. Soc. Chem. Ind., 54, 178T.

Langevin, P. 1910. Le Radium, 7, 249.

Levinthal, C. and Davison, P. F. 1961. J. Mol. Biol., 3, 674.

Lucas, R. 1939. Rev. Acoust., 8, 121.

Macleod, R. 1966. Ph.D. Thesis, University of Illinois.

Nomoto, O., Kishimoto, T. and Ikeda, T. 1952. Bull. Kobyashi Institute, 2, 72.

Oka, S. 1940. Z. Physik, 116, 632 also Kolloid, Z. 1939. 87, 37.

Peterlin, A. 1950. J. Phys. Radium, 11, 45.

Peterlin, A. 1967a. J. Poly. Sci. A., 5, 21.

Raman and Krishnan. 1928. Phil. Mag. 5, 769.

Raman, C. V. and Nath, N. S. N. 1935. Proc. Indian Acad. Sci., 2, p. 406.

Riley, W. and Klein, R. 1967. J. Acoust. Soc. Amer., 42, 1258.

Riley, W. and Klein, R. 1969. J. Acoust. Soc. Amer., 45, 578.

Rouse, P. E. 1953. J. Chem. Phys. 21, 1272.

Stokes, G. G. 1845. Trans. Cambridge Phil. Soc., 8, 1.

Welkowitz, W. and Fry, W. J. 1956. J. Cell. and Comp. Physiol., 48, 435.

Yariv, Amnon. Introduction to Optical Electronics. New York: Holt, Rinehart and Winston, Inc., 1971, p. 273.

Zvetkov, V., Mindlina, A. and Makarov, G. 1946. Acta Physio. Chim. U.R.S.S., 21, 135.

APPENDIX 1

A FORTRAN LANGUAGE COMPUTER PROGRAM TO EVALUATE THE ACOUSTIC DIFFRACTION FUNCTION

A complete program for evaluating the components of the electric vector in the various diffraction orders produced when light is diffracted by an acoustic wave has been written and was used to produce tables from which the experimental data could be evaluated. Klein and Cook (1967) derived a recurrence relation for the diffraction function

$$\frac{d\psi_n}{dz} = \frac{nQ}{2d}(n - 2\alpha) - \frac{v}{2d}(\psi_{n-1} - \psi_{n+1}) \qquad \text{(A1-1)}$$

This relation was treated as a set of coupled, difference differential equations and the program described below is a modification of a method for integrating a differential equation using numerical techniques (Henrici, 1962).

The main program consists of an initialization section, a modified Hamming predictor-corrector method of integration, and an output section which also checks the accumulated error. The information required to be input has the following items: NMAX is the maximum number of orders used during recurrence. All larger orders are then considered to be negligible. The use of a small NMAX reduces the calculation time but decreases the accuracy of the results. For most of the tables given in Appendix 2, the value of NMAX is 10.

STEP is the number of steps the program should take when integrating from 0 to Z, i.e., the width of the sound beam. The minimum number of steps is four since the procedure begins with a Runge-Kutta integration and no error estimate is available. The number of steps needed is directly related to the desired accuracy. This accuracy is written in the program as 10^{-4} but before running the tables, a number was inserted by hand into the computer to give an accuracy of 10^{-5}. If the accumulated error over all the diffraction orders exceeds 10^{-5}, then the program will automatically double the number of steps for the integration, put out a message, and then begin the integration procedure over again.

ALPHA is the normalized angle of incidence of the light beam and is given by Klein and Cook as

$$\alpha = -(n_0 k' \sin\theta)/k$$

where θ is the actual angle of incidence, the geometry factor Q is given as

$$Q = \frac{k^2 d}{n_0 k'}$$

Q is used as itself in the program.

VMAX is the value of v for which the integration is taking place. It is not possible to integrate the Eq. A1-1 and yield as intermediate results values of ψ for intermediate values of v. In order to make a table, VMAX is entered and used as the first value for integration. Then, the VMAX

is stepped in intervals of 0.1 up to the value given by VST, the last v desired in the table.

NDAT is the diffraction order for which the table is desired.

The program is liberally commented so that an additional description will not be given here. The integration procedure is a modified version of subroutine HPCG given in the IBM 360 computer Scientific Subroutine Package as described in IBM manual H20-205.

```
C
C       THE FOLLOWING PROGRAM EVALUATES THE INTENSITY
C       OF LIGHT IN VARIOUS DIFFRACTION ORDERS WHEN
C       LIGHT IS DIFFRACTED BY ULTRASONIC WAVES.
C       THE PROCEDURE INTEGRATES THE RECURRENCE RELATION
C       DEVELOPED BY W.R. KLEIN USING A HAMMING MODIFIED
C       PREDICTOR-CORRECTOR METHOD.  SINCE THE METHOD
C       IS NOT SELF STARTING, A RUNGE-KUTTA METHOD
C       SUGGESTED BY RALSTON IS USED TO OBTAIN THE FIRST
C       THREE STEPS AFTER THE INITIAL VALUES ARE
C       GIVEN.  THE HAMMING METHOD IS USED FROM THEN ON.
C
C       ..................................................
C
        COMMON PHI,DERIV,NMAX,ALPHA,Q,VMAX,VACT
        DIMENSION PHI(42),DERIV(42),WORK(9,1)
C
C       OBTAIN THE INTEGRATION PARAMETERS.
40      READ (1,100) NMAX,STEP,ALPHA,Q,VMAX,NDAT,VST
100     FORMAT('NO. OF ORDERS USED = ',I4/
       1'NO. OF STEPS = ',F7.2/'ANGLE OF INCIDENT LIGHT = '
       2,F7.2/'Q FACTOR = ',F7.2/'FIRST V = ',F7.2,/
       3'OUTPUT ORDER NO. = ',I4,/'STOP TABLE AT V = ',F7.2)
C
C       PHI IS THE CALCULTED FUNCTION VALUE
C       DERIV IS THE DERIVATIVE AT THAT V
C       WORK STORES THE VALUES OF PREVIOUS STEPS.
C       NMAX IS THE MAXIMUM NUMBER OF DIFFRACTION ORDERS
C         USED IN THE RECURRENCE FORMULA AND IS = OR < 10
C       STEP IS THE NO. OF STEPS TO INTEGRATE.
C       ALPHA IS THE ANGLE THE LIGHT MAKES WITH
C         THE SOUND BEAM (NORMALIZED)
C       Q IS THE GEOMETRY FACTOR FOR THE SOUND AND LIGHT.
C       VMAX IS THE ENDPOINT OF THE INTEGRATION.
C       NDAT IS THE NO. OF THE ORDER TO BE OUTPUT.
C       VST IS THE LAST TABLE ENTRY TO BE OUTPUT.
C          THE TABLE ALWAYS HAS STEPS OF .1
C
C
C       CONVERT STEPS TO STEP SIZE IN UNITS OF Z/L.
        STEP=.5/STEP
        NOR=2*NMAX+1
        NDIM=2*NOR
C
C       CALCULATE THE SUBSCRIPT FOR THE ORDER TO BE
C       OUTPUT.
        ID=NMAX+1+NDAT
        JD=ID+NOR
C
C       INITIALIZE PHI AT V=0.
C
41      DO 1 I=1,NDIM
1       PHI(I)=0.
        PHI(NMAX+1)=1.
```

```
C
C       PUT OUT HEADING.
        V=0.
        CALL RECUR (V)
        WRITE (1,110)
110     FORMAT(/4X,'V',8X,'REAL',12X,'IMAG'/)
C
C       BEGIN RUNGE-KUTTA STARTING PROCEDURE.
        DO 2 I=1,NDIM
        WORK(5,I)=DERIV(I)
2       WORK(1,I)=PHI(I)
C
C       ..................................................
C
C       FOURTH ORDER RUNGE-KUTTA.
C
        DO 56 J=1,3
        DO 51 I=1,NDIM
        Z=WORK(J+4,I)*STEP
        WORK(4,I)=Z
51      PHI(I)=WORK(J,I)+.4*Z
C
C       WORK(4,I),WORK(8,I),WORK(9,I),AND Z
C       ARE USED AS TEMPORARY STORAGE LOCATIONS.
C
        Z=V+.4*STEP
        CALL RECUR (Z)
        DO 52 I=1,NDIM
        Z=DERIV(I)*STEP
        WORK(8,I)=Z
52      PHI(I)=WORK(J,I)+.29697609*WORK(4,I)+.15875964 5*Z
C
        Z=V+.45573725 4*STEP
        CALL RECUR (Z)
        DO 53 I=1,NDIM
        Z=STEP*DERIV(I)
        WORK(9,I)=Z
53      PHI(I)=WORK(J,I)+.21810038 8*WORK(4,I)-3.05096515
     1*WORK(8,I)+3.83286476*Z
C
        Z=V+STEP
        CALL RECUR (Z)
        DO 54 I=1,NDIM
54      PHI(I)=WORK(J,I)+.17476028 2*WORK(4,I)-.55148066 3
     1*WORK(8,I)+1.20553560*WORK(9,I)+.17118478 1*STEP
     2*DERIV(I)
C
        V=Z
        CALL RECUR (V)
        DO 55 I=1,NDIM
        WORK(J+1,I)=PHI(I)
55      WORK(J+5,I)=DERIV(I)
C
56      CONTINUE
C
```

```
C     ..................................................
C
C     REFINE RUNGE-KUTTA WITH FOURTH ORDER
C     INTERPOLATION FORMULAS.
C
      V=0.
      DO 3 I=1,NDIM
3     PHI(I)=WORK(1,I)+STEP*(.375*WORK(5,I)+.791666667
     1*WORK(6,I)-.208333333*WORK(7,I)+.0416666667*DERIV(I))
C
      N=1
4     V=V+STEP
      CALL RECUR (V)
      N=N+1
      IF(N-4)5,11,11
5     DO 6 I=1,NDIM
      WORK(N,I)=PHI(I)
6     WORK(N+4,I)=DERIV(I)
      IF(N-3)7,9,11
C
7     DO 8 I=1,NDIM
      Z=WORK(6,I)*4.
8     PHI(I)=WORK(1,I)+.333333333*STEP*(WORK(5,I)+Z
     1+WORK(7,I))
      GO TO 4
C
9     DO 10 I=1,NDIM
      Z=(WORK(6,I)+WORK(7,I))*3.
10    PHI(I)=WORK(1,I)+.375*STEP*(WORK(5,I)+Z+WORK(8,I))
      GO TO 4
C
C     RUNGE-KUTTA REFINEMENT DONE.  BEGIN HAMMING METHOD.
C
11    DO 111 I=1,NDIM
111   WORK(9,I)=0.
      GO TO 14
C
C     INTERCHANGE ROWS TO UPDATE.
12    DO 13 J=2,4
      DO 13 I=1,NDIM
      WORK(J-1,I)=WORK(J,I)
13    WORK(J+3,I)=WORK(J+4,I)
C
C     COMPUTE PREDICTOR FOR NEXT PHI
C
14    DO 15 I=1,NDIM
      WORK(4,I)=PHI(I)
15    WORK(8,I)=DERIV(I)
      V=V+STEP
      DO 16 I=1,NDIM
      Z=WORK(1,I)+1.33333333*STEP*(WORK(8,I)*2.-WORK(7,I)
     1+WORK(6,I)*2.)
C
C     COMPUTE MODIFIER.  PREDICTOR IS STORED IN ROW 11
C     AND MODIFIER IS STORED IN PHI.
```

```
      PHI(I)=Z-.925619835*WORK(9,I)
16    WORK(9,I)=Z
C
C     GET DERIVATIVE OF MODIFIED PREDICTOR.
C
      CALL RECUR (V)
C
C     COMPUTE THE CORRECTOR.
C
      DO 17 I=1,NDIM
      Z=.125*(9.*WORK(4,I)-WORK(2,I)+3.*STEP*(DERIV(I)
     1+WORK(8,I)*2.-WORK(7,I)))
C
C     WORK ROW 9 WILL NOW HOLD THE DIFFERENCE
C     BETWEEN THE PREDICTOR AND THE CORRECTOR.
C
      WORK(9,I)=WORK(9,I)-Z
C
C     THE FINAL VALUE OF PHI IS NOW COMPUTED.
C
17    PHI(I)=Z+.0743801653*WORK(9,I)
C
C     NOW COMPUTE AN ESTIMATE OF THE TRUNCATION ERROR.
C
      CALL RECUR (V)
      Z=0.
      DO 18 I=1,NDIM
18    Z=Z+ABS(WORK(9,I))
      Z=Z/FLOAT(NDIM)
      IF(Z-1.E-4) 19,30,30
C
C     THE ERROR IS REASONABLE.  IS THE INTEGRATION FINISHED?
C
19    IF(V-.499999) 12,20,20
C
C     INTEGRATION FINISHED.  OUTPUT TABLE VALUES.
C
20    WRITE (1,120) VACT,PHI(ID),PHI(JD)
120   FORMAT (F6.3,2E16.8)
C
C     IS TABLE FINISHED?
C
      VMAX=VMAX+.1
      IF(VMAX-VST-.0001) 41,21,21
C
C     DONE.  PUT OUT ERROR ESTIMATE AND SUM OF THE
C     DIFFRACTION ORDERS SQUARED.
C
21    WRITE (1,125),
125   FORMAT (/'THE LOCAL TRUNCATION ERROR IS = ',E12.4/
     1'THE SUM OF THE DIFFRACTION ORDERS SQUARED = ',F13.9//)
      CALL IOH(Z)
      Z=.0
      DO 22 I=1,NOR
      J=I+NOR
```

```
22      Z=Z+PHI(I)*PHI(I)+PHI(J)*PHI(J)
        CALL IOH(Z)
        FINI
        PAUSE
        GO TO 40
30      STEP=.5*STEP
        WRITE(1,130)
130     FORMAT ('**** UNSTABLE.  HALVE STEP SIZE.'/)
        GO TO 41
        END
```

```
C     ..................................................
C
C     THE FOLLOWING SUBROUTINE IS USED TO COMPUTE THE
C     DERIVATIVE OF PHI FOR USE WITH THE HAMMING METHOD
C     FOR INTEGRATING SIMULTANEOUS DIFFERENTIAL EQUATIONS.
C     ALL NEEDED PARAMETERS ARE PASSED THROUGH COMMON
C
C     ..................................................
C
      SUBROUTINE RECUR (X)
      COMMON PHI,DERIV,NMAX,ALPHA,Q,VMAX,V
      DIMENSION PHI(42),DERIV(42)
C
C     BEGIN AT HIGHEST + ORDER.
      V=VMAX*X*2.
      NOR=2*NMAX+1
      EN=NMAX
      Z=EN*Q*(EN-2.*ALPHA)
      IJ=2*NOR
      DERIV(NOR)=-(VMAX*(PHI(NOR-1))+Z*PHI(IJ))
      DERIV(IJ)=-(VMAX*(PHI(IJ-1))-Z*PHI(NOR))
C
C     BEGIN RECURRENCE OF INTERMEDIATE ORDERS.
C
      I=NOR-2
      DO 1 KN=1,I
      EN=NMAX-KN
      Z=EN*Q*(EN-2.*ALPHA)
      IJ=NOR-KN
      DERIV(IJ)=-VMAX*(PHI(IJ-1)-PHI(IJ+
     11))-Z*PHI(IJ+NOR)
      IJ=NOR*2-KN
1     DERIV(IJ)=-VMAX*(PHI(IJ-1)-PHI(
     1IJ+1))+Z*PHI(IJ-NOR)
C
C     FINISH LAST ORDER.
C
      EN=-NMAX
      Z=EN*Q*(EN-2.*ALPHA)
      IJ=NOR+1
      DERIV(1)=VMAX*PHI(2)-Z*PHI(IJ)
      DERIV(IJ)=VMAX*PHI(IJ+1)+Z*PHI(1)
      RETURN
      END
```

APPENDIX 2

TABLES OF THE ACOUSTIC DIFFRACTION FUNCTION

NO. OF ORDERS USED = 10
NO. OF STEPS = 4.
ANGLE OF INCIDENT LIGHT = 0.
Q FACTOR = .1825
FIRST V = .1
DIFF. ORDER = 0
STOP AT V = 9.9

V	REAL	IMAG
.100	.99750331E+00	-.75914699E-04
.200	.99003185E+00	-.30251850E-03
.300	.97764147E+00	-.67640494E-03
.400	.96042476E+00	-.11919441E-02
.500	.93851019E+00	-.18413536E-02
.600	.91206113E+00	-.26147967E-02
.700	.88127449E+00	-.35005056E-02
***** UNSTABLE. HALVE STEP SIZE.		
.800	.84637957E+00	-.44863788E-02
.900	.80763448E+00	-.55551753E-02
1.000	.76532615E+00	-.66912281E-02
1.100	.71976680E+00	-.78767915E-02
1.200	.67129155E+00	-.90931329E-02
1.300	.62025562E+00	-.10320772E-01
1.400	.56703148E+00	-.11539731E-01
1.500	.51200586E+00	-.12729784E-01
***** UNSTABLE. HALVE STEP SIZE.		
1.600	.45558177E+00	-.13870624E-01
1.700	.39815632E+00	-.14942327E-01
1.800	.34014324E+00	-.15925496E-01
1.900	.28195383E+00	-.16801507E-01
2.000	.22399721E+00	-.17552772E-01
2.100	.16667708E+00	-.18162980E-01
2.200	.11038839E+00	-.18617326E-01
2.300	.55514444E-01	-.18902702E-01
2.400	.24235654E-02	-.19007904E-01
2.500	-.48533671E-01	-.18923790E-01
2.600	-.97027093E-01	-.18643424E-01
2.700	-.14274947E+00	-.18162203E-01
2.800	-.18541906E+00	-.17477941E-01
2.900	-.22478143E+00	-.16590938E-01
3.000	-.26061154E+00	-.15504018E-01
3.100	-.29271520E+00	-.14222530E-01
3.200	-.32093051E+00	-.12754330E-01
***** UNSTABLE. HALVE STEP SIZE.		
3.300	-.34512834E+00	-.11108300E-01
3.400	-.36521595E+00	-.92998744E-02
3.500	-.38113231E+00	-.73426842E-02
3.600	-.39285204E+00	-.52537950E-02
3.700	-.40038450E+00	-.30522253E-02
3.800	-.40377309E+00	-.75875785E-03
3.900	-.40309458E+00	.16042775E-02
4.000	-.39845848E+00	.40132229E-02
4.100	-.39000502E+00	.64433723E-02
4.200	-.37790444E+00	.88692010E-02

4.300	-.36235480E+00	.11264676E-01
4.400	-.34357999E+00	.13603538E-01
4.500	-.32182753E+00	.15859582E-01
4.600	-.29736644E+00	.18006976E-01
4.700	-.27048436E+00	.20020551E-01
4.800	-.24148502E+00	.21876087E-01
4.900	-.21068536E+00	.23550614E-01
5.000	-.17841267E+00	.25022684E-01
5.100	-.14500167E+00	.26272629E-01
5.200	-.11079134E+00	.27282825E-01
5.300	-.76122125E-01	.28037893E-01
5.400	-.41332723E-01	.28524938E-01
5.500	-.67571989E-02	.28733700E-01
5.600	.27277819E-01	.28656722E-01
5.700	.60456074E-01	.28289473E-01
5.800	.92474286E-01	.27630446E-01
5.900	.12364478E+00	.26681225E-01
6.000	.15189770E+00	.25446485E-01
6.100	.17878337E+00	.23934024E-01
6.200	.20347421E+00	.22154708E-01
6.300	.22576659E+00	.20122402E-01
6.400	.24548229E+00	.17853863E-01
***** UNSTABLE. HALVE STEP SIZE.		
6.500	.26246979E+00	.15368373E-01
6.600	.27660699E+00	.12688747E-01
6.700	.28779748E+00	.98390116E-02
6.800	.29597534E+00	.68458069E-02
6.900	.30110394E+00	.37376789E-02
7.000	.30317606E+00	.54478756E-03
7.100	.30221349E+00	-.27013855E-02
7.200	.29826661E+00	-.59683325E-02
7.300	.29141338E+00	-.92228819E-02
7.400	.28175846E+00	-.12431527E-01
7.500	.26943209E+00	-.15560755E-01
7.600	.25458803E+00	-.18577433E-01
7.700	.23740251E+00	-.21449162E-01
7.800	.21807196E+00	-.24144575E-01
7.900	.19681084E+00	-.26633747E-01
8.000	.17384988E+00	-.28888492E-01
8.100	.14943319E+00	-.30882672E-01
8.200	.12381624E+00	-.32592523E-01
8.300	.97263003E-01	-.33996903E-01
8.400	.70043779E-01	-.35077579E-01
8.500	.42432075E-01	-.35819405E-01
8.600	.14702333E-01	-.36210563E-01
8.700	-.12872827E-01	-.36242695E-01
8.800	-.40025087E-01	-.35911040E-01
8.900	-.66493081E-01	-.35214520E-01
9.000	-.92024718E-01	-.34155818E-01
9.100	-.11637941E+00	-.32741333E-01
9.200	-.13933054E+00	-.30981218E-01
9.300	-.16066717E+00	-.28889302E-01
9.400	-.18019609E+00	-.26482956E-01
9.500	-.19774352E+00	-.23782975E-01
9.600	-.21315651E+00	-.20813415E-01
9.700	-.22630419E+00	-.17601336E-01
9.800	-.23707906E+00	-.14176607E-01
9.900	-.24539738E+00	-.10571562E-01

NO. OF ORDERS USED = 10
NO. OF STEPS = 4.
ANGLE OF INCIDENT LIGHT = 0.
Θ FACTOR = .1825
FIRST V = .1
DIFF. ORDER = 1
STOP AT V = 6.4

V	REAL	IMAG
.100	-.49868454E-01	-.22749336E-02
.200	-.99364404E-01	-.45215298E-02
.300	-.14811845E+00	-.67117818E-02
.400	-.19576735E+00	-.88183404E-02
.500	-.24195706E+00	-.10814832E-01
.600	-.28634568E+00	-.12676170E-01
.700	-.32860623E+00	-.14378844E-01
***** UNSTABLE. HALVE STEP SIZE.		
.800	-.36842562E+00	-.15900797E-01
.900	-.40551958E+00	-.17222998E-01
1.000	-.43961916E+00	-.18327986E-01
1.100	-.47048213E+00	-.19201060E-01
1.200	-.49789284E+00	-.19830232E-01
1.300	-.52166409E+00	-.20206376E-01
1.400	-.54163842E+00	-.20323342E-01
1.500	-.55768948E+00	-.20178035E-01
***** UNSTABLE. HALVE STEP SIZE.		
1.600	-.56972134E+00	-.19768456E-01
1.700	-.57767526E+00	-.19101057E-01
1.800	-.58152130E+00	-.18180552E-01
1.900	-.58126413E+00	-.17016149E-01
2.000	-.57694161E+00	-.15619990E-01
2.100	-.56862387E+00	-.14007020E-01
2.200	-.55641321E+00	-.12194834E-01
2.300	-.54044260E+00	-.10203476E-01
2.400	-.52087470E+00	-.80552337E-02
2.500	-.49790022E+00	-.57743831E-02
2.600	-.47173628E+00	-.33869294E-02
2.700	-.44262432E+00	-.92031149E-03
2.800	-.41082800E+00	.15969005E-02
2.900	-.37663093E+00	.41353233E-02
3.000	-.34033393E+00	.66650951E-02
3.100	-.30225271E+00	.91562084E-02
3.200	-.26271477E+00	.11578856E-01
***** UNSTABLE. HALVE STEP SIZE.		
3.300	-.22206669E+00	.13902118E-01
3.400	-.18063344E+00	.16100395E-01
3.500	-.13876936E+00	.18145239E-01
3.600	-.96820668E-01	.20010966E-01
3.700	-.55131001E-01	.21673697E-01
3.800	-.14038337E-01	.23111663E-01
3.900	.26127872E-01	.24305453E-01
4.000	.65049308E-01	.25238247E-01
4.100	.10242164E+00	.25896042E-01
4.200	.13795688E+00	.26267807E-01

4.300	.17138581E+00	.26345647E-01
4.400	.20246020E+00	.26124912E-01
4.500	.23095463E+00	.25604261E-01
4.600	.25666843E+00	.24785729E-01
4.700	.27942710E+00	.23674710E-01
4.800	.29908365E+00	.22279929E-01
4.900	.31551965E+00	.20613376E-01
5.000	.32864604E+00	.18690200E-01
5.100	.33840350E+00	.16528560E-01
5.200	.34476302E+00	.14149468E-01
5.300	.34772552E+00	.11576551E-01
5.400	.34732189E+00	.88358427E-02
5.500	.34361215E+00	.59554988E-02
5.600	.33668487E+00	.29655059E-02
5.700	.32665614E+00	-.10261551E-03
5.800	.31366798E+00	-.32161659E-02
5.900	.29788732E+00	-.63415921E-02
6.000	.27950379E+00	-.94448707E-02
6.100	.25872818E+00	-.12491852E-01
6.200	.23579008E+00	-.15448652E-01
6.300	.21093586E+00	-.18282011E-01
6.400	.18442615E+00	-.20959658E-01

NO. OF ORDERS USED = 10
NO. OF STEPS = 4.
ANGLE OF INCIDENT LIGHT = 0.
Q FACTOR = .1825
FIRST V = .1
DIFF. ORDER = 2
STOP AT V = 8.

V	REAL	IMAG
.100	.12308511E-02	.18856927E-03
.200	.49112167E-02	.75202316E-03
.300	.11004646E-01	.16836247E-02
.400	.19450768E-01	.29722274E-02
.500	.30165848E-01	.46023973E-02
.600	.43043570E-01	.65545811E-02
.700	.57956027E-01	.88053201E-02
***** UNSTABLE. HALVE STEP SIZE.		
.800	.74754162E-01	.11330670E-01
.900	.93271596E-01	.14095551E-01
1.000	.11332303E+00	.17068527E-01
1.100	.13470783E+00	.20213567E-01
1.200	.15721142E+00	.23492377E-01
1.300	.18060734E+00	.26864825E-01
1.400	.20465930E+00	.30289375E-01
1.500	.22912342E+00	.33723545E-01
***** UNSTABLE. HALVE STEP SIZE.		
1.600	.25374567E+00	.37124215E-01
1.700	.27828148E+00	.40448378E-01
1.800	.30247441E+00	.43653526E-01
1.900	.32607308E+00	.46698030E-01
2.000	.34883009E+00	.49541648E-01
2.100	.37050432E+00	.52145960E-01
2.200	.39086329E+00	.54474824E-01
2.300	.40968512E+00	.56494750E-01
2.400	.42676082E+00	.58175303E-01
2.500	.44189611E+00	.59489438E-01
2.600	.45491337E+00	.60413815E-01
2.700	.46565308E+00	.60929064E-01
2.800	.47397562E+00	.61020037E-01
2.900	.47976239E+00	.60675976E-01
3.000	.48291703E+00	.59890663E-01
3.100	.48336631E+00	.58662515E-01
3.200	.48106089E+00	.56994629E-01
***** UNSTABLE. HALVE STEP SIZE.		
3.300	.47597701E+00	.54892082E-01
3.400	.46811290E+00	.52372413E-01
3.500	.45749353E+00	.49450112E-01
3.600	.44416783E+00	.46146478E-01
3.700	.42820899E+00	.42486973E-01
3.800	.40971367E+00	.38500998E-01
3.900	.38880123E+00	.34221593E-01
4.000	.36561281E+00	.29685133E-01
4.100	.34030988E+00	.24930935E-01
4.200	.31307297E+00	.20000904E-01

4.300	.28410013E+00	.14939082E-01
4.400	.25360497E+00	.97912172E-02
4.500	.22181497E+00	.46042797E-02
4.600	.18896942E+00	-.57397566E-03
4.700	.15531723E+00	-.56955520E-02
4.800	.12111479E+00	-.10712669E-01
4.900	.86623649E-01	-.15578281E-01
5.000	.52108217E-01	-.20246540E-01
5.100	.17833473E-01	-.24673293E-01
5.200	-.15937506E-01	-.28816545E-01
5.300	-.48945745E-01	-.32636889E-01
5.400	-.80938831E-01	-.36097942E-01
5.500	-.11167286E+00	-.39166702E-01
5.600	-.14091492E+00	-.41813945E-01
5.700	-.16844490E+00	-.44014497E-01
5.800	-.19405752E+00	-.45747540E-01
5.900	-.21756412E+00	-.46996822E-01
6.000	-.23879433E+00	-.47750886E-01
6.100	-.25759743E+00	-.48003127E-01
6.200	-.27384381E+00	-.47751974E-01
6.300	-.28742597E+00	-.47000856E-01
6.400	-.29825940E+00	-.45758201E-01
***** UNSTABLE. HALVE STEP SIZE.		
6.500	-.30628592E+00	-.44036211E-01
6.600	-.31146544E+00	-.41855756E-01
6.700	-.31378720E+00	-.39238281E-01
6.800	-.31326367E+00	-.36211093E-01
6.900	-.30993169E+00	-.32805643E-01
7.000	-.30385197E+00	-.29057272E-01
7.100	-.29510862E+00	-.25004848E-01
7.200	-.28380820E+00	-.20690337E-01
7.300	-.27007873E+00	-.16158449E-01
7.400	-.25406843E+00	-.11456138E-01
7.500	-.23594455E+00	-.66321736E-02
7.600	-.21589142E+00	-.17365962E-02
7.700	-.19410915E+00	.31797286E-02
7.800	-.17081142E+00	.80656772E-02
7.900	-.14622379E+00	.12870370E-01
8.000	-.12058155E+00	.17543692E-01

NO. OF ORDERS USED = 10
NO. OF STEPS = 4.
ANGLE OF INCIDENT LIGHT = 0.
Q FACTOR = .1825
FIRST V = .1
DIFF. ORDER = 3
STOP AT V = 8.

V	REAL	IMAG
.100	-.19563402E-04	-.64648810E-05
.200	-.15621817E-03	-.51613911E-04
.300	-.52561365E-03	-.17360688E-03
.400	-.12405299E-02	-.40956089E-03
.500	-.24094805E-02	-.79504418E-03
.600	-.41353586E-02	-.13635879E-02
.700	-.65141416E-02	-.21462211E-02
***** UNSTABLE. HALVE STEP SIZE.		
.800	-.96374802E-02	-.31718633E-02
.900	-.13578405E-01	-.44640775E-02
1.000	-.18407700E-01	-.60444428E-02
1.100	-.24182569E-01	-.79300105E-02
1.200	-.30948180E-01	-.10133525E-01
1.300	-.38736970E-01	-.12663198E-01
1.400	-.47568085E-01	-.15522526E-01
1.500	-.57446964E-01	-.18710174E-01
***** UNSTABLE. HALVE STEP SIZE.		
1.600	-.68364678E-01	-.22223457E-01
1.700	-.80298851E-01	-.26045200E-01
1.800	-.93212560E-01	-.30162069E-01
1.900	-.10705503E+00	-.34553298E-01
2.000	-.12176188E+00	-.39193508E-01
2.100	-.13725552E+00	-.44052918E-01
2.200	-.15344585E+00	-.49097621E-01
2.300	-.17023090E+00	-.54289884E-01
2.400	-.18749779E+00	-.59588523E-01
2.500	-.20512365E+00	-.64949291E-01
2.600	-.22297680E+00	-.70325340E-01
2.700	-.24091786E+00	-.75667690E-01
2.800	-.25880113E+00	-.80925738E-01
2.900	-.27647598E+00	-.86047784E-01
3.000	-.29378818E+00	-.90981602E-01
3.100	-.31058154E+00	-.95674981E-01
3.200	-.32669932E+00	-.10007630E+00
***** UNSTABLE. HALVE STEP SIZE.		
3.300	-.34198006E+00	-.10413196E+00
3.400	-.35628147E+00	-.10779874E+00
3.500	-.36944971E+00	-.11102776E+00
3.600	-.38134156E+00	-.11377542E+00
3.700	-.39182119E+00	-.11600148E+00
3.800	-.40076123E+00	-.11766953E+00
3.900	-.40804439E+00	-.11874745E+00
4.000	-.41356476E+00	-.11920783E+00
4.100	-.41722880E+00	-.11902835E+00
4.200	-.41895664E+00	-.11819206E+00

4.300	-.41868302E+00	-.11668768E+00
4.400	-.41635806E+00	-.11450987E+00
4.500	-.41194792E+00	-.11165926E+00
4.600	-.40543559E+00	-.10814269E+00
4.700	-.39682113E+00	-.10397316E+00
4.800	-.38612185E+00	-.99169798E-01
4.900	-.37337271E+00	-.93757841E-01
5.000	-.35862589E+00	-.87768416E-01
5.100	-.34195081E+00	-.81238363E-01
5.200	-.32343378E+00	-.74209987E-01
5.300	-.30317715E+00	-.66730646E-01
5.400	-.28129899E+00	-.58852465E-01
5.500	-.25793199E+00	-.50631847E-01
5.600	-.23322258E+00	-.42128998E-01
5.700	-.20732975E+00	-.33407422E-01
5.800	-.18042386E+00	-.24533326E-01
5.900	-.15268523E+00	-.15575065E-01
6.000	-.12430275E+00	-.66025085E-02
6.100	-.95472202E-01	.23136455E-02
6.200	-.66394852E-01	.11102423E-01
6.300	-.37275468E-01	.19693356E-01
6.400	-.83209204E-02	.28017065E-01
***** UNSTABLE. HALVE STEP SIZE.		
6.500	.20252903E-01	.36000953E-01
6.600	.48257979E-01	.43589272E-01
6.700	.75483903E-01	.50715490E-01
6.800	.10173370E+00	.57321135E-01
6.900	.12681727E+00	.63352010E-01
7.000	.15055296E+00	.68758659E-01
7.100	.17276917E+00	.73496907E-01
7.200	.19330594E+00	.77528304E-01
7.300	.21201626E+00	.80820492E-01
7.400	.22876742E+00	.83347585E-01
7.500	.24344234E+00	.85090421E-01
7.600	.25594032E+00	.86036779E-01
7.700	.26617825E+00	.86181549E-01
7.800	.27409123E+00	.85526795E-01
7.900	.27963317E+00	.84081780E-01
8.000	.28277741E+00	.81862933E-01

NO. OF ORDERS USED = 10
NO. OF STEPS = 4.
ANGLE OF INCIDENT LIGHT = 0.
Q FACTOR = .1825
FIRST V = .1
DIFF. ORDER = 4
STOP AT V = 8.

V	REAL	IMAG
.100	.21687395E-06	.13254038E-06
.200	.34649441E-05	.21173510E-05
.300	.17498832E-04	.10691339E-04
.400	.55117589E-04	.33667465E-04
.500	.13397822E-03	.81813023E-04
.600	.27633763E-03	.16868146E-03
.700	.50872579E-03	.31039988E-03
***** UNSTABLE. HALVE STEP SIZE.		
.800	.86207143E-03	.52362392E-03
.900	.13694658E-02	.83135513E-03
1.000	.20679944E-02	.12546260E-02
1.100	.29967919E-02	.18168586E-02
1.200	.41967530E-02	.25424187E-02
1.300	.57098937E-02	.34562075E-02
1.400	.75786848E-02	.45832360E-02
1.500	.98453639E-02	.59481856E-02
***** UNSTABLE. HALVE STEP SIZE.		
1.600	.12554233E-01	.75766901E-02
1.700	.15739864E-01	.94888172E-02
1.800	.19441851E-01	.11706794E-01
1.900	.23694498E-01	.14249637E-01
2.000	.28528396E-01	.17133874E-01
2.100	.33969776E-01	.20373142E-01
2.200	.40039915E-01	.23977829E-01
2.300	.46754556E-01	.27954731E-01
2.400	.54123406E-01	.32306762E-01
2.500	.62149664E-01	.37032680E-01
2.600	.70829641E-01	.42126884E-01
2.700	.80152429E-01	.47579241E-01
2.800	.90099658E-01	.53374963E-01
2.900	.10064531E+00	.59494550E-01
3.000	.11175565E+00	.65913773E-01
3.100	.12338919E+00	.72603713E-01
3.200	.13549679E+00	.79530879E-01
***** UNSTABLE. HALVE STEP SIZE.		
3.300	.14801815E+00	.86658934E-01
3.400	.16089584E+00	.93942465E-01
3.500	.17405617E+00	.10133697E+00
3.600	.18742183E+00	.10879270E+00
3.700	.20090961E+00	.11625668E+00
3.800	.21443085E+00	.12367303E+00
3.900	.22789214E+00	.13098354E+00
4.000	.24119607E+00	.13812808E+00
4.100	.25424192E+00	.14504517E+00
4.200	.26692659E+00	.15167254E+00

4.300	.27914542E+00	.15794772E+00
4.400	.29079316E+00	.16380863E+00
4.500	.30176484E+00	.16919422E+00
4.600	.31195681E+00	.17404506E+00
4.700	.32126773E+00	.17830402E+00
4.800	.32959942E+00	.18191681E+00
4.900	.33685811E+00	.18483266E+00
5.000	.34295507E+00	.18700486E+00
5.100	.34780777E+00	.18839129E+00
5.200	.35134076E+00	.18895501E+00
5.300	.35348640E+00	.18866473E+00
5.400	.35418581E+00	.18749522E+00
5.500	.35338950E+00	.18542770E+00
5.600	.35105803E+00	.18245021E+00
5.700	.34716272E+00	.17855788E+00
5.800	.34168606E+00	.17375318E+00
5.900	.33462204E+00	.16804599E+00
6.000	.32597672E+00	.16145374E+00
6.100	.31576811E+00	.15400146E+00
6.200	.30402658E+00	.14572165E+00
6.300	.29079468E+00	.13665419E+00
6.400	.27612710E+00	.12684613E+00
***** UNSTABLE. HALVE STEP SIZE.		
6.500	.26009617E+00	.11635172E+00
6.600	.24276956E+00	.10523152E+00
6.700	.22424145E+00	.93551993E-01
6.800	.20461183E+00	.81385512E-01
6.900	.18399064E+00	.68809623E-01
7.000	.16249707E+00	.55906403E-01
7.100	.14025878E+00	.42761901E-01
7.200	.11741079E+00	.29465343E-01
7.300	.94094872E-01	.16108555E-01
7.400	.70457986E-01	.27250356E-02
7.500	.46651670E-01	-.10410679E-01
7.600	.22830507E-01	-.23383916E-01
7.700	-.84895960E-03	-.36040654E-01
7.800	-.24229483E-01	-.48288320E-01
7.900	-.47154320E-01	-.60036650E-01
8.000	-.69468671E-01	-.71198518E-01

NO. OF ORDERS USED = 10
NO. OF STEPS = 4.
ANGLE OF INCIDENT LIGHT = 0.
Q FACTOR = ,540
FIRST V = .1
DIFF. ORDER = 0
STOP AT V = 7.0

V	REAL	IMAG
.100	.99751669E+00	-.22390139E-03
.200	.99008492E+00	-.89229337E-03
.300	.97775928E+00	-.19952796E-02
.400	.96063019E+00	-.35165008E-02
***** UNSTABLE. HALVE STEP SIZE.		
.500	.93882337E+00	-.54340688E-02
.600	.91249833E+00	-.77186256E-02
.700	.88184771E+00	-.10336367E-01
.800	.84709546E+00	-.13247963E-01
.900	.80849491E+00	-.16409361E-01
1.000	.76632698E+00	-.19772324E-01
1.100	.72089776E+00	-.23285025E-01
1.200	.67253607E+00	-.26892686E-01
***** UNSTABLE. HALVE STEP SIZE.		
1.300	.62159319E+00	-.30538334E-01
1.400	.56843194E+00	-.34163044E-01
1.500	.51343474E+00	-.37707480E-01
1.600	.45699374E+00	-.41112066E-01
1.700	.39950958E+00	-.44317889E-01
1.800	.34138784E+00	-.47267448E-01
1.900	.28303604E+00	-.49905393E-01
2.000	.22486044E+00	-.52179256E-01
2.100	.16726274E+00	-.54040130E-01
2.200	.11063697E+00	-.55443350E-01
2.300	.55366512E-01	-.56349077E-01
2.400	.18209248E-02	-.56722895E-01
2.500	-.49646688E-01	-.56536295E-01
2.600	-.98702482E-01	-.55767115E-01
***** UNSTABLE. HALVE STEP SIZE.		
2.700	-.14503365E+00	-.54398236E-01
2.800	-.18835423E+00	-.52424383E-01
2.900	-.22840184E+00	-.49842988E-01
3.000	-.26494318E+00	-.46660297E-01
3.100	-.29777489E+00	-.42890028E-01
3.200	-.32672494E+00	-.38553313E-01
3.300	-.35165381E+00	-.33678582E-01
3.400	-.37245538E+00	-.28301385E-01
3.500	-.38905753E+00	-.22464095E-01
3.600	-.40142238E+00	-.16215556E-01
3.700	-.40954656E+00	-.96106253E-02
3.800	-.41346066E+00	-.27096503E-02
3.900	-.41322896E+00	.44220670E-02
4.000	-.40894857E+00	.11714983E-01
4.100	-.40074811E+00	.19095994E-01
4.200	-.38878692E+00	.26489156E-01

4.300	-.37325288E+00	.33816565E-01
4.400	-.35436095E+00	.40999098E-01
4.500	-.33235121E+00	.47957330E-01
4.600	-.30748633E+00	.54612386E-01
4.700	-.28004945E+00	.60886851E-01
4.800	-.25034147E+00	.66705602E-01
4.900	-.21867846E+00	.71996704E-01
5.000	-.18538879E+00	.76692250E-01
5.100	-.15081027E+00	.80729188E-01
5.200	-.11528714E+00	.84050069E-01
5.300	-.79167261E-01	.86603792E-01
5.400	-.42798795E-01	.88346277E-01
5.500	-.65275866E-02	.89241049E-01
5.600	.29306045E-01	.89259789E-01
5.700	.64370053E-01	.88382779E-01
5.800	.98343583E-01	.86599276E-01
5.900	.13091944E+00	.83907761E-01
6.000	.16180690E+00	.80316200E-01
***** UNSTABLE. HALVE STEP SIZE.		
6.100	.19073105E+00	.75839798E-01
6.200	.21744681E+00	.70510175E-01
6.300	.24172278E+00	.64361362E-01
6.400	.26355565E+00	.57438966E-01
6.500	.28216821E+00	.49797376E-01
6.600	.29801103E+00	.41499579E-01
6.700	.31076344E+00	.32616408E-01
6.800	.32033431E+00	.23226172E-01
6.900	.32666270E+00	.13413793E-01
7.000	.32971812E+00	.32701765E-02

NO. OF ORDERS USED = 10
NO. OF STEPS = 4.
ANGLE OF INCIDENT LIGHT = 0.
Q FACTOR = .540
FIRST V = .1
DIFF. ORDER = 1
STOP AT V = 7.0

V	REAL	IMAG
.100	-.49334701E-01	-.66954433E-02
.200	-.98309856E-01	-.13309166E-01
.300	-.14656881E+00	-.19760372E-01
.400	-.19376064E+00	-.25970096E-01
***** UNSTABLE. HALVE STEP SIZE.		
.500	-.23954153E+00	-.31861821E-01
.600	-.28358209E+00	-.37363205E-01
.700	-.32556430E+00	-.42405836E-01
.800	-.36518728E+00	-.46926606E-01
.900	-.40216892E+00	-.50868307E-01
1.000	-.43624816E+00	-.54180282E-01
1.100	-.46718708E+00	-.56819012E-01
1.200	-.49477263E+00	-.58748615E-01
***** UNSTABLE. HALVE STEP SIZE.		
1.300	-.51881826E+00	-.59938816E-01
1.400	-.53916616E+00	-.60374230E-01
1.500	-.55568704E+00	-.60042328E-01
1.600	-.56828214E+00	-.58941143E-01
1.700	-.57688363E+00	-.57077571E-01
1.800	-.58145506E+00	-.54467332E-01
1.900	-.58199168E+00	-.51134853E-01
2.000	-.57852020E+00	-.47113008E-01
2.100	-.57109863E+00	-.42442822E-01
2.200	-.55981566E+00	-.37173055E-01
2.300	-.54478974E+00	-.31359676E-01
2.400	-.52616827E+00	-.25065322E-01
2.500	-.50412605E+00	-.18358625E-01
2.600	-.47886376E+00	-.11313477E-01
***** UNSTABLE. HALVE STEP SIZE.		
2.700	-.45060958E+00	-.40090414E-02
2.800	-.41960521E+00	.34737926E-02
2.900	-.38612072E+00	.11049710E-01
3.000	-.35044149E+00	.18632031E-01
3.100	-.31286850E+00	.26133140E-01
3.200	-.27371569E+00	.33465461E-01
3.300	-.23330736E+00	.40542428E-01
3.400	-.19197551E+00	.47279427E-01
3.500	-.15005702E+00	.53594744E-01
3.600	-.10789094E+00	.59410478E-01
3.700	-.65815566E-01	.64653433E-01
3.800	-.24165771E-01	.69255966E-01
3.900	.16729713E-01	.73156736E-01
4.000	.56551165E-01	.76301459E-01
4.100	.94990130E-01	.78643566E-01
4.200	.13175227E+00	.80144748E-01

4.300	.16655951E+00	.80775503E-01
4.400	.19915229E+00	.80515459E-01
4.500	.22929163E+00	.79353766E-01
4.600	.25676103E+00	.77289254E-01
4.700	.28136800E+00	.74330564E-01
4.800	.30294581E+00	.70496167E-01
4.900	.32135432E+00	.65814226E-01
5.000	.33648141E+00	.60322447E-01
5.100	.34824341E+00	.54067756E-01
5.200	.35658586E+00	.47105868E-01
5.300	.36148359E+00	.39500853E-01
5.400	.36294101E+00	.31324503E-01
5.500	.36099154E+00	.22655664E-01
5.600	.35569745E+00	.13579486E-01
5.700	.34714890E+00	.41865953E-02
5.800	.33546323E+00	-.54278091E-02
5.900	.32078357E+00	-.15164870E-01
6.000	.30327767E+00	-.24923121E-01
***** UNSTABLE. HALVE STEP SIZE.		
6.100	.28314430E+00	-.34595280E-01
6.200	.26057963E+00	-.44085413E-01
6.300	.23582186E+00	-.53286857E-01
6.400	.20911894E+00	-.62098146E-01
6.500	.18073363E+00	-.70420454E-01
6.600	.15094120E+00	-.78158714E-01
6.700	.12002683E+00	-.85222661E-01
6.800	.88283327E-01	-.91527733E-01
6.900	.56008237E-01	-.96996112E-01
7.000	.23501478E-01	-.10155754E+00

NO. OF ORDERS USED = 10
NO. OF STEPS = 4.
ANGLE OF INCIDENT LIGHT = 0.
Q FACTOR = .540
FIRST V = .1
DIFF. ORDER = 2
STOP AT V = 7.0

V	REAL	IMAG
.100	.10958793E-02	.52796909E-03
.200	.43733879E-02	.21058993E-02
.300	.98022241E-02	.47159209E-02
.400	.17332174E-01	.83284507E-02
***** UNSTABLE. HALVE STEP SIZE.		
.500	.26892665E-01	.12906839E-01
.600	.38396352E-01	.18393024E-01
.700	.51735986E-01	.24727307E-01
.800	.66787632E-01	.31837676E-01
.900	.83411203E-01	.39643066E-01
1.000	.10145169E+00	.48054179E-01
1.100	.12074048E+00	.56974417E-01
1.200	.14109683E+00	.66300845E-01
***** UNSTABLE. HALVE STEP SIZE.		
1.300	.16232446E+00	.75923600E-01
1.400	.18423137E+00	.85732667E-01
1.500	.20660638E+00	.95611609E-01
1.600	.22923650E+00	.10544315E+00
1.700	.25190524E+00	.11510939E+00
1.800	.27439431E+00	.12449301E+00
1.900	.29648566E+00	.13347850E+00
2.000	.31796327E+00	.14195341E+00
2.100	.33861506E+00	.14980941E+00
2.200	.35823475E+00	.15694354E+00
2.300	.37662354E+00	.16325922E+00
2.400	.39359204E+00	.16866733E+00
2.500	.40896176E+00	.17308712E+00
2.600	.42256664E+00	.17644711E+00
***** UNSTABLE. HALVE STEP SIZE.		
2.700	.43425600E+00	.17868314E+00
2.800	.44389099E+00	.17974968E+00
2.900	.45135232E+00	.17960499E+00
3.000	.45653736E+00	.17822151E+00
3.100	.45936200E+00	.17558389E+00
3.200	.45976134E+00	.17168910E+00
3.300	.45769041E+00	.16654670E+00
3.400	.45312453E+00	.16017877E+00
3.500	.44605968E+00	.15261973E+00
3.600	.43651234E+00	.14391613E+00
3.700	.42451962E+00	.13412632E+00
3.800	.41013910E+00	.12331990E+00
3.900	.39344809E+00	.11157711E+00
4.000	.37454327E+00	.98988182E-01
4.100	.35353984E+00	.85652469E-01
4.200	.33057068E+00	.71677577E-01

4.300	.30578518E+00	.57178363E-01
4.400	.27934806E+00	.42275825E-01
4.500	.25143823E+00	.27096069E-01
4.600	.22224695E+00	.11769009E-01
4.700	.19197665E+00	-.35727912E-02
4.800	.16083911E+00	-.18795356E-01
4.900	.12905365E+00	-.33764686E-01
5.000	.96845616E-01	-.48347913E-01
5.100	.64444202E-01	-.62414686E-01
5.200	.32080753E-01	-.75838402E-01
5.300	-.13078416E-04	-.88497418E-01
5.400	-.31607373E-01	-.10027629E+00
5.500	-.62475698E-01	-.11106685E+00
5.600	-.92397079E-01	-.12076935E+00
5.700	-.12115769E+00	-.12929342E+00
5.800	-.14855273E+00	-.13655903E+00
5.900	-.17438790E+00	-.14249719E+00
6.000	-.19848123E+00	-.14705088E+00
***** UNSTABLE. HALVE STEP SIZE.		
6.100	-.22066584E+00	-.15017247E+00
6.200	-.24078615E+00	-.15183642E+00
6.300	-.25870602E+00	-.15202127E+00
6.400	-.27430591E+00	-.15072229E+00
6.500	-.28748451E+00	-.14794833E+00
6.600	-.29815973E+00	-.14372200E+00
6.700	-.30626927E+00	-.13807943E+00
6.800	-.31177106E+00	-.13106999E+00
6.900	-.31464369E+00	-.12275596E+00
7.000	-.31488642E+00	-.11321198E+00

NO. OF ORDERS USED = 10
NO. OF STEPS = 4.
ANGLE OF INCIDENT LIGHT = 0.
Q FACTOR = .540
FIRST V = .1
DIFF. ORDER = 3
STOP AT V = 7.0

V	REAL	IMAG
.100	-.11211314E-04	-.15350624E-04
.200	-.89545719E-04	-.12257926E-03
.300	-.30140367E-03	-.41243770E-03
.400	-.71174666E-03	-.97343659E-03
***** UNSTABLE. HALVE STEP SIZE.		
.500	-.13878829E-02	-.18915954E-02
.600	-.23842906E-02	-.32466357E-02
.700	-.37600810E-02	-.51144141E-02
.800	-.55680588E-02	-.75639988E-02
.900	-.78563927E-02	-.10657206E-01
1.000	-.10668072E-01	-.14477780E-01
1.100	-.14040420E-01	-.18980666E-01
1.200	-.18004643E-01	-.24291359E-01
***** UNSTABLE. HALVE STEP SIZE.		
1.300	-.22578686E-01	-.30411590E-01
1.400	-.27791368E-01	-.37345290E-01
1.500	-.33648547E-01	-.45101719E-01
1.600	-.40153555E-01	-.53674120E-01
1.700	-.47302277E-01	-.63044609E-01
1.800	-.55083072E-01	-.73184177E-01
1.900	-.63476795E-01	-.84052823E-01
2.000	-.72456835E-01	-.95599782E-01
2.100	-.81989277E-01	-.10776387E+00
2.200	-.92033116E-01	-.12047400E+00
2.300	-.10254047E+00	-.13364963E+00
2.400	-.11345703E+00	-.14720158E+00
2.500	-.12472233E+00	-.16103272E+00
2.600	-.13627027E+00	-.17503880E+00
***** UNSTABLE. HALVE STEP SIZE.		
2.700	-.14802762E+00	-.18910525E+00
2.800	-.15992256E+00	-.20312414E+00
2.900	-.17187345E+00	-.21697247E+00
3.000	-.18379718E+00	-.23052778E+00
3.100	-.19560885E+00	-.24366587E+00
3.200	-.20721840E+00	-.25626194E+00
3.300	-.21853941E+00	-.26819191E+00
3.400	-.22948179E+00	-.27933362E+00
3.500	-.23995660E+00	-.28956798E+00
3.600	-.24987588E+00	-.29878029E+00
3.700	-.25915361E+00	-.30686136E+00
3.800	-.26770639E+00	-.31370870E+00
3.900	-.27545403E+00	-.31922757E+00
4.000	-.28232055E+00	-.32333206E+00
4.100	-.28823453E+00	-.32594600E+00
4.200	-.29313013E+00	-.32700391E+00

```
 4.300  -.29694744E+00  -.32645178E+00
 4.400  -.29963308E+00  -.32424769E+00
 4.500  -.30114094E+00  -.32036255E+00
 4.600  -.30143230E+00  -.31478044E+00
 4.700  -.30047652E+00  -.30749903E+00
 4.800  -.29825134E+00  -.29852990E+00
 4.900  -.29474302E+00  -.28789852E+00
 5.000  -.28994666E+00  -.27564433E+00
 5.100  -.28386639E+00  -.26182064E+00
 5.200  -.27651530E+00  -.24649426E+00
 5.300  -.26791562E+00  -.22974525E+00
 5.400  -.25809843E+00  -.21166633E+00
 5.500  -.24710375E+00  -.19236230E+00
 5.600  -.23498014E+00  -.17194922E+00
 5.700  -.22178451E+00  -.15055373E+00
 5.800  -.20758175E+00  -.12831193E+00
 5.900  -.19244427E+00  -.10536845E+00
 6.000  -.17645160E+00  -.81875351E-01
***** UNSTABLE.  HALVE STEP SIZE.
 6.100  -.15969260E+00  -.57997433E-01
 6.200  -.14225348E+00  -.33885306E-01
 6.300  -.12423440E+00  -.97116551E-02
 6.400  -.10573741E+00   .14354465E-01
 6.500  -.86868168E-01   .38143203E-01
 6.600  -.67735753E-01   .61485137E-01
 6.700  -.48451506E-01   .84212832E-01
 6.800  -.29128342E-01   .10616210E+00
 6.900  -.98799239E-02   .12717351E+00
 7.000   .91801194E-02   .14709363E+00
```

```
NO. OF ORDERS USED = 10
NO. OF STEPS = 4.
ANGLE OF INCIDENT LIGHT = 0.
@ FACTOR =1.737
FIRST V = .1
DIFF. ORDER = 0
STOP AT V = 5.4

     V          REAL                IMAG

   .100    .99765445E+00   -.69609085E-03
   .200    .99063213E+00   -.27754873E-02
***** UNSTABLE.  HALVE STEP SIZE.
   .300    .97897642E+00   -.62128636E-02
***** UNSTABLE.  HALVE STEP SIZE.
***** UNSTABLE.  HALVE STEP SIZE.
***** UNSTABLE.  HALVE STEP SIZE.
***** UNSTABLE.  HALVE STEP SIZE.
   .400    .96276123E+00   -.10963173E-01
   .500    .94208085E+00   -.16966205E-01
   .600    .91706532E+00   -.24145034E-01
   .700    .88786798E+00   -.32407189E-01
   .800    .85466776E+00   -.41645586E-01
   .900    .81766828E+00   -.51739582E-01
  1.000    .77709656E+00   -.62556214E-01
  1.100    .73320074E+00   -.73951453E-01
  1.200    .68624980E+00   -.85771761E-01
  1.300    .63653068E+00   -.97855486E-01
  1.400    .58434652E+00   -.11003458E+00
  1.500    .53001664E+00   -.12213635E+00
  1.600    .47387156E+00   -.13398507E+00
  1.700    .41625305E+00   -.14540384E+00
  1.800    .35751129E+00   -.15621649E+00
  1.900    .29800260E+00   -.16624920E+00
  2.000    .23808733E+00   -.17533256E+00
  2.100    .17812757E+00   -.18330305E+00
  2.200    .11848452E+00   -.19000513E+00
  2.300    .59517078E-01   -.19529257E+00
  2.400    .15784451E-02   -.19903032E+00
  2.500   -.54984977E-01   -.20109578E+00
  2.600   -.10983686E+00   -.20138051E+00
  2.700   -.16265198E+00   -.19979100E+00
  2.800   -.21311897E+00   -.19625044E+00
  2.900   -.26094205E+00   -.19069924E+00
  3.000   -.30584283E+00   -.18309614E+00
```

3.100	-.34756200E+00	-.17341873E+00
3.200	-.38586100E+00	-.16166411E+00
3.300	-.42052356E+00	-.14784917E+00
3.400	-.45135653E+00	-.13201056E+00
3.500	-.47819211E+00	-.11420517E+00
3.600	-.50088727E+00	-.94509378E-01
3.700	-.51932644E+00	-.73019023E-01
3.800	-.53342025E+00	-.49848609E-01
3.900	-.54310760E+00	-.25130898E-01
4.000	-.54835473E+00	.98449702E-03
4.100	-.54915670E+00	.28331613E-01
4.200	-.54553558E+00	.56729822E-01
4.300	-.53754180E+00	.85985074E-01
4.400	-.52525301E+00	.11589115E+00
4.500	-.50877330E+00	.14623165E+00
4.600	-.48823244E+00	.17678154E+00
4.700	-.46378573E+00	.20730891E+00
4.800	-.43561171E+00	.23757699E+00
4.900	-.40391208E+00	.26734606E+00
5.000	-.36890893E+00	.29637554E+00
5.100	-.33084438E+00	.32442571E+00

```
NO. OF ORDERS USED = 10
NO. OF STEPS = 64.
ANGLE OF INCIDENT LIGHT = 0.
Q FACTOR = 1.737
FIRST V = .3
DIFF. ORDER = 1
STOP AT V = 5.1

     V          REAL                IMAG

  .300   -.13070681E+00   -.60229133E-01
***** UNSTABLE.  HALVE STEP SIZE.
  .400   -.17310512E+00   -.79362894E-01
  .500   -.21450912E+00   -.97699551E-01
  .600   -.25468182E+00   -.11505343E+00
  .700   -.29339384E+00   -.13124760E+00
  .800   -.33042470E+00   -.14611568E+00
  .900   -.36556426E+00   -.15950314E+00
 1.000   -.39861407E+00   -.17126887E+00
 1.100   -.42938819E+00   -.18128626E+00
 1.200   -.45771547E+00   -.18944472E+00
 1.300   -.48343896E+00   -.19565020E+00
 1.400   -.50641780E+00   -.19982635E+00
 1.500   -.52652861E+00   -.20191538E+00
 1.600   -.54366485E+00   -.20187816E+00
 1.700   -.55773856E+00   -.19969493E+00
 1.800   -.56868039E+00   -.19536546E+00
 1.900   -.57644017E+00   -.18890897E+00
 2.000   -.58098734E+00   -.18036417E+00
 2.100   -.58231037E+00   -.16978865E+00
 2.200   -.58041807E+00   -.15725884E+00
 2.300   -.57533815E+00   -.14286893E+00
 2.400   -.56711795E+00   -.12673032E+00
 2.500   -.55582372E+00   -.10897057E+00
 2.600   -.54154027E+00   -.89732377E-01
 2.700   -.52437012E+00   -.69172161E-01
 2.800   -.50443345E+00   -.47458942E-01
 2.900   -.48186647E+00   -.24772765E-01
 3.000   -.45682140E+00   -.13029991E-02
 3.100   -.42946448E+00    .22753104E-01
 3.200   -.39997597E+00    .47192264E-01
 3.300   -.36854806E+00    .71807023E-01
```

3.400	-.33538395E+00	.96387332E-01
3.500	-.30069682E+00	.12072271E+00
3.600	-.26470778E+00	.14460374E+00
3.700	-.22764511E+00	.16782432E+00
3.800	-.18974231E+00	.19018318E+00
3.900	-.15123684E+00	.21148587E+00
4.000	-.11236832E+00	.23154623E+00
4.100	-.73377240E-01	.25018835E+00
4.200	-.34503286E-01	.26724790E+00
4.300	.40164454E-02	.28257389E+00
4.400	.41948457E-01	.29602959E+00
4.500	.79064809E-01	.30749420E+00
4.600	.11514451E+00	.31686368E+00
4.700	.14997477E+00	.32405178E+00
4.800	.18335267E+00	.32899092E+00
4.900	.21508615E+00	.33163273E+00
5.000	.24499548E+00	.33194843E+00
5.100	.27291414E+00	.32992929E+00

NO. OF ORDERS USED = 10.
NO. OF STEPS = 64.
ANGLE OF INCIDENT LIGHT = 0.
Q FACTOR = 1.737
FIRST V = .4
DIFF. ORDER = 2
STOP AT V = 5.5

V	REAL	IMAG
***** UNSTABLE. HALVE STEP SIZE.		
.400	.23224385E-02	.14777527E-01
.500	.36148319E-02	.22951822E-01
.600	.51808201E-02	.32808982E-01
.700	.70123359E-02	.44270554E-01
.800	.90999166E-02	.57245399E-01
.900	.11432762E-01	.71630396E-01
1.000	.13998768E-01	.87311355E-01
1.100	.16784564E-01	.10416392E+00
1.200	.19775661E-01	.12205471E+00
1.300	.22956363E-01	.14084217E+00
1.400	.26309999E-01	.16037800E+00
1.500	.29818972E-01	.18050836E+00
1.600	.33464700E-01	.20107490E+00
1.700	.37227913E-01	.22191630E+00
1.800	.41088674E-01	.24286959E+00
1.900	.45026438E-01	.26377125E+00
2.000	.49020290E-01	.28445892E+00
2.100	.53048886E-01	.30477236E+00
2.200	.57090881E-01	.32455506E+00
2.300	.61124623E-01	.34365523E+00
2.400	.65128796E-01	.36192727E+00
2.500	.69082102E-01	.37923278E+00
2.600	.72963869E-01	.39544187E+00
2.700	.76753678E-01	.41043374E+00
2.800	.80432031E-01	.42409827E+00
2.900	.83980190E-01	.43633636E+00
3.000	.87380374E-01	.44706111E+00
3.100	.90616066E-01	.45619788E+00
3.200	.93672014E-01	.46368562E+00
3.300	.96534444E-01	.46947678E+00

3.400	.99191079E-01	.47353737E+00
3.500	.10163161E+00	.47584836E+00
3.600	.10384742E+00	.47640403E+00
3.700	.10583210E+00	.47521355E+00
3.800	.10758119E+00	.47229968E+00
3.900	.10909260E+00	.46769922E+00
4.000	.11036632E+00	.46146183E+00
4.100	.11140517E+00	.45365064E+00
4.200	.11221404E+00	.44434016E+00
4.300	.11280051E+00	.43361716E+00
4.400	.11317472E+00	.42157855E+00
4.500	.11334916E+00	.40833122E+00
4.600	.11333905E+00	.39399053E+00
4.700	.11316204E+00	.37867984E+00
4.800	.11283820E+00	.36252872E+00
4.900	.11238998E+00	.34567245E+00
5.000	.11184209E+00	.32825019E+00
5.100	.11122134E+00	.31040404E+00
5.200	.11055661E+00	.29227797E+00
5.300	.10987851E+00	.27401586E+00
5.400	.10921932E+00	.25576098E+00
5.500	.10861279E+00	.23765429E+00

APPENDIX 3

THE THEORY OF THE FRACTIONAL WAVEPLATE

(A ROTARY MICA COMPENSATOR)

The fractional waveplate consists of a thin sheet of mica oriented with its optical axis perpendicular with the plane of the sheet. Consider a system with only a polarizer, an analyzer, and the wave plate. If the electric vector is horizontal and the fast axis of the wave plate makes an angle with the horizontal θ, then the electric vector just before arriving at the waveplate has components

$$E_f = E_{IN} \cos\theta \sin\omega t$$
$$E_s = E_{IN} \sin\theta \sin\omega t$$

where E_f is the component of the electric vector in the fast axis direction and E_s is the component of the electric vector in the slow axis direction. After leaving the wave plate the electric vector E_f is phase shifted δ_r so that (Fig. 1)

$$E_f = E_{IN} \cos\theta \sin(\omega t + \delta_r)$$
$$E_s = E_{IN} \sin\theta \sin(\omega t)$$

where δ_r is the maximum retardation of the waveplate. The vectors are now decomposed into x and y components

$$E_{sx} = E_{IN} \sin^2\theta \sin\omega t$$
$$E_{sy} = -E_{IN} \sin\theta \cos\theta \sin\omega t$$

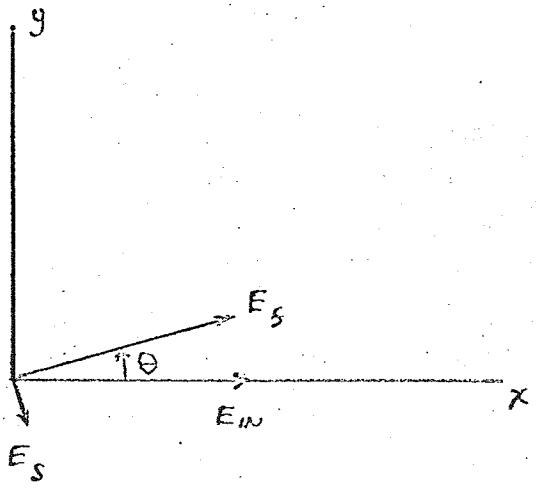

(a)

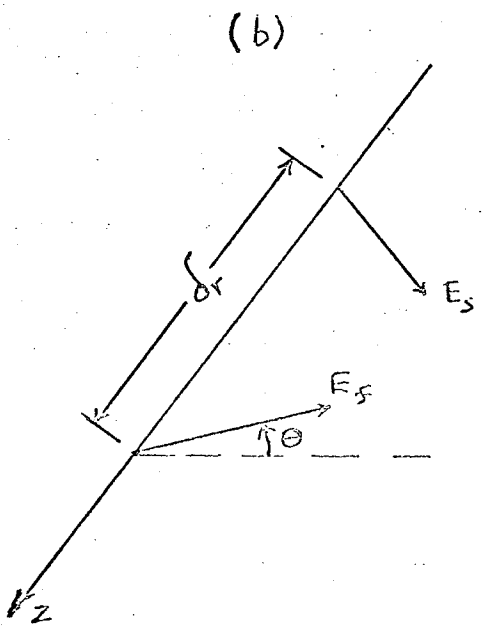

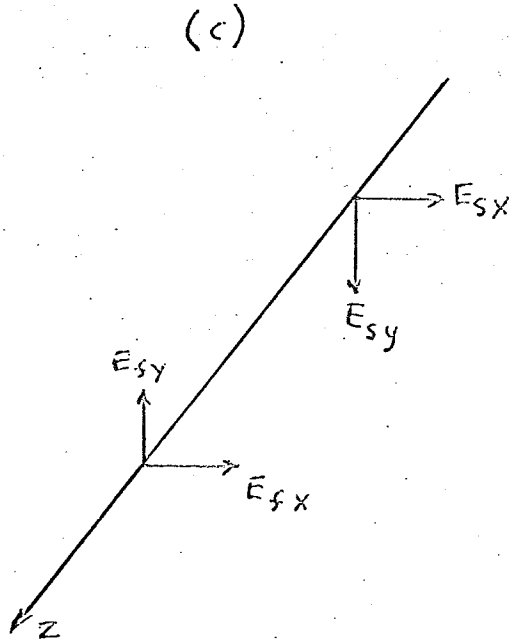

Figure 1. Vector diagram for (a), the light vectors, just before entering the wave plate, (b) the light vectors just before sample chamber, and (c) vector decomposition of the light vectors just before sample chamber.

$$E_{fx} = E_{IN} \cos^2 \theta \sin(\omega t + \delta_r)$$

$$E_{fy} = E_{IN} \cos\theta \sin\theta \sin(\omega t + \delta_r)$$

The vector sum of the y components is

$$\frac{E_Y}{E_{IN}} = \sin\theta\cos\theta \left[\sin(\omega t + \delta_r) - \sin\omega t \right]$$

$$= \frac{1}{2} \sin 2\theta \sin(\omega t + \phi) \sqrt{2 - 2\cos\delta_r}$$

with the x components being canceled by the analyzer. The current in the photomultiplier is

$$i = i_{90^\circ} \sin^2 2\theta \, (1 - \cos\delta_r)/2$$

To obtain the value of the maximum retardation of the twentieth wave plate at the laser wave length, a calibration was performed. Using a polarizer and analyzer combination, the laser intensity is calibrated by rotating the analyzer from null and recording the photomultiplier current as a function of angle. Since the intensity of light leaving the analyzer prism is proportional to $\sin^2\theta$ where θ is the angle of rotation of the analyzer, the maximum current, i_{90°, is then calculated. With the analyzer set for extinction, the wave plate is inserted between the prisms and the

position for null obtained. The wave plate is rotated and the photomultiplier current measured as a function of angle. Then the retardation is found from

$$\sin^2 \frac{\delta_r}{2} = \frac{1}{\sin^2 2\theta} \cdot \frac{i}{i_{90°}}$$

VITA

Aaron Joseph Averbuch was born in Chicago, Illinois on April 17, 1939. He attended public schools in Chicago and graduated from South Shore High School in 1956. In the fall of 1956, he entered the Illinois Institute of Technology. In 1960, he left school to work for a year at the Lindberg Engineering Company, Chicago, Illinois. He returned to school in 1961 and graduated in June 1962 with a bachelor's degree in electrical engineering with a minor in electronics. During the summer of 1962, he attended Roosevelt University.

In September, 1962, Mr. Averbuch entered the Department of Electrical Engineering at the University of Illinois. He completed his master's thesis in 1965 on the subject of the role of depolarizing agents in the conduction and transmission of action potentials in amphibian skeletal muscles.

From 1965 until 1968, Mr. Averbuch was a research and teaching assistant in the Department of Electrical Engineering. He taught laboratory sections in control systems and pulse techniques. During this same period, he worked on his doctoral dissertation at the Bio-acoustics Research Laboratory under the supervision of Dr. Floyd Dunn. His dissertation was concerned with a method of detecting acoustically induced birefringence in liquids.

In 1968, Mr. Averbuch became a research associate in the Department of Electrical Engineering. Since that time, he has been concerned with the effect of high intensity acoustic

stimulation on the inner ear, the effect of high intensity ultrasonic waves on the central nervous system, and the measurement of the threshold of hearing using evoked potentials. Concurrently, he has taught both lecture and laboratory sections of pulse techniques.